

EXTRACTIVE DESULFURIZATION OF FUEL OILS USING IONIC LIQUIDS

by

© Hanan M. Ashoshan

A thesis submitted to the School of Graduate Studies in partial fulfillment of
the requirements for the degree of

Doctor of Philosophy

Faculty of Engineering and Applied Science

Memorial University of Newfoundland

January 2022

St. John's, Newfoundland

Abstract

The sulphur content of transportation fuels must be reduced in high-sulphur crude oil by desulfurization. Traditionally, desulfurization methods have required harsh reaction conditions and are not very effective at removing refractory sulfur compounds such as benzothiophene (BT), dibenzothiophene (DBT) and 4,6-dimethyldibenzothiophene (4,6-DMDBT). Alternative methods, such as ionic liquid (IL)-mediated desulfurization, are both effective and environmentally friendly. Solvents ideal for desulfurization are required to be recyclable, insoluble in oil, selective for compounds containing sulphur, and eco-friendly. These properties are offered by ILs based on pyridinium. Therefore, the primary objectives of this thesis were to: (1) investigate the properties of N-butyl-pyridinium tetrafluoroborate ([BPy][BF₄]) and N-carboxymethyl pyridinium hydrogen sulfate ([CH₂COOHPy][HSO₄]); (2) understand the effects of reaction parameters (temperature, volume ratio, oxidant dosage, quantities of sulphur compound extracted, etc.) on desulfurization efficiency; (3) clarify the interactions between ILs and sulphur compounds; and (4) investigate the recycling and regeneration of ILs. Experimental results showed that the desulfurization efficiency of [BPy][BF₄] increased with temperature and oxidant dosage and declined with IL to fuel volume ratio. It was observed that at 30°C, 1:1 ratio of IL to model fuel [BPy][BF₄] could remove up to 79% of DBT in 80 min in the presence of oxidant H₂O₂. [CH₂COOHPy][HSO₄] was found to be more effective in desulfurization, capable of removing up to 99.9% of DBT in the presence of oxidant H₂O₂ within 40 min at 25°C, 1:1 ratio of IL to model fuel. The recycled [CH₂COOHPy][HSO₄] marginally lost effectiveness

after 8 recycles. It was also found that the effectiveness of both ILs was lower in real diesel compared to model fuels.

Computational density functional theory-based structural analysis revealed that there were two types of possible π - π interactions between [BPy] [BF₄] and DBT/DBTO₂, resulting in the formation of complexes with different geometries. [CH₂COOHPy][HSO₄] also exhibits similar potential π - π interactions with DBT/DBTO₂. Moreover, both ILs undergo the same oxidative mechanism of desulfurization, as they involve π - π interactions and hydrogen bonds.

Acknowledgements

This work is funded by the Ministry of Higher Education of Libyan Government and my supervisors who helped me to finish this work, which is managed by the CBIE in Canada, and the author acknowledges both of them for their support. I want to express my grace of Allah Almighty and my great gratitude to my thesis advisors Dr. Syed Imtiaz and Dr. Yan Zhang, who made most of the help and reviews to make this work exist. I'd also like to thank Dr. Shofiur Rahman for his kind support.

Words cannot express my thankfulness to the support and encouragement provided by my parents (My father Mohamed and my mother Zohra), my lovely husband during my studies.

Many thanks are due to my brothers and sisters for their sweet wishes and kind support.

My friends and all my family members who never stop encouraging me during my study, many thanks to you.

Table of Contents

Abstract	ii
Acknowledgements	iv
Table of Contents	v
List of Tables	ix
List of Figures	x
List of Abbreviations and Symbols.....	xvi
Chapter 1: Introduction	1
1.1 Background	1
1.2 Research Objectives	4
1.3 Organization of the Thesis	4
References	8
Chapter 2: Literature Review	9
2.1 Introduction	9
2.2 Sulfur Compounds in Raw Petroleum	10
2.3 Desulfurization Methods	13
2.3.1 Hydrodesulfurization	14
2.3.2 Biodesulfurization	15
2.3.3 Adsorption.....	16
2.3.4 Oxidative Desulfurization	17
2.3.5 Extractive Desulfurization	19
2.4 Ionic Liquids	19
2.4.1 Definition and Classification	19
2.4.2 Synthesis and Purification of ILs	22
2.4.3 Properties of ILs.....	27
2.5 Desulfurization Using ILs	29
2.6 Density Functional Theory Study in Desulfurization by ILs	40

2.6.1 Density Functional Theory	40
2.6.2 Evaluation of Desulfurization Mechanism Using DFT Simulation.....	44
2.7 Summary	48
References	49
Chapter 3: Oxidative Desulfurization by the Pyridinium-Based Ionic Liquid <i>N</i> -Butyl-Pyridinium Tetrafluoroborate	57
3.1 Introduction.....	57
3.2 Experimental Methods	61
3.2.1 Chemicals and Reagents	61
3.2.2 Synthesis of <i>N</i> -butyl-pyridinium tetrafluoroborate ([BPy][BF ₄]).....	61
3.2.3 Desulfurization of Model Fuels by IL.....	65
3.2.4 Recycling of the IL	67
3.2.5 Desulfurization of Aromatic Compounds from Diesel Fuel by IL	69
3.3 Analytical Methods.....	69
3.3.1 Proton Nuclear Magnetic Resonance (Hydrogen-1 NMR or ¹ H-NMR) and Carbon-13 NMR (¹³ C-NMR).....	69
3.3.2 Ultraviolet-Visible-Infrared (UV-Vis-IR) Spectrophotometric Analysis	69
3.4 Results and Discussion	69
3.4.1 ¹ H-NMR, ¹³ C-NMR and FTIR Characterization of [BPy][BF ₄]	69
3.4.2 Effect of Operating Parameters on Desulfurization Efficiency	72
3.4.3 Interaction of Various Operating Parameters to Determine Desulfurization Efficiency	77
3.4.4 Regeneration of the IL	85
3.4.5 Desulfurization of DBT from Diesel Fuel with [BPy][BF ₄].....	90
3.5 Conclusion	91
References	93
Chapter 4: Oxidative-Extractive Desulfurization by the Acidic Ionic Liquid <i>N</i> -Carboxymethyl Pyridinium Hydrogen Sulfate	95
4.1 Introduction.....	95
4.2 Experimental Methods	98

4.2.1	Chemicals and Reagents	98
4.2.2	Synthesis of the Acidic IL N-Carboxymethyl Pyridinium Hydrogen Sulfate	98
4.2.3	Desulfurization of Model Fuel by the Synthesized IL	101
4.2.4	Recycling of the IL	103
4.2.5	Desulfurization of Aromatic Compounds from Diesel Fuel by IL	104
4.3	Analytical Methods	105
4.3.1	Proton Nuclear Magnetic Resonance (hydrogen-1 NMR, or $^1\text{H-NMR}$) and Carbon-13 NMR ($^{13}\text{C-NMR}$)	105
4.3.2	Agilent 1260 High Performance Liquid Chromatography-UV Spectroscopy	105
4.4	Results and Discussion	106
4.4.1	$^1\text{H-NMR}$ and $^{13}\text{C-NMR}$ Characterization of $[\text{CH}_2\text{COOHPy}][\text{HSO}_4]$	106
4.4.2	Effect of Operating Parameters on Desulfurization Efficiency	108
4.4.3	Desulfurization of DBT from Diesel Fuel by Using Acidic IL	112
4.4.4	Recycling of Used IL	113
4.5	Conclusion	118
	References	119
	Chapter 5: Molecular Simulation Using Density Functional Theory	121
5.1	Introduction	121
5.2	A DFT Study on Oxidative and Extractive Desulfurization by ILs	121
5.2.1	N-Butyl-Pyridinium Tetrafluoroborate ($[\text{BPy}][\text{BF}_4]$) IL	121
5.2.2	N-Carboxymethyl Pyridinium Hydrogen Sulfate ($[\text{CH}_2\text{COOHPy}][\text{HSO}_4]$)	130
5.3	Conclusion	139
	References	141
	Chapter 6: Conclusions and Future Works	142
6.1	Conclusions	142
6.2	Future Perspectives	145
	Appendix A	146

A.1 ^1H -NMR and ^{13}C -NMR Analyses of [BPy][BF ₄]	146
A.2 FTIR Analysis of [BPy][BF ₄]	147
A.3 Calibration Curve Obtained Using UV-Vis Spectrophotometer to Analyze Sulfur Removal	149
A.4 Diesel Sample Analysis by Gas Chromatography	150
Appendix B	153
B.1 HPLC-UV-vis-TOF of the Model Oil Layer after Desulfurization with IL.....	153

List of Tables

Table 2.1: Physical Properties of Th, BT and DBT.....	13
Table 2.2: Summary of EDS using ILs as extractants.....	31
Table 2.3: Summary of OEDS using ILs as both extractants and catalysts.....	33
Table 2.4: A summary of DFT approaches.....	47
Table 3.1: Magnitude and nature of interaction between different operating parameters of the desulfurization reaction.....	83
Table 5.1: Calculated interaction energies (Δ IE kJ/mol) for the ionic liquid [BPY][BF ₄] with DBT and DBTO ₂ sulfur-containing compounds in model fuel (hexane) and CCl ₄ solvent system.....	123
Table 5.2: Calculated interaction energies (DIE kJ/mol) for the ionic liquid [CH ₂ COOHPy] [HSO ₄] when interacting with DBT and DBTO ₂ sulfur-containing compounds in a model fuel gas phase and various solvents.....	132
Table A.1: Comparison of ¹ H-NMR chemical shifts of [BPy][BF ₄] with references.....	147
Table A.2: Comparison of ¹³ C-NMR chemical shifts of [BPy][BF ₄] with references.....	148
Table A.3: FTIR spectrum of [BPy][BF ₄].....	149
Table A.4: Components of diesel fuel identified using gas chromatography.....	152

List of Figures

Figure 1.1: Thesis organization.....	7
Figure 2.1: Chemical structure of crude oil S-containing compounds.....	12
Figure 2.2: Structures of some common IL cations and anions. R, R ₁ , and R ₂ = side groups (predominantly alkyl chains).....	22
Scheme 2.1: Synthesis of halide precursor IL through nucleophilic substitution...	26
Figure 3.1: Synthesis of the IL N-Butylpyridinium tetrafluoroborate: Step 1 – Synthesis of N-Butylpyridinium bromide.....	62
Figure 3.2: Synthesis of the IL N-Butylpyridinium tetrafluoroborate: Step 2 – Synthesis of N-Butylpyridinium from N-Butylpyridinium bromide.....	63
Scheme 3.1: Synthetic route for [BPy][BF ₄].....	64
Figure 3.3: Oxidative-extractive desulfurization of sulfur compounds by using the IL.....	67
Figure 3.4: Recycling of the IL.....	68
Figure 3.5: (a) ¹ H-NMR (300 MHz), DMSO- <i>d</i> ₆), (b) ¹³ C-NMR (75 MHz, DMSO- <i>d</i> ₆) spectra of [BPy][BF ₄].....	70
Figure 3.6: FTIR spectrum of the IL [BPy][BF ₄].....	71
Figure 3.7: Oxidation extraction desulfurization efficiency at different temperatures and IL:Oil volume ratios. ([DBT] _{ini} = 1000 ppm; V(H ₂ O ₂): V(model oil) = 1 %, <i>t</i> = 40 min).....	73

Figure 3.8: Desulfurization efficiency of EDS and OEDS at different time. ([DBT] _{ini} =1000 ppm; $T = 30\text{ }^{\circ}\text{C}$).....	74
Figure 3.9: Desulfurization efficiency of EDS and OEDS at different volume ratios of H ₂ O ₂ to model fuel. ([DBT] _{ini} = 1000 ppm; $T = 30\text{ }^{\circ}\text{C}$ and $t = 40\text{ min}$).....	76
Figure 3.10: Desulfurization efficiency of EDS and OEDS at different volume ratios of IL to model fuel. ([DBT] _{ini} = 1000 ppm; $V(\text{H}_2\text{O}_2): V(\text{model oil}) = 40\%$, $T = 30\text{ }^{\circ}\text{C}$ and $t = 40\text{ min}$).....	77
Figure 3.11: Graphic representation of temperature (T) and IL to model fuel ratio on DBT removal. Legend on the right shows colored mapping of DBT removal in %.....	78
Figure 3.12: Graphic representation of H ₂ O ₂ dosage and IL to model fuel ratio on DBT removal. Legend on the right shows colored mapping of DBT removal in %.....	80
Figure 3.13: Graphic representation of the effect of H ₂ O ₂ and IL to model fuel ratios on DBT removal. Legend on the right shows colored mapping of DBT removal in %.....	79
Figure 3.14: Graphic representation of the effect of temperature (T) and H ₂ O ₂ to model fuel ratio on DBT removal. Legend on the right shows colored mapping of DBT removal in %.....	80
Figure 3.15: Graphic representation of temperature (T) and IL to model fuel ratio on DBT removal. Legend on the right shows colored mapping of DBT removal in %.....	81

Figure 3.16: Graphic representation of time and H ₂ O ₂ to model fuel ratio on DBT removal. Legend on the right shows colored mapping of DBT removal in %.....	82
Figure 3.17: Graphic representation of extraction time and IL to model fuel ratio on DBT removal. Legend on the right shows colored mapping of DBT removal in %.....	82
Figure 3.18: Magnitude and nature of interaction between different operating parameters of the desulfurization reaction.....	84
Figure 3.19: Interaction of 3 variables – H ₂ O ₂ to model fuel ratio, IL to model fuel ratio and temperature on the desulfurization efficiency of the IL.....	85
Figure 3.20: Interaction of model fuel and H ₂ O ₂ volumes at low and high temperatures in the desulfurization reaction.....	85
Figure 3.21: (a) ¹ H-NMR (300 MHz), DMSO- <i>d</i> ₆ , (b) ¹³ C-NMR (75 MHz, DMSO- <i>d</i> ₆) spectra of [BPy][BF ₄].....	87
Figure 3.22: ¹ H-NMR spectra of regenerated IL.....	88
Figure 3.23: ¹³ C-NMR spectra of regenerated IL.....	89
Figure 3.24: OEDS of DBT by regenerated [BPy][BF ₄]. ([DBT] _{ini} = 1000 ppm, V(IL): V(model oil) = 1:1, V(H ₂ O ₂): V(model oil) = 40 %, T = 30 °C).....	90
Figure 3.25: Desulfurization efficiency of DBT in diesel fuel. ([DBT] _{ini} = 1000 ppm, V(IL): V(model oil) = 1:1, V(H ₂ O ₂): V(model oil) = 40 %, T = 40 °C).....	91
Scheme 4.1: Synthetic route for ([CH ₂ COOHPy] [HSO ₄]).....	99
Figure 4.1: Synthesis of N-carboxymethyl pyridinium hydrogen sulfate.....	100

Figure 4.2: Using a separatory funnel to separate the ionic liquid phase from the model fuel or diesel phase after desulfurization.....	102
Figure 4.3: Recycling the IL.....	104
Figure 4.4: (a) ¹ H-NMR (300 MHz, Deuterium Oxide), (b) ¹³ C-NMR (75 MHz, Deuterium Oxide)) spectra of ([CH ₂ COOHPy] [HSO ₄]).....	107
Figure 4.5: Desulfurization of model fuel by ([CH ₂ COOHPy] [HSO ₄]) at different extraction times. Reaction conditions: volume ratio (IL: DBT): 1:1, T: 30°C, (V) H ₂ O ₂ : 0.4mL.....	109
Figure 4.6: Desulfurization efficiency of OEDS at H ₂ O ₂ : model fuel (O:S) volume ratio of 1:300; temperature = 25°C at different extraction times.....	111
Figure 4.7: Desulfurization efficiency of OEDS at volume ratio of H ₂ O ₂ to model fuel = 2:75, temperature = 25 °C at different extraction times.....	112
Figure 4.8: Desulfurization of DBT in model fuel and real diesel as a function of extraction time. Reaction conditions: V DBT= 20ml; V(IL)=1.2 ml, T= 25 °C; O/S=6.....	113
Figure 4.9: ¹ H-NMR spectrum of the recycled IL.....	114
Figure 4.10: ¹³ C-NMR spectrum of the recycled IL.....	115
Figure 4.11: Desulfurization efficiency of OEDS of DBT under the following reaction conditions: volume ratio of H ₂ O ₂ to oil fuel = 2:75, IL= 1.2 mL, temperature = 25 °C at extraction time 40 min.....	117

Figure 4.12: Desulfurization efficiency of OEDS of DBT under the following reaction conditions: volume ratio of H ₂ O ₂ to real diesel fuel = 2:75, IL= 1.2 mL, temperature = 25 °C at extraction times 40 min.....	117
Figure 4.13: Desulfurization of DBT using recycled IL that has residual H ₂ O ₂	118
Figure 5.1: The geometry optimized structures of [BPy][BF ₄], dibenzothiophene (DBT), dibenzothiophene sulfone (DBTO ₂), ([BPy][BF ₄]) ⊃ DBT and ([BPy][BF ₄]) ⊃ DBTO ₂ in hexane solvent system. Color code: carbon = grey; hydrogen= white; nitrogen= blue; oxygen = red; sulfur = yellow, boron = magenta and fluorine = green.....	126
Scheme 5.1: Desulfurization mechanism reaction by pyridine-based ionic liquid to remove DBT.....	130
Figure 5.2: The geometry optimized structures of (a) [CH ₂ COOHPy] [HSO ₄], (b) DBT, (c) DBTO ₂ , (d) [CH ₂ COOHPy] [HSO ₄] ⊃ DBTO ₂ in gas phase, and (e) [CH ₂ COOHPy] [HSO ₄] ⊃ DBT in gas phase. Color code: carbon = grey; hydrogen= white; nitrogen= blue; oxygen = red; sulphur = yellow.....	133
Figure 5.3: Geometry optimized structures of (a, b, c, e) [CH ₂ COOHPy] [HSO ₄] ⊃DBTO ₂ , and (d, f) [CH ₂ COOHPy] [HSO ₄] ⊃ DBT in solvents – CCl ₄ , hexane, hexadecane. Color code: carbon = grey; hydrogen = white; nitrogen = blue; oxygen atom = red; sulphur atom = yellow.....	136
Figure 5.4: Reaction mechanism of desulfurization of DBT in fuel by using IL and H ₂ O ₂	138

Scheme 5.2: Desulfurization mechanism reaction by the acidic ionic liquid [CH ₂ COOHPy] [HSO ₄] to remove DBT.....	139
Figure A.1: FTIR spectrum of [BPy][BF ₄].....	149
Figure A.2: Calibration curve used to measure DBT removal.....	151
Figure A.3: Gas chromatogram of real diesel fuel.....	152
Figure B.1: HPLC-UV-vis-TOF calibration curve for BT.....	154
Figure B.2: HPLC-UV-vis-TOF calibration curve for DBT.....	155
Figure B.3: HPLC-UV-vis-TOF calibration curve for 4,6-DMDBT.....	155
Figure B.4: Multi-standard HPLC-UV chromatogram (at wavelength 284 nm) for the three sulfur compounds BT, DBT and 4,6-DMDBT. Peaks from left to right: BT, DBT and 4,6-DMDBT.....	156
Figure B.5: HPLC-UV chromatogram (at wavelength 284 nm) used for qualitative determination of the efficacy of BT removal.....	157
Figure B.6: HPLC-UV chromatogram (at wavelength 284 nm) used for qualitative determination of the efficacy of DBT removal.....	157
Figure B.7: HPLC-UV chromatogram (at wavelength 284 nm) used for qualitative determination of the efficacy of 4,6-DMDBT removal.....	158

List of Abbreviations and Symbols

Abbreviations			
<i>1-NMR</i>	¹ H-Nuclear magnetic resonance	<i>13-NMR</i>	¹³ C-Nuclear magnetic resonance
<i>4,6 DMDBT</i>	4,6-Dimethyldibenzothiophene	<i>[BPy] [BF₄]</i>	Butyl-Pyridinium tetrafluoroborate
<i>ODS</i>	Oxidative desulfurization	<i>[CH₂COOHPy] [HSO₄]</i>	N-carboxy-methyl pyridine hydrogen sulfate
<i>BT</i>	Benzothiophene	<i>CCl₄</i>	Carbon tetrachloride
<i>DBT</i>	Dibenzothiophene	<i>DBTO</i>	Dibenzothiophene 5-oxide (C ₁₂ H ₈ OS)
<i>DMSO</i>	Dimethyl sulfoxide	<i>DBTO₂</i>	Dibenzothiophene sulfone (C ₁₂ H ₈ O ₂ S)
<i>DFT</i>	Density Functional Theory	<i>FT-IR</i>	Fourier-transform infrared spectroscopy
<i>BPy</i>	Buty pyridine	<i>GC-TOF-MS</i>	Gas chromatography time-of-flight mass spectrometry, Agilent
<i>BF₄</i>	potassium tetrafluoroborate	<i>H₂O₂</i>	Hydrogen peroxide
<i>D₂O</i>	Deuterium oxide	<i>HDS</i>	Hydrodesulfurization
<i>EODS</i>	Extractive and Oxidative desulfurization	<i>HPLC</i>	High-performance liquid chromatography
<i>ILs</i>	Ionic Liquids	<i>PCM</i>	
<i>EDS</i>	Extractive desulfurization	<i>UV-vis</i>	Agilent Cary 6000i Ultraviolet–visible spectroscopy

ppm parts per million -
commonly used as a unit
of concentration Parts per
million

Symbols

C_0	The initial concentration of DBT in the model oil
C_x	The concentration of sulfur compound in the oil phase after the reaction began for a certain amount of time
E	known as ionization energy of compound
W_t	Weight
V/V	Volume per volume
PCM	The polarizable continuum model
$\Delta IEkJ/mol$	The first ionization energy of an element is the energy needed to remove the outermost, or highest energy, electron from a neutral atom in the phase
\supset	The combination (union) between two compounds as a complex
δ	The energy axis (delta), the units are given in part per million (ppm) Most often the signal area for organic compounds ranges from 0-12 ppm
λ	Wavelength
$\pi-\pi$	Non-covalent interaction (Hydrogen 'bond' donor) in cation-ionic liquid and S- compound

Chapter 1: Introduction

1.1 Background

With the rapid growth of the global petrochemical industry alongside the automobile industry, there is a subsequent rapid increase in air pollution resulting from diesel sulfur oxide (SO_x) emissions. These emissions combine in the air with rainwater, forming sulfurous acid, popularly known as acid rain.^{1,2} A classic example of the deadly nature of SO_x pollution is 1952 smog event in London, England. Around 5,000 people died due to the combination of foggy weather and air pollutants in high concentrations.³ Due to the adverse environmental effects that are caused by sulfur oxides in engine exhaust emissions, environmental protection agencies around the world are now mandating sulfur content specifications for different types of fuels.⁴ The desulfurization of diesel and gasoline fuels is, therefore required to meet the allowable sulfur limits. For instance, in the United States, the sulfur content in diesel has been restricted to 15 ppm since 2006, while in the European Union, sulfur-free gasoline has been mandated since 2011.¹⁻⁵ The response of refineries to these regulations was swift. Still, they experienced significant challenges in complying with the stated fuel sulfur specifications, which also included reductions in aromatics contents. These measures were followed up a few years later with further regulations announced by the EPA to reduce non-road diesel fuel sulfur to 500 ppm from 3400 ppm by 2007, and then down even more to 15 ppm by 2010 in keeping with the US Clean Air Act.²

Environmental movements are now a major driving force in government policy not only in the US but globally. As a result, the desulfurization of fuels has become a rapidly expanding

research area. The main thrust of this research field is finding ways to adhere to ever-stricter government regulations amidst oil reserve depletion that is resulting in lower petroleum quality. Because the reservoirs of “sweet” (i.e., low sulfur content) crude oil are now almost depleted, drillers are left with mostly “sour” (i.e., high sulfur content) petroleum, which requires different refining. Even so, the demand for oil worldwide continues to surge.²

Sulfur compounds (S-compounds) cause significant complications during the refining process and impact fractional distillation efficiency. To date, no fully feasible methods exist that are able to completely remove S-compounds from crude oil.⁶ Depending on the type of S-compounds to be removed, two main elimination strategies, namely hydrodesulfurization (HDS) and non-hydrodesulfurization (including adsorptive, extractive, oxidative desulfurization) have been widely used.⁷ HDS is a heterogeneous catalytic reaction process, which involves the reaction of S-compounds with H₂ at the presence of catalysts to form hydrocarbons and H₂S that can be removed by amine washing using the Claus process.²⁻⁸ HDS is operated at high temperature (300–400 °C) and pressure (20–130 atm) and consumes large amount of H₂. Although HDS is efficient in removal aliphatic S-compounds from crude oil, it is less effective in removing refractory aromatic S-compounds such as dibenzothiophene (DBT), benzothiophene (BT), and their alkyl derivatives. More cost-effective methods need to be developed for the desulfurization of aromatic S-compounds from crude oil.

Recently, removal of refractory S-compounds by extractive/oxidative processes using ionic liquids (ILs) at ambient temperature and pressure shows great potential in the production of clean fuels. ILs are molten salts with melting points below 100°C and are typically

composed of large asymmetric cations, and inorganic/organic anions.⁸ ILs feature several characteristics that make them especially attractive for desulfurization, such as their general all-around stability, non-volatility, non-toxicity, fuel oil insolubility. Over the past two decades, ILs with different combinations of cations (imidazolium, pyridinium, pyrrolidinium, and quinolinium) and anions (tetrafluoroborate, hexafluorophosphate, and trifluoromethanesulfonate) have been explored for extractive/oxidative desulfurization with satisfactory removal efficiency (ranging of 40–100%).⁹⁻¹⁰ Experimental and theoretical investigations to manifest the underlying mechanisms on effectiveness of ILs in the extraction of S-compounds have also been carried out. Most of the studies reported that the extraction efficiency of S-compounds was dependent upon size and structure of both the cation and anion, as well as the aromaticity of the S-compound being extracted.¹¹⁻¹² More recently, Zhao and co-workers correlated the sulfur partition coefficient (removal efficiency) with the Kamlet–Taft parameter π^* (an indicator of the dipolarity and polarizability of ILs) for $[\text{C}_4\text{C}_{11}\text{im}]^+$ based ILs by exploring the influence of the alkyl chain length of the cations on desulfurization rate.¹³

Although extensive studies have been carried out to extract S-compounds from crude oils, a comprehensive understanding of how the structure and properties of ILs influence the removal of aromatic S-compounds remains elusive. Desulfurization using ILs is still very costly. It remains a big challenge to synthesize ILs of high yield using the minimum synthetic steps. Moreover, further research efforts are required to develop effective methods for the regeneration of ILs without significant loss of the activity.

1.2 Research Objectives

The current research continues the trend by looking at ways to remove BT, DBT, and 4,6-dimethyldibenzothiophene (4,6-DMDBT) present in diesel fuels. Several researchers have already found that deep eutectic solvent (DESs) and ILs are highly effective in removing thiophene from model oils. However, literature on optimization of reaction steps and parameters to achieve optimum desulfurization using ILs is sparse. Moreover, very few studies focus on deducing the mechanism of desulfurization by an IL. A comprehensive study on parameter optimization and mechanism of IL-based desulfurization can help develop high-yield ILs for industrial applications. Main research objectives of this study are as follows:

1. Synthesize a Brønsted acidic ionic liquid ($[\text{CH}_2\text{COOHPy}] [\text{HSO}_4]$) and protic IL $[\text{BPy}][\text{BF}_4]$ in a cost-effective manner.
2. Optimize the extraction conditions for thiophenic compounds (BT, DBT and 4,6 DMDBT) extraction out of diesel fuel and model oils.
3. Evaluate the activity of recycled ionic liquids as a means to explore their industrial application ability to remove S-compounds in the post-regeneration phase.
4. Explain the mechanism of sulfur removal by ($[\text{CH}_2\text{COOHPy}] [\text{HSO}_4]$) and $[\text{BPy}][\text{BF}_4]$ using Density Function Theory (DFT) simulation.

1.3 Organization of the Thesis

This study focuses on investigating the use of ionic liquids for the removal of thiophene from both model fuels and diesel. To achieve this purpose, we employ carboxyl methyl

pyridinium- and butyl-pyridinium-based ionic liquids. The study intends to measure the extraction efficiency of carboxyl methyl pyridinium and butyl-pyridinium-based ionic liquids for DBT from hexane (our model fuel oil). The aim in doing this is to deeply examine the extraction thermodynamics in order to better understand extraction conditions for thiophene species. We analyze the samples extracted during the fuel oil phase using HPLC-UV-MS and UV-visible spectroscopy. In addition, we use DFT simulation to explain the mechanism. The thesis has six chapters in total. The organization of the thesis is as follows:

Chapter 1 presents the thesis problem, thesis objectives, and research scope.

Chapter 2 provides a literature review on the ordinary desulfurization methods, the synthesis, purification and properties of ILs, as well as the application of ILs to extractive/oxidative desulfurization.

Chapter 3 develops and presents a methodology for synthesizing N-butyl-pyridinium tetrafluoroborate ([BPy] [BF₄]) ionic liquid and its characterization. This study evaluates the desulfurization of DBT (an aromatic sulfur compound) from both model and real (diesel) fuels.

Chapter 4 investigates the use of acidic ILs in a variety of desulfurization experiments with different parameters. The experiments are conducted in order to find both optimal and actual extraction retention time for model and diesel fuels. The three aromatic sulfur species tested are BT, DBT, and 4,6 DMDBT. Additionally, the ILs' abilities after the removal of DBT are also validated.

Chapter 5 discusses density functional theory (DFT), which is used to explore how two ILs interact with the sulfur-containing compounds DBT and DBTO₂. The chapter also compares the results.

Chapter 6 provides conclusions for the thesis research and summarizes its contributions. In addition, recommendations are made for future research work on the physicochemical characteristics (e.g., melting point, viscosity, thermal stability, etc.) of ILs post-synthesis and recycling.

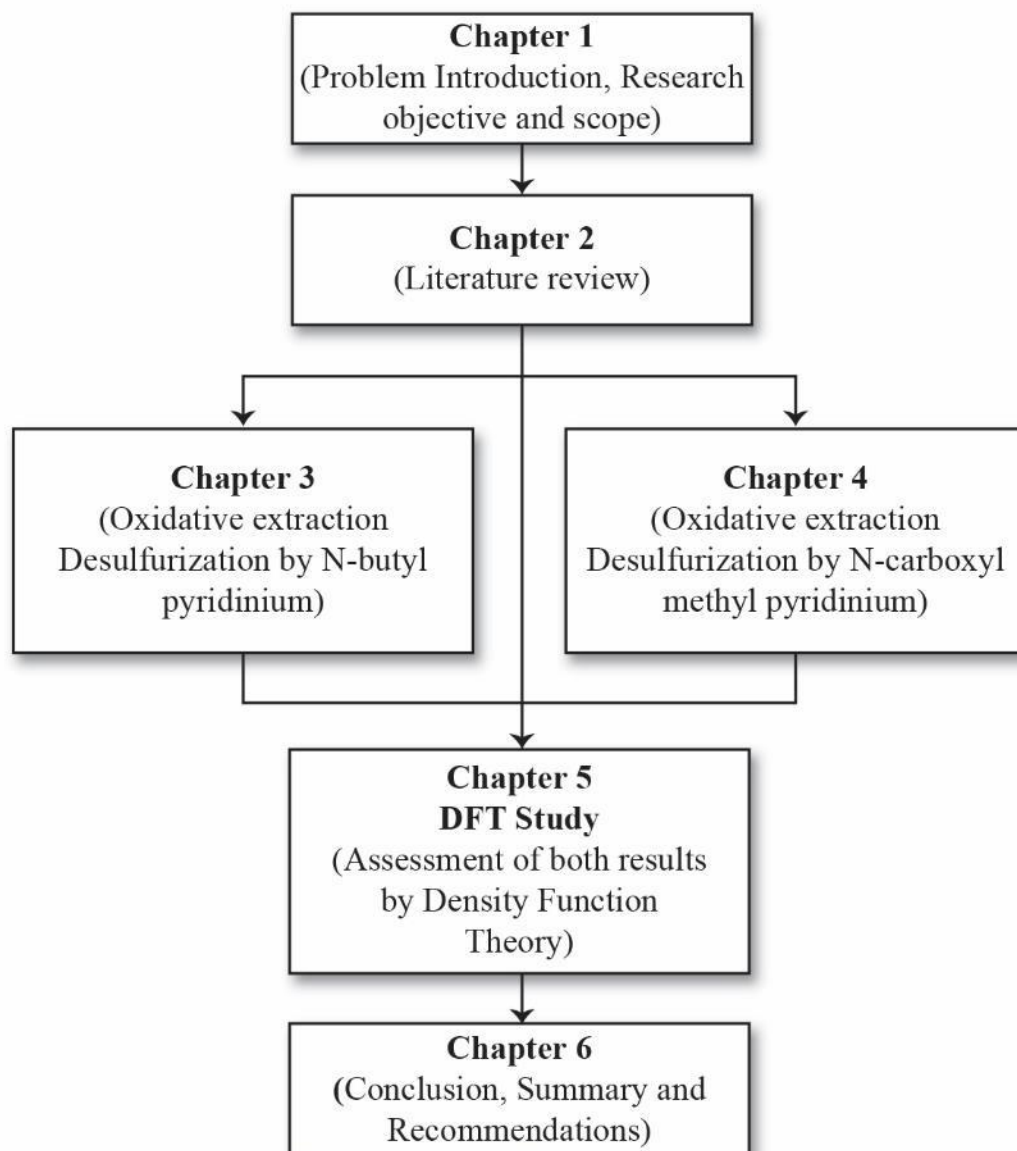


Figure 1.1: Thesis organization.

References

1. Xuemei, C., Yufeng, H., Jiguang, L., Liang, Q., Yansheng, L., Zhang, X., Xiaoming, P., Wenjia, Y. Desulfurization of diesel fuel by extraction with [BF₄]⁻-based ionic liquids, *Chinese Journal of Chemical Engineering* 16 (2008), 881–884.
2. Ibrahim, M.H., Hayyan, M., Hashim, M.A., Hayyan, A. The role of ionic liquids in desulfurization of fuels: A review, *Renewable and Sustainable Energy Reviews* 76 (2017), 1534–1549.
3. Roman, P. Biotechnological Removal of H₂S and Thiols from Sour Gas Streams Under Haloalkaline Conditions. Doctoral dissertation, Wageningen University, Wageningen, NL, 2016.
4. Lu, L., Cheng, S., Gao, J., Gao, G., He, M.Y. Deep oxidative desulfurization of fuels catalyzed by ionic liquid in the presence of H₂O₂. *Energy & Fuels* 21 (2007), 383–384.
5. Francisco, M., Arce, A., Soto, A. Ionic liquids on desulfurization of fuel oils. *Fluid Phase Equilibria* 294 (2010), 39–48.
6. Lui, M.Y.Y. Special Solvation Behaviour of Salts in Ionic Liquid. Doctoral dissertation, Imperial College London, London, UK, 2012.
7. Kulkarni, P.S., Afonso, C.A.M. Deep desulfurization of diesel fuel using ionic liquids: current status and future challenges, *Green Chemistry*, 12(2010), 1139–1149.
8. Player, L.S., Chan, B., Lui, M.Y., Masters, A.F., Maschmeyer, T. Toward an understanding of the forces behind extractive desulfurization of fuels with ionic liquids, *ACS Sustainable Chemistry & Engineering* 7(2019), 4087–4093.
9. Gholap, A.R., Venkatesan, R., Daniel, T., Lahoti, R.J., Sirinivasan, K.V. Ultrasound promoted acetylation of alcohols in room temperature ionic liquid under ambient conditions, *Green Chemistry* 5 (2003), 693–696.
10. Zhu, W., Wu, P., Yang, L., Chang, Y., Chao, Y., Li, H., Jiang, Y., Jiang, W., Xun, S. Pyridinium-based temperature-responsive magnetic ionic liquid for oxidative desulfurization of fuels, *Chemical Engineering Journal* 229 (2013), 250–256.
11. Zhang, S., Zhang, Q., Zhang, Z. C. Extractive desulfurization and denitrogenation of fuels using ionic liquids, *Industrial & Engineering Chemistry Research* 43 (2004), 614–622.
12. Elwan, H.A., Zaky, M.T., Farag, A.S., Soliman, F.S., Hassan, M.E.D. A coupled extractive-oxidative process for desulfurization of gasoline and diesel fuels using a bifunctional ionic liquid, *Journal of Molecular Liquids* 248 (2017), 549–555,
13. Zhao, H., Baker, G.A., Wagle, D.V., Ravula, S., Zhang, Q. Tuning task-specific ionic liquids for the extractive desulfurization of liquid fuel, *ACS Sustainable Chemistry & Engineering* 4 (2016), 4771–4780.

Chapter 2: Literature Review

2.1 Introduction

Desulfurization is the removal of sulfur from crude oils to prevent contamination. Desulfurization has variations, including hydrodesulfurization (HDS), extractive desulfurization (EDS), oxidative desulfurization (ODS), and biodesulfurization (BDS). Due to its importance, desulfurization has long been a hot research topic. The quality of reservoir oil is decreasing due to dwindling oil reserves, on the other hand more and more stringent environmental regulations are being introduced around refinement. At the same time, global petroleum demand is spiking. Because the more easily accessible crude oil reserves that are low in sulfur are nearly depleted, the next option is crude oil with higher sulfur content, which requires a different mode of refinement.¹

Depending on the crude oil's origin, sulfur content ranges anywhere between 0% and 8+% (w/w). Crude oil, during the refining stage, is separated into different fractions according to different boiling points. The heavier fractions contain higher concentrations of sulfur. HDS is typically used to remove sulfur. HDS uses immense amounts of energy. It also requires hydrogen, which is in short supply in the refinery, and expensive to buy from marketplace.¹

As an alternative refining option, other methods that are more environmentally friendly are starting to replace HDS or to be used in conjunction with it. The most popular of these new methods are ODS, EDS, BDS, and adsorption.² Due to the characteristic properties of ILs,

they are drawing increasing attention as the extraction solvent or catalysts in EDS and ODS processes.

In the following sections, an overall review on the S-compounds in crude oil, ordinary desulfurization methods, the synthesis and properties of ILs, as well as the application of ILs in EDS and ODS will be presented.

2.2 Sulfur Compounds in Raw Petroleum

Despite the increasing trend towards sustainable energy sources, petroleum and its derivatives remain the most popular option for the world's energy needs. However, crude oil contributes enormously to emissions of carbon dioxide as well as nitrogen (NO_x) and sulfur oxides (SO_x), increasing both the occurrence of acid rain and the greenhouse effect. To counteract the release of this pollution into the atmosphere, it is important to control emissions by removing sulfur from crude oil.^{3,4}

Sulfur makes up a large part of crude oil. As well, it occurs in diesel (aromatic organosulfur compounds) and in gasoline (alkyl S-compounds). The primary issue with S-containing compounds is their oxidation, during combustion, into SO_x. The result of this oxidation is air pollution. Therefore, in order to decrease the S-content in fuels, methods need to be developed that are “green”, and will not contribute to harmful emissions or other forms of pollution.⁴

In crude oil, organosulfur compounds can be challenging components to deal with, as they affect not only the refinery process performance, but also the transportation and storage of the fuel. As mentioned above, S-containing fuels contribute to a significant proportion of

the world's air pollution through airborne particulate emissions, thereby endangering public health. Sulfur impurities that may occur in many crude oils can release noxious sulfur oxides when combusted. Examples of impurities include BT, DBT, and thiophene (TS).^{5,6} Furthermore, sulfur content in crude oil can negatively affect prices, boosting the cost of products derived from the oil.^{5,6}

In transportation fuels (e.g., diesel and gasoline) and petroleum distillates, S-compounds are mostly comprised of a hydrocarbon mixture that is classified according to boiling range. The heavier distillates generally contain heterocyclic aromatic sulfur species, whereas the lighter distillates are made up of sulfides, disulfides, and mercaptans.^{7,8} The mid-weight distillates contain alkylated and BT derivatives⁹, while in diesel, the main contaminants are DBT and its derivatives.¹⁰ The next section presents an overview of the main organic sulfur compounds (OSCs) that exists in petroleum fractions.

Most small to mid-range vehicles use gasoline as fuel. Within the crude oil family, gasoline is classified as a light fraction. It features a boiling point range of approximately 25 °C to 225 °C¹¹ and is mostly comprised of: thiophenes (2-methyl thiophene, 3-methylthiophene, 2,4 dimethyl thiophene, BT, and 2-methylbenzothiophene).¹¹ Diesel is primarily used for fuel in buses, heavy trucks, and heavy equipment, such as that used in construction. For refinery purposes, diesel is classified as a middle distillate stream and has a boiling point range of approximately 160 °C to 380 °C¹¹. Diesel fuel (C₁₀H₂₂ – C₁₅H₃₂) contains 75% naphthalene (cycloalkanes) and aliphatic hydrocarbons paraffin (alkanes), along with a smaller proportion of aromatic hydrocarbons (alkylbenzene and olefins [styrene]).¹² Derivatives of BT and DBT make up the majority of S-bearing compounds in diesel.¹³

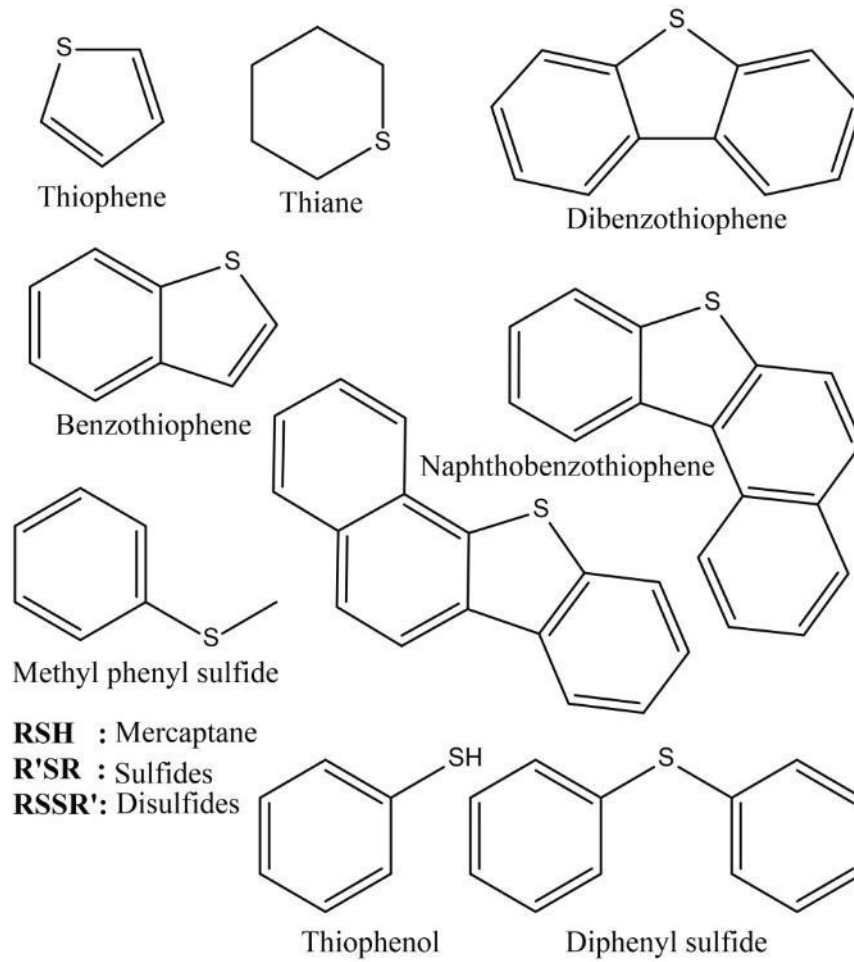


Figure 2.1: Chemical structure of crude oil S-containing compounds.¹⁴

Table 2.1: Physical Properties of Th, BT and DBT.¹⁴

Properties	Th	BT	DBT
Chemical formula	C ₄ H ₄ S	C ₈ H ₆ S	C ₁₂ H ₈ S
Molar mass (g/mol)	84.14	134.20	184.26
Appearance	Liquid (colorless)	Solid (white)	Crystalline Solid (colorless)
Density (g/mL)	1.059	1.150	1.252
Vaporization enthalpy (kJ/mol)	32.5	52.1	78.3
Formation enthalpy (kJ/mol)	82.1	100.6	120.3
Combustion enthalpy (kJ/mol)	-2807.0	-4708.2	-6571.0
Flash point (°C)	-6.7	101.5	170.0
Boiling point (°C)	84.2	221.0	332.5
Melting point (°C)	-38.3	32.0	97.0
Dipole moment (D)	0.53	0.62	0.83

2.3 Desulfurization Methods

The most popular conventional technique for desulfurization is hydrodesulfurization (HDS).¹⁵ This is, however, a very energy-intensive approach and also requires hydrogen, which is in short supply in any refinery. Alternative methods for desulfurization are therefore being researched, with the aim to develop an easier and more environmentally friendly way to produce cleaner gasoline and diesel products. The desulfurization technologies that are most promising are ODS, BDS, EDS, and adsorption.^{16,17} All of these approaches can be used either to replace or complement HDS.

2.3.1 Hydrodesulfurization

Currently, HDS is the most popular method used for desulfurizing fuels.¹⁸ Most oil refineries in developed countries have three or more HDS units for processing different types of feeds.¹⁹ Since being patented in 1950 by Paul Nahin and Raymond Fleck of Union Oil, HDS has been the predominant desulfurization technique used in most refineries.^{20,21} A trickle bed reactor is normally utilized to perform processing.²² Desulfurization includes several steps, the main one involves sulfur compounds reacting with H_2 , from which H_2S gas and hydrocarbons are formed. These are subsequently removed via amine washing (Claus process) at between 300 °C and 400 °C, with 20 to 130 atm pressure in the reactor. Note that, when using this process, heavier feeds may require higher temperatures and more extreme pressure, which may lead to an increase in olefin (alkenes) saturation. When this occurs, the octane rating of the affected gasoline is decreased. Higher temperatures can also cause enhanced coke formation, possibly resulting in catalyst deactivation.^{19,23}

In general, the design of the individual unit limits the HDS process.²⁴ For example, sterically-hindered compounds like 4,6-dimethyl dibenzothiophene have a relatively slow reaction. This is due to the catalyst surface being shielded from the S-atom by alkyl substituents across four to six positions and the planar characteristic of the BT core, which is caused by its aromaticity.¹⁹ In this case, there must first be a saturation of the sterically-hindered compound until two 6-carbon rings lose their aromatic property. When this occurs, the molecule is able to twist and the catalyst surface can then access the S-atom.¹⁹ HDS is able to remove S-compounds from sulfides, thiols, and thiophenes, but the removal

of these compounds from BT, DBT, and alkyl derivatives can be challenging, leading to their categorization as refractory sulfur compounds.

Over the past several decades, HDS has been positioned in the industry as a cost-effective desulfurization technique, but it is actually quite expensive.²⁵ It would be even more expensive to adapt HDS technology and equipment to totally remove refractory sulfur. The costs would necessitate higher capital and operating costs, increased hydrogen consumption, and a shorter catalyst lifespan.^{26,27} While current HDS technology could be adapted with less of an outlay simply by improving the reactor design or developing more efficient catalysts, alternative approaches to HDS are also being researched and developed.^{28,29}

2.3.2 Biodesulfurization

One promising desulfurization process is biodesulfurization (BDS), which removes sulfur from petroleum using biological methods. Microorganisms need sulfur both for physical activities and growth, and it occurs naturally in some proteins (e.g., disulfur bonds, methionine and cysteine), enzyme cofactors (e.g., biotin, thiamine, and Coenzyme A), and amino acids.³⁰ However, some microorganisms may be able to source sulfur elsewhere. For instance, some organisms are able to consume sulfur found in thiophene compounds (e.g., DBT), and in this way decrease the sulfur content. Using microorganisms for desulfurization has numerous advantages, such as relatively mild temperature and pressure conditions (thus saving energy) and the use of biocatalysts (enzymes), making the process highly selective.³¹

Overall, the benefits of using BDS in desulfurization are as follows: it causes lower amounts of acid rain gases^{32,33}; it leverages the specificity of the selected enzymes towards DBT and its derivatives; it has lower operating costs^{32,34,35}; and it uses relatively mild temperatures (20-30°C) and pressure (normal atmospheric pressure).^{32,34-36} Meanwhile, the main disadvantages of using BDS for desulfurization are that it requires the separation of oil/microbial biomass^{32,37,38}; it is a fairly lengthy process³⁴⁻³⁷; and deep desulfurization has not yet been attained (reduced to 10–100 ppm sulfur) with the method.²⁷

2.3.3 Adsorption

Adsorption is another desulfurization method for removing sulfur from fuel. During the process of both non-destructive and non-reactive adsorption, selective adsorption of the sulfur compound occurs via adsorbents. Adsorbents are positioned on unreactive porous substrates in such a way as to increase surface area. Alumina, aluminosilicates, activated carbon, zeolites and zinc oxide are some examples of adsorbents that have been studied for desulfurization. The findings show that adsorbents are generally quite efficient, especially when used in refractory sulfur compounds (e.g., 4,6-dimethyl dibenzothiophene).³⁷

The main advantages of using adsorption in desulfurization include the low sulfur levels it achieves and its relatively mild operating temperatures.³⁹ However, most of the adsorbents tested showed low adsorption capacity, which would necessitate multiple adsorbent beds to maintain a continuous process. This would not be cost-effective. As an alternative, lower-cost adsorbent materials that feature higher surfaces are currently being researched.³⁷

2.3.4 Oxidative Desulfurization

Another promising technique to achieve deep sulfurization in fuel oil is ODS.⁴⁰ Oxidative desulfurization has two main stages: (i) oxidation, and (ii) separation. In this process, S-compounds oxidize into sulfones through the application of an oxidant, which attacks the oil components. The sulfone compounds can then be easily removed from the oil with a solvent. This approach takes good advantage of their higher polarity.⁴¹ In ODS, S-compounds are oxidized into corresponding sulfones and sulfoxides. The oxidation process results in an increase in polarity and molecular weight, which then assists in the removal by distillation or extraction adsorption.³⁷ Furthermore, ODS reacts oxidants and fuel oil to the point where the S-compounds have oxidized, but the other is still less reactive.

Nowadays, the most commonly applied oxidants are hydroperoxides, ozone, nitrogen oxides, and peroxy salts.⁴² Earlier research also utilized nitric oxide oxidants such as NO/NO₂ gases or nitric acid^{43,44}, but it was discovered that these oxidants left too much residue (high-sulfur-containing semi-solid residue) behind during the process.⁴⁵ Moreover, as sulfur levels in diesel became increasingly limited due to environmental regulations, other approaches, such as the use of hydroperoxides (e.g., hydrogen peroxide, tert-butyl hydroperoxide) were combined either with a catalyst or in-situ produced per-acids. Research findings indicated that these were efficient at making sulfones out of organosulfur compound oxidation without the issue of residue formation.²⁷

In ODS, the extractive solvent and the oxidant comprise the main features. However, some oxidants, such as nitric oxides and nitric acid, react non-specifically with S-free hydrocarbons, which leads to a reduction in fuel quality. Further, an unsuitable extractant

(for example, acetonitrile) could cause undesirable co-extraction of S-free hydrocarbons, such as olefins (alkenes) and aromatics, and cause them to be removed together with the sulfones.^{41,46} The loss of the alkenes and aromatics would decrease the fuel quality.

Some advantages of using ODS are that it can operate using conventional equipment found in most refineries, and requires only mild operating conditions, like BDS and adsorption. Additionally, this approach can complement HDS, with ODS oxidizing via an oxidant, and HDS achieving reduction via hydrogen gas.³⁴⁻⁴⁷ Further, H_2O_2 is the most environment-friendly oxidant when it comes to the waste treatment of the produced sulfone compounds or regeneration of the extractant or adsorbent.^{16,47} It is also clear that high sulfur removal is attained with simultaneous oxidation and extraction.

Nonetheless, some improvements could still be introduced to the ODS process. The three main improvements would be:

1. A reduction in the H_2O_2/S ratio.
2. An increase in mass transfer between the oil and the polar phase.
3. Better post-treatment of the produced sulfones.

Another concern with the current ODS process involves the use of conventional solvents such as nitric acid, dimethyl sulfoxide (DMSO) and acetic acid.^{16,45} While these may be effective in many cases, the use of volatile organic compounds (VOCs), is not only bad for the environment, but also poses a fire hazard. This property can make them dangerous to work with.¹⁶ As alternatives to ODS, ILs are attracting notable research attention due to their ability to act as both catalyst and extractant and their low volatility. Section 2.5 provides more details about the use of ILs in ODS.

2.3.5 Extractive Desulfurization

Extractive desulfurization (EDS) of fuels utilizes extractant solvents for selectively removing S-compounds. Traditionally, the main solvents used as extractants are dimethylformamide (DMF), acetonitrile (AcN), pyrrolidones, and dimethyl sulfoxide (DMSO). EDS does not need either catalysts or hydrogen, and is conducted under relatively mild conditions.²⁷ As well, EDS is able to selectively remove sulfur compounds without reducing the fuel quality. In EDS, extractant selectivity is critically important due to the similarity in the polarities of aromatic S-free hydrocarbons and aromatic sulfur compounds in the fuels.²⁷ Currently in the literature, the most researched extractants are ionic liquids (ILs), as they are considered to be the most promising among emerging extractants. The application of the EDS process using ILs is discussed after section 2.4.

To date, EDS is able to achieve only low levels of sulfur removal (less than 50%), while at the same time causing many of the desired S-free hydrocarbons to be removed as well. To counteract this issue, selectivity can be increased through the oxidization of sulfur molecules prior to extraction. This process, known as ODS, increases polarity and thus simplifies and improves the extraction process.²⁷

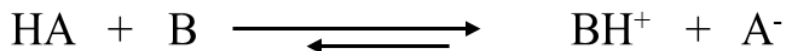
2.4 Ionic Liquids

2.4.1 Definition and Classification

Ionic liquids (ILs) are defined as salts that melt below 100°C.¹⁹ They are composed of an asymmetric organic cation and a weakly coordinating anion. The large number of possible combinations of such cations and anions gives rise to an exponentially high number of possible ILs. These ILs can broadly be divided into two categories: aprotic or protic.

Aprotic ILs are permanently charged, while protic ILs exist in a state of equilibrium between a cation and the conjugate acid of an IL anion.^{20,21} In this state, the ionized side dominates the non-ionized side, as shown in [Equation 2.1](#).

For the feasibility of many of its applications, ILs should be in a liquid state at room temperature. Variations in size and charge delocalization arising from differences in cations and anions can significantly affect the melting point of an IL. For example, ILs with a low melting point are asymmetric, large-sized, bulky ions with a high degree of charge delocalization. When the size of the ions is extensive, ion-ion interactions are low. The low strength of inter-ionic interactions prevents the ions from packing neatly in a crystal structure, affecting the IL's physical state. The presence of an inorganic anion commonly results in a liquid form IL. However, it should be noted that ILs may also contain organic anions.



BH^+ = Brønsted acid, or the conjugate acid of basic anion B
 A^- = Conjugate base of acid HA

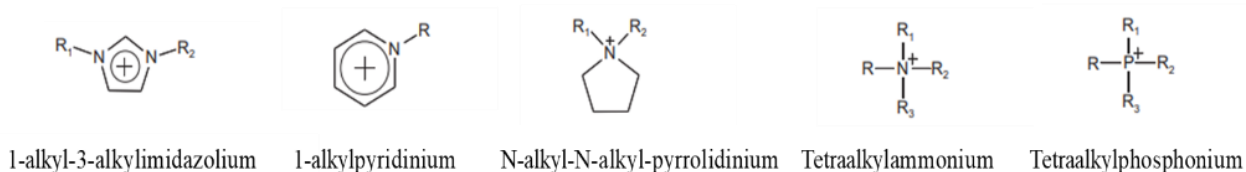
Equation 2.1: Equilibrium between neutral and ionized species in protic ILs.

ILs are characterized by the large organic ions and have been classified in many ways. For example, there can be protic or aprotic ionic liquids and complex or straightforward anions. Some of these classes are shown in [Figure 2.1](#).⁶ ILs based on the imidazolium cation are among the most widely studied. In general, ILs have been used in many fields, such as

electrochemistry, synthesis, industrial applications, energy, extraction processes, and catalysis.⁶

A typical class of ILs contains salts with the imidazolium cation (Figure 2.2). Other common IL cations include pyrrolidinium, piperidinium, and ammonium (Figure 2.2). Meanwhile, IL anions are predominantly inorganic. They range from mono-atomic and charge-localized halides such as Cl⁻ and Br⁻, to polyatomic, coordination complex, and bulky ions such as hexafluorophosphate (PF₆⁻) and bis(trifluoromethylsulfonyl)imide (TFSI or NTf₂) (Figure 2.2). As mentioned previously, the sheer number of cations and anions that can form an IL and the ease with which these ions can be altered in their structure and length leads to a wide diversity in ILs. Such diversity also facilitates the development of tailor-made ILs for specific tasks (task-specific ILs).^{4,5} ILs have attracted the attention of many chemists due to their unique properties as solvents for chemical transformations in the “task-specific” ILs, whereby the role of ILs goes beyond that of a solvent. Such ILs find application in various areas, including catalysis, synthesis, gas absorption, and analysis.⁶ Moreover, some investigations reported that the cations of ILs as hydrogen-bond donors are influential active sites for electrophiles in organic reactions.^{7, 8} Additionally, the anions of ILs also play an essential role as active sites for nucleophiles as hydrogen-bond acceptors.^{9,10} This is referred to as cooperative catalysis by ILs.¹¹⁻¹³

Examples of IL Cations



Examples of IL Anions

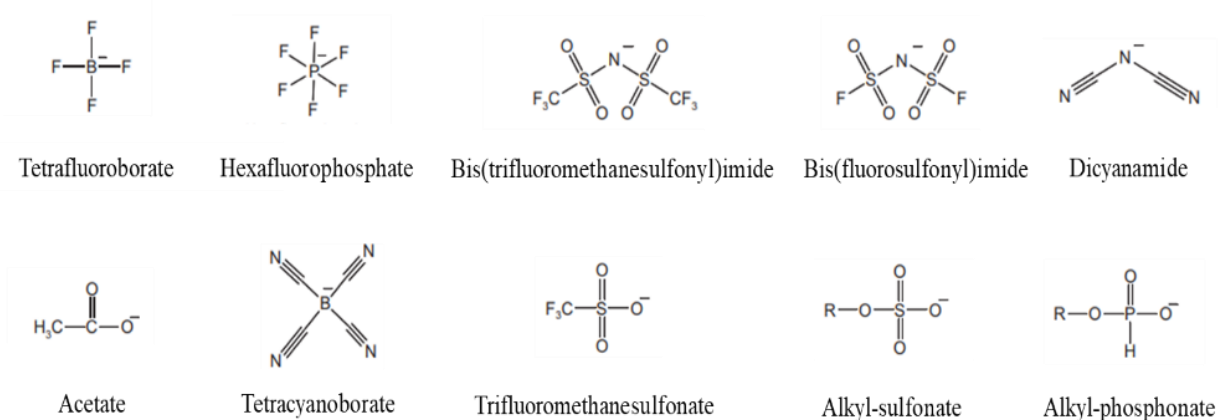


Figure 2.2: Structures of some common IL cations and anions. R, R₁, and R₂ = side groups (predominantly alkyl chains).⁴⁸

2.4.2 Synthesis and Purification of ILs

The synthesis of ILs is a critical part of the research on IL-based desulfurization. Over several years, the processes of IL synthesis have witnessed significant developments. Indeed, these developments have resulted in a transition from colored ILs containing a high proportion of impurities (like water and halides) to colorless ILs with a high purity level. Most ILs are synthesized by employing two-step introductory chemistry. The first step is typically the formation of the IL cation, and the second step involves anion exchange if required.

Two main methods form IL cations. The first approach is protonation with the help of free acid. The second method is a quaternization reaction between a Lewis base (an amine, a phosphine, or a sulfide) and a haloalkane (Scheme 2.1). Protic ILs are most commonly synthesized by mixing an acid and a base^{49,50}, but the second alkylation method with a haloalkane offers several benefits. For example, it is simple, and several different haloalkanes (including chloroalkanes, bromoalkanes, and iodoalkanes) can be used to carry out this step. Iodoalkanes are the most reactive haloalkanes, followed by bromoalkanes and chloroalkanes. Another advantage of quaternization is that it is an irreversible reaction under normal temperature conditions. It should, however, be noted that the synthesis of protic ILs is challenging at high temperatures, especially if the IL has a discernible vapor pressure due to residual acid-base equilibrium.⁵¹

Once the cation is synthesized, the anion can be incorporated in a variety of ways. For example, cation synthesis can be followed by an anion exchange reaction to ultimately lead to the formation of Lewis acidic ILs, Bronsted acidic ILs or ion exchange resin based ILs.⁵² This is called anion metathesis.⁵¹⁻⁵³ The compound containing the anion for anion exchange generally has a group 1 metal ion (Li^+ , Na^+ , K^+), an ammonium ion, or a silver ion as the cation.⁵¹ The corresponding anions that are desired in the final IL are typically CH_3COO^- , BF_4^- , SO_4^{2-} , NO_2^- , PF_6^- , NO_3^- , etc.⁵² In some cases, halide salts of IL cations are available commercially for researchers to use after conducting the necessary anion exchange reactions.⁵² Depending on the cation, the miscibility of the IL produced by that method changes. For example, metathesis involving silver cation results in water miscible ILs, whereas metathesis using group 1 or ammonium cation results in water immiscible ILs.⁵¹

However, the use of silver is not cost-effective and produces substantial quantities of silver halides as by-products.⁵¹ In fact, the presence of large quantities of by-product, and consequently, impurity of ILs, is a major concern with any anion metathesis method of IL synthesis.⁵¹ Some studies have demonstrated the synthesis of ILs, such as 1,3-disubstituted imidazolium tetrafluoroborate ILs, using a halogen-free, one-step method that utilizes methylamine. Other halogen-free IL synthesis methods include synthesis using carbenes, phosphines, sulphonates and sulphates as precursors.⁵¹ Using Lewis acids (or metal halides), such as AlCl_3 , FeCl_3 , CuCl etc., is also an important means of synthesizing ILs.⁵² When Lewis acids are used, ILs are formed via an addition reaction, wherein the halides in the Lewis acids add to the halide ion(s) already present in the IL precursor.⁵²

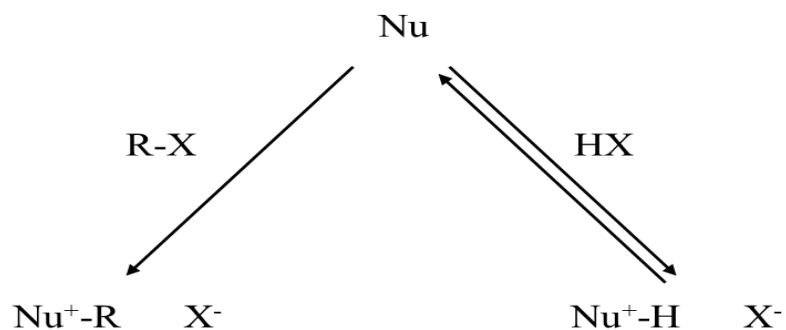
Microwave irradiation and ultrasound-assisted synthesis (using sonication) are relatively new methods of synthesizing ILs.^{52,53} Microwave irradiation method is a solvent-free synthesis technique which allows for high IL yields in shorter reaction times.^{53,54} Alkylimidazolium-based ILs have been synthesized using this method.^{52,53-55} In one study, ILs of 1-alkyl-3-methylimidazolium halides and dialkyl-3-methylimidazolium dihalides were synthesized with yields greater than 70% in under 2 min.⁵⁵

Like microwave irradiation, ultrasound-assisted methods also work in solvent-free environments and have resulted in high IL yields.⁵² In reaction systems involving two immiscible liquids, ultrasound can help accelerate product formation at the interface.⁵² One study reported higher yield, shorter reaction time, and enhanced product quality and purity when ultrasound was used to synthesize 1-butyl-3-methylimidazolium salts (with BF_4^- , PF_6^- , CF_3SO_3^- and BPh_4^- anions).⁵⁶ Another study demonstrated the ultrasound-assisted synthesis

of 1-alkyl-3-methylimidazolium halide-based ILs, reporting lower reaction time as well temperature requirements as compared to conventional thermal heating method.⁵⁷ In yet another study, ultrasound irradiation and conventional thermal heating approaches were compared in the synthesis of imidazolium-based ILs and dramatically lower reaction times and higher yields were reported.⁵⁸

Task-specific ILs can also be synthesized using specialized approaches. Task-specific ILs are ILs that primarily have their cations functionalized with a reactive group that helps achieve a specific task such as catalysis, separation of compounds, organic synthesis, etc.⁵¹ Such functionalization reactions could involve the addition of urea, thiourea, amine, thiol, sulphonate, metal complexes etc. to the cation.⁵¹⁻⁵⁹

In addition to synthesis, it is also essential to ensure that the synthesized ILs have a high purity level.⁶⁰⁻⁶¹ However, removing impurities from synthesized ILs is a highly complex and challenging. Hence, high purity reagents and precursors are generally used for IL synthesis to minimize the requirement of purification. To synthesize high purity ILs, all precursors and reagents should be distilled (wherever possible) before the reaction is started. To aid in the purification process, synthesis methods should be used so that the number of by-products released is minimal or that the released products can be easily separated from the synthesized ILs.



Nu = Nucleophile
 X = Halide ion
 R = Alkyl group

Nucleophilic substitution in IL preparation

Scheme 2.1: Synthesis of halide precursor IL through nucleophilic substitution. ⁴⁹

For conventional materials, a variety of purification techniques are available for use. ILs are, however, more complex. Since ILs have low volatility, it is not feasible to use distillation. At the same time, the low volatility of ILs allows for the removal of volatile precursors under conditions of low pressure without wasting any of the final synthesized product. ILs that have melting points higher than room temperature may be purified via recrystallization.

An essential determinant of IL purity is colorlessness. Many synthesized ILs have either a yellow, orange or brownish color due to different impurities.⁶⁰ These impurities are often not detectable even through experimental techniques such as ¹H-NMR spectroscopy and CHN elemental analysis. The most likely presence of these impurities in newly synthesized

ILs are impurities present in haloalkanes or the occurrence of unwanted and unintended side reactions (e.g., polymerization or oligomerization of free amines). To minimize contaminants in ILs, a quaternization reaction (as discussed in the previous section) is most commonly conducted. It is carried out in an inert atmosphere in a round-bottom flask or a reflux condenser to obtain a colorless IL as the product. Moreover, to further improve the purity of the halide salt formed in the reaction, a dry acetonitrile and ethyl ethanoate mixture is used to recrystallize it. If the halide salts formed are not solid, they are washed rigorously with an immiscible solvent to increase the purity of the IL. Standard washing solvents for this purpose include diethyl ether and 1,1,1-trichloroethane.³⁵

Even though colorlessness is a significant purity indicator, it is almost impossible to obtain colorless ILs in some cases. Instances of this include when anions like cyanamides, iodides, or thiocyanates are used. Moreover, while the presence or absence of color may not seem necessary for many IL applications, color can significantly affect results during photochemical or spectroscopic studies. In some cases, colorless ILs can be prepared by purifying (or using ultra-pure) reagents and precursors for obtaining high-purity ILs. In cases where colored ILs are obtained even after using highly pure precursor materials, sorbents such as silica, alumina, or activated charcoal may be used to purify and decolorize synthesized ILs.⁶⁰⁻⁶³

2.4.3 Properties of ILs

The unique characteristics of ionic liquids have sparked the academic community's interest in this research area.²⁹ ILs were initially known for their lack of vapor pressure. However, in the past few years, evaporation of ILs has been observed under high vacuum at high

temperatures (near 300 °C).^{32,37-39} Yet, many ILs do not undergo distillation below their thermal decomposition temperature under atmospheric conditions.³² This low volatility allows immense control over emissions, which is why ILs act as green alternatives for solvents in industrial-scale organic reactions. However, ILs can pollute the aquatic environment due to their decomposition in water. For instance, $[\text{BF}_4]^-$ and $[\text{PF}_6]^-$ undergo very slow hydrolysis to form the toxic and corrosive HF.³³

ILs are safer to store and handle than traditional solvents because they are generally not flammable and have good combustion stability, with no detectable flashpoints below 200 °C.³⁴ ILs are also more viscous than traditional solvents like ethanol or water.^{35,36} The stronger the cation-anion hydrogen bonds and the larger the alkyl chain on the IL cation, the higher the IL viscosity.³⁶ A low glass transition temperature (T_g) can also lead to low viscosity. Moreover, the T_g of an IL may drop with increasing ion size when ionic interactions dominate, although this may not be true for ions with long side chains as other forces (e.g., van der Waals interactions) come into play.⁶⁵

Most ILs are immiscible with non-polar organic solvents (hexane, octane) but mix well with polar ones.²⁷ Further, ILs can themselves be both solvents and catalysts for nucleophilic reactions.³⁸ Nucleophilic substitution reactions with a salt nucleophile are often carried out with a phase-transfer catalyst (PTC), which acts as a shuttle for the anion, carrying it between a polar phase with the salt reactant and a non-polar phase with the organic reactant.⁴² Since ILs also have bulky organic cations, they can act as both catalysts and solvents for reactions involving PTCs.

2.5 Desulfurization Using ILs

ILs are ideal for application as chemical reactant solvents, given their tenability and unique solvent properties. Catalytic effects are detected where molecular solvents are changed to ILs, but catalysts may also be fabricated in ILs (e.g., chloroaluminates) or could be the outcome of cation-anion interactions. Traces of IL-decomposing products may act as catalysts as well, particularly in instances where $[\text{PF}_6]$ salts are applied as solvents, such that $[\text{PF}_6]$ decomposes into $[\text{PF}_4]$ and HF when in contact with water and heated.^{66,67}

Overall, then, ILs offer promising solutions across a broad range of chemical uses, especially in cases where a lower environmental impact is important or processing costs need to be lowered. In the hydrocarbon and petroleum industries, many different solvents have been used for absorption, distillation, extraction, etc., such as alcohols, ethers and amines, but these solvents are limited in their application with regard to recyclability and environmental concerns. ILs do not have the same limitations.^{68,69}

Furthermore, because aromatic sulfide compounds polarity is similar to sulfur-free aromatic hydrocarbon polarity, finding an extractant that is able to selectively remove S-compounds while retaining a high volume of feed is a key aspect in the EDS process. Ionic liquids are emerging as potential extractants.⁷⁰ In fact, some ILs that are alkyl sulfate anion- or alkyl phosphate-based show evidence of having higher sulfur derivative extractability than that shown in molecular solvents. The desulfurization ability of ILs in aromatic S-compounds is cation-dependent.⁷¹

Even so, several important challenges remain unsolved, including the efficiency limitations of some ILs and their cross-solubility in hydrocarbons. Sulfur may, however, be used as an

oxidant to improve extraction selectivity.⁷² Research also indicates that molybdic compounds are able to be dissolved in ILs as a way to oxidize S-compounds using H₂O₂ in moderate conditions, with ILs assuming the dual role of extractant / catalyst solvent.⁷³ Nonetheless, despite their many advantages like not requiring H₂, ionic liquids still lag behind traditional extractants.⁷⁴ Table 2.3 presents a summary of results for extraction and oxidative desulfurization (EODS) with ILs. As can be seen, the solvents and/or extractants were used together with an H₂O₂ oxidant in gasoline, diesel, and model oil and show the superiority of conventional extractants.

Other recent research shows that ILs that are metal halide anion-based or Brønsted acid-based can well act as extractants or reaction media or as catalysts in either extraction or oxidative desulfurization processes.^{75,76} In these studies, additional catalysts were not required, which thus avoided the need for catalytic separation and regeneration. Table 2.2 and Table 2.3 provide a summary of research results regarding EDS process employing ILs as extractant or ILs as both extractant and catalyst in extractive-oxidative desulfurization.

Table 2.2: Summary of EDS using ILs as extractants.

Entry	Substrate	Oil	S (ppm)	IL	n(H ₂ O ₂)/ n(Oil)	T/ °C	t/ min/h	V(Oil): V(IL) (mL)	S Removal %	Ref
1	DBT	n-octane	1000	[BMIM][BF ₄]	10	70	3 h	5: 2	93.0	77
2	DBT	n-octane	1000	[BMIM][PF ₆]	10	70	3 h	5: 2	96.9	77
3	DBT	n- octane	1000	[(CH ₂) ₃ SO ₃ HM IM] [BF ₄]	4	70	3h	5: 1	99.5	78
4	4,6- DMDBT	n- octane	1000	[EMIM][DEP]	0.2	50	3h	5: 1	84.46	79
5	4,6- DMDBT	n- octane	1000	[BMIM][DBP]	0.2	50	3h	5: 1	89.2	79
6	Thiophene	n-octane	700	[HNMP]BF ₄	10	60	5h	4	99.4	80
7	Thiophene	n-octane	700	[HNMP]HSO ₄	10	60	5h	4	63.5	80
8	Thiophene	n-octane	700	[HMIM]BF ₄	10	60	5h	4	47.1	80
9	DBT	n-octane	1000	[BMIM][BF ₄]	60: 20	30	30 min	5: 1	78.0	81
10	4,6- DMDBT	n-octane	500	[BMIM][PF ₆]	5: 1	30	3h	10:1	86.0	82
11	DBT	n-octane	500	[BMIM][PF ₆]	5: 1	30	3h	10:1	96.0	82
12	DBT	gasoline	599	[BMI][N(CN) ₂]	-	25	5 min	1:1	48.5	83
13	DBT	diesel	599	[BMI][N(CN) ₂]	-	25	5 min	1:1	68.7	83
14	DBT	n- dodecane	160	([BPy][BF ₄])	-	25	15 min	5:1	45.0	84

15	DBT	n-dodecane	160	[HPy][BF ₄]	-	25	15 min	5:1	59.37	84
16	DBT	n-dodecane	160	[OPy][BF ₄]	-	25	15 min	5:1	68.75	84
17	DBT	n-octane	1550	([HNMP]BF ₄)	6	60	30 min	1:1	99	85
18	DBT	gasoline	780	[BPy]BF ₄	0.4	55	30 min	1:1	74.2	86
19	Thiophene	gasoline	780	[BPy]BF ₄	0.4	55	30 min	1:1	44.5	86
20	BT	iso-octane	1000	[HMIM]BF ₄	10	90	6h	3.2:5	51.0	87
21	DBT	iso-octane	1000	[HMIM]BF ₄	10	90	6h	3.2:5	93.0	87
22	Thiophene	iso-octane	1000	[HMIM]BF ₄	10	90	6h	3.2:5	49.0	87
23	DBT	Diesel	1000	[HMIM]BF ₄	10	90	6h	3.2:5	50.0	87
24	DBT	Diesel	0.0711%	[C ₈ Py] [BF ₄]	-	25	20 min	1:1	16.17	88
25	DBT	Diesel	0.0711%	[C ₈ MIM] [BF ₄]	-	25	20 min	1:1	29.96	88
26	DBT	N-Dodecane	1000	[BMIM]Cl	-	30	30 min	5:1	77.15	89
27	DBT	n-octane	500	[BMIM]Br	-	30	30 min	1:1	86.3	90
28	DBT	n-octane	500	[EMIM]Br	-	30	30 min	1:1	84.1	90
29	DBT	n-octane	500	[BMIM]Cl	-	30	30 min	1:1	80.8	90

30	DBT	n-octane	500	[BMIM]PF ₆	-	30	30 min	1:1	77.2	90
31	DBT	n-octane	300	[C ₄ Py] [N(CN) ₂]	-	25	15 min	1:1	70.0	91
32	DBT	n-hexane	500	[C ₄ Py] [BF ₄] ⁻	-	40	30 min	1:1	90.78	62
33	DBT	n-hexane	1000	[C ₄ Py] [BF ₄] ⁻	-	40	30 min	1:1	99.63	62
34	DBT	n-hexane	2000	[C ₄ Py] [BF ₄] ⁻	-	40	30 min	1:1	99.64	62
35	DBT	n- dodecane	500	[BMIM]BF ₄	-	30	30 min	1:1	73.02	30
36	DBT	n- decane	500	[OMIM][NO ₃]	-	25	60 min	1:1	94.9	31
37	DBT	n- decane	500	[Bmim][NO ₃]	-	25	60 min	1:1	74.1	31
38	DBT	n- decane	500	[OPy][NO ₃]	-	25	60 min	1:1	74.7	31
39	DBT	n- decane	500	[BPy][NO ₃]	-	25	60 min	1:1	68.2	31
40	DBT	Diesel	500	[EMIM][BF ₄]	-	30	2h	1:3	97.5	92

Table 2.3: Summary of OEDS using ILs as both extractants and catalysts.

Entry	Substrate	Oil	S (ppm)	IL	n(H ₂ O ₂)/ n(Oil)	T/ °C	t/ min/h	V(Oil): V(IL) (mL)	S Removal %	Ref
1	DBT	n-octane	1000	([BPy]HSO ₄)	4	60	70 min	1:1	93.3	75
2	DBT	gasoline	1000	([BPy]HSO ₄)	4	60	70 min	1:1	87.7	75

3	DBT	n-octane	1000	(C ₄ H ₉) ₄ NBr· 2C ₆ H ₁₁ NO	16	50	30 min	1:1	98.8	93
4	DBT	n-octane	2000	[HMMP][H ₂ PO ₄]	16:1	60	5h	1:1	99.8	94
5	DBT	Diesel	2000	[HNMP][H ₂ PO ₄]	16:1	60	5h	1:1	64.3	94
6	DBT	n-octane	1000	[BMIM]Cl/F eCl ₃	3:1	30	30 min	3:1	99.2	95
7	BT	n-octane	1000	[BMIM]Cl/F eCl ₃	3:1	30	30 min	3:1	75.9	95
8	4,6- DMDBT	n-octane	1000	[BMIM]Cl/F eCl ₃	3:1	30	30 min	3:1	90.3	95
9	DBT	Diesel	1000	[BMIM]Cl/F eCl ₃	20:1	30	30 min	1.5:1	71.3	95
10	DBT	n-octane	500	[BPY][FeCl ₄]	8:1	40	10 min	5:1	95.3	96
11	BT	n-octane	250	[BPY][FeCl ₄]	8:1	40	10 min	5:1	75.0	96
12	4,6- DMDBT	n-octane	250	[BPY][FeCl ₄]	8:1	40	10 min	5:1	54.8	96

13	DBT	Diesel	200	[(CH ₂) ₂ COO HMIM] [HSO ₄]	0.5:3	25	20 min	1:1	89.8	97
14	DBT	n-octane	1000	[HCPL][TFA]	6:1	30	2h	1:1	100	98
15	BT	n-octane	1000	[HCPL][TFA]	6:1	30	2h	1:1	100	98
16	DBT	n-octane	1000	[HDMF][TF A]	6:1	30	2h	1:1	99.21	98
17	BT	n-octane	1000	[HDMF][TF A]	6:1	30	2h	1:1	80.12	98
18	DBT	n-octane	1000	[HCPL][HS O ₄]	6:1	30	2h	1:1	73.34	98
19	BT	n-octane	1000	[HCPL] [HSO ₄]	6:1	30	2h	1:1	56.52	98
20	DBT	Diesel	225	[(CH ₂) ₄ SO ₃ H MIM] [HSO ₄]	40:1	70	30 min	2:1	98.0	99
21	4,6- DMDBT	tetradeca ne	500	[(CH ₂) ₂ COO HMIM] [HSO ₄]	1:10	25	1h	10:2.5	95.1	100

22	DBT	tetradecane		[(CH ₂) ₂ COO HMIM] [HSO ₄]	1:10	25	1h	10:2.5	96.7	100
23	DBT	n-octane	1000	[C ₄ MIM] HSO ₄	5	25	2h	1:2	99.6	101
24	DBT	Diesel	97	[C ₄ MIM] HSO ₄	5	25	2h	1:2	85.5	101
25	DBT	commercial Diesel	64	[C ₄ MIM] Cl/2ZnCl ₂	0.1	25	1h	-	77.5	102
26	DBT	n-octane	1000	[CH ₂ COOHP Y] [HSO ₄]	6	30	60 min	20:1.2	99.9	103
27	BT	n-octane	1000	[CH ₂ COOHP Y] [HSO ₄]	6	30	60 min	20:1.2	82.5	103
28	4,6- DMDBT	n-octane	1000	[CH ₂ COOHP Y] [HSO ₄]	6	30	60 min	20:1.2	89.1	103
29	DBT	n-octane	1000	(((CH ₂) ₂ CO OHPy) [HSO ₄])	6	30	60 min	20:1.2	75.9	103
30	DBT	n-octane	1000	[AMIM]Cl/F eCl ₃	6:1	25	20 min	1:1	90.64	104

31	DBT	n-octane	1000	[(CH ₂) ₂ COO HMIM] Cl/ZnCl ₂	8:1	60	4h	3:1	99.62	104
32	DBT	n-octane	500	[AMIM]Cl/F eCl ₃	8:1	25	20 min	3:1	96.96	104
33	DBT	gasoline	1000	[C ₆ ³ MPy]Cl/ nFeCl ₃	4:1	25	20 min	3:1	100	64
34	DBT	gasoline	1000	[C ₆ MIM] Cl/FeCl ₃	4:1	25	20 min	3:1	80.0	64
35	DBT	n-octane	500	[C ₄ ³ MPy] FeCl ₄	-	25	15 min	1:1	86.0	105
36	DBT	n-octane	500	[C ₆ ³ MPy] FeCl ₄	-	25	15 min	1:1	88.6	105
37	DBT	n-octane	500	[C ₈ ³ MPy] FeCl ₄	-	25	15 min	1:1	89.0	105
38	DBT	n-octane	279	[BMIM]Cl/Z nCl ₂	-	25	30 min	1:1	97.8	106
39	Thiophene	n-octane	1000	[C ₄ MIM] TFA	0.125	60	60 min	20:0.5	86.47	107
40	DBT	n-octane	500	[C ₄ MIM] ₃ Fe (CN) ₆	4	40	5h	5:1	97.9	108

41	DBT	n-octane	500	[C ₂ MIM] ₃ Fe (CN) ₆	4	40	5h	5:1	86.7	108
42	DBT	n-octane	500	[C ₈ MIM] ₃ Fe (CN) ₆	4	40	5h	5:1	91.1	108
43	DBT	n-octane	1000	[BMIM]HSO ₄ /FeCl ₃	-	25	1h	1:1	100	109
44	DBT	n-octane	1000	[BMIM]Br/F eCl ₃	-	25	1h	1:1	93.1	109
45	DBT	n-octane	1000	[BMIM]Cl/F eCl ₃	-	25	1h	1:1	99.8	109
46	DBT	iso- dodecane	500	[P4444] [MeSO ₄]	-	30	15 min	1: 1	69.0	110
47	BT	+ hexadeca	500	[P4444] [MeSO ₄]	-	30	15 min	1:1	62.0	110
48	Thiophene	ne+ toluene	500	[P4444] [MeSO ₄]	-	30	15 min	1:1	61.0	110
49	DBT	n-heptane	500	[TBCMP][Br]	-	25	15 min	1:0.5	69	111
50	BT	n-heptane	500	[TBCMP][Br]	-	25	15 min	1:0.5	53	111
51	4,6- DMDBT	n-heptane	500	[TBCMP][Br]	-	25	15 min	1:0.5	40	111

52	DBT	n-octane	1000	[HDBN] Cl/nZnCl ₂	6:1	40	120 min	5:1	99.9	112
53	DBT	Diesel	500	[HDBN] Cl/nZnCl ₂	6:1	60	2h	5:1	98.8	112
54	DBT	n-octane	1000	[HDBN]Cl/2 ZnCl ₂	6:1	40	120 min	5:1	72.6	112
55	DBT	n-octane	1000	[HDBN]Cl/3 ZnCl ₂	6:1	40	120 min	5:1	52.8	112
56	DBT	Diesel	150	[(CH ₂) ₄ SO ₃ HMIM] [Tos]	40:1	25	3h	2:1	94.6	113
57	DBT	n-octane	1000	[ODBU]Cl/3 ZnCl ₂	6:1	49	120 min	10:1	93.8	113

2.6 Density Functional Theory Study in Desulfurization by ILs

2.6.1 Density Functional Theory

Density functional theory (DFT) describes a computational quantum mechanics modeling strategy that is mainly applied in chemistry, physics, and materials science. The primary purpose of using DFT is to explore nuclear or electronic structures, i.e., the ground state of systems that contain countless bodies, such as molecules, atoms, or condensed phases. DFT approaches enable the recovering of correlation energy at a meager computational cost. Moreover, DFT can derive molecular properties by considering a molecule's electron density.¹¹⁴

Electron density describes molecules' core physical characteristics. As such, it differs significantly from the wavefunction in that the latter is not a physical reality but instead is a mathematical construct, as calculated using the Hartree-Fock approximation technique. Therefore, if a function may be defined as "a function of a function," a molecule's energy may thus be defined as "a function of electron density." More specifically, electron density describes a function that features three variables, namely the x , y , and z positions of the relevant electrons. Furthermore, wavefunction may grow in complexity with increasing numbers of electrons, electron density remains independent of this factor.¹¹⁴

Density functional methods can be divided into three main classifications. First, local density approximation (LDA) approaches operate on the assumption of uniform molecule density. However, this is not a very useful method, as most molecules have different densities at different areas (i.e., they are not uniform). The second classification is gradient corrected (GC) methods. These strategies actively seek to find non-uniformity in electron density. Finally, hybrid

approaches incorporate features from both LDA and GC while also adding modifications to the DFT mathematics. Hybrid techniques, such as B3LYP, are particularly popular in chemistry applications.¹¹⁵

Nowadays, most industry-related software packages for DFT calculation include Spartan, Gaussian, HyperChem, and GAMESS. These software packages provide user-friendly environment for DFT calculation, thus being widely used for both educational and research purposes. For example, the North Carolina High School Computational Chemistry Server WebMO interface uses DFT methods as standard user options. The user can also customize calculations that involve advanced DFT strategies like time-dependent DFT when determining excited states.¹¹⁴

Although DFT methods are considered complex in application, they all fall into three main classifications: Local Density Approximation, Generalized Density Approximation, and Hybrid Functionals. Local density approximation (LDA) is formulated in line with electron density properties. For molecules that have numerous gaseous electrons, the density of the molecule is typically uniform. The LDA technique works best with electronic band structures occurring in solids because these structures feature an electron energy range of being permissible or forbidden. However, LDA is less suited for applications outside this range.¹¹⁶ Strategies involving generalized gradient approximation (GGA) combine gradient correction and electron density factors. Gradients, in mathematical terms, describe a function used to determine property change rates. Thus, in GGA, gradients attempt to offset electron density non-uniformity as a form of gradient correction that is non-local.^{117,118}

In the hybrid functionals approach, DFT and Hartree-Fock approximations are combined to formulate exchange energy in addition to an electron correlation functional. To date, hybrid strategies are the most popular DFT, especially for molecular calculations, where B3LYP is

increasingly adopted. B3LYP utilizes exchange functional B along with correlation functional LYP and another three parameters, which limits the amount of HF exchange energy that may be used. Fitting molecule training sets molecules is most frequently used in general hybrid functionals. A major advantage of DFT strategies is their high computational accuracy. For example, B3LYP/6-31G(d) is used as a standard chemistry model in numerous applications. However, DFT still suffers from difficulties around choosing the best approach for a given application. The relevant published literature remains the best source for supporting suitability choices, but less sophisticated users may find that option overwhelming. As a fallback, many users choose B3LYP/6-31g(d) as a default.¹¹⁹

Kohn and Hohenberg developed a theory to exploit density when formulating system characteristics.¹¹⁶ Their approach, however, was limited in its application scope at the time.¹¹⁶ Since then, the Kohn-Hohenberg technique has been applied in systems with particle interaction, thus forming two interconnected theories. One theory features a system of N electrons in a non-degenerate ground state associated with an external potential V_{ext} , its total energy can be expressed by Equation 2.1:

$$E[\rho(r)] = F[\rho(r)] + \int \rho(r)V_{\text{ext}}(r)dr \quad (2.1)$$

where $E[\rho(r)]$ represents the total energy of the electron system; $\int \rho(r)V_{\text{ext}}(r)dr$ represents electron-nucleus interaction; and $F[\rho(r)]$ denotes the Kohn-Hohenberg function, which can be defined as a singular function in multi-electron as below:

$$F[\rho(r)] = T[\rho(r)] + V_{e-e}[\rho(r)] \quad (2.2)$$

where $T[\rho(r)]$ denotes kinetic energy of electronic system, and $V_{e-e}[\rho(r)]$ represents electron-electron interaction energy. In this instance, the Kohn-Hohenberg technique is unable to formulate analytical expressions related to quantity.

The other theory for the Kohn-Hohenberg function shows an electron density's basic state corresponding to the lowest value of total energy. In this method, the basic state turns into an electron density function, as follows:

$$E[\rho_0(r)] = \min(E[\rho(r)]) \quad (2.3)$$

where $\rho_0(r)$ denotes basic state density.

When using the Kohn-Hohenberg approach, we should find total energy as well as the charge density for the base state of external potential, but the theory, as it stands, is unable to make this calculation.

Extending earlier research, Kohn and Sham developed DFT by applying simulated equations. In this work, the authors utilized the Schrödinger formulation for calculating wave functions related to the lowest value of total energy. The reworking of Schrödinger's equation is given in [Equation 2.4](#):

$$H_{ks}\psi(r) = E_i\psi_i(r) \quad (2.4)$$

$$\text{where } H_{ks} = [-\hbar^2/2m \nabla^2 + V_{ion}(r) + V_H(r) + V_{xc}(r)] \quad (2.5)$$

and $\psi_i(r)$ is the electron wave function i ; E_i refers to energy; $V_{ion}(r)$ represents nucleation potential; $V_H(r)$ is Hartree's potential; $V_{xc}(r)$ is the crossover and interconnection potentials; \hbar is Planck's constant divided by 2π ; and m represents the mass of the particle.

Table 2.4: A summary of DFT approaches.¹¹⁶

Name of the method	Type	Acronym
Hartree-Fock Slater functional	Hartree-Fock with local density approximation exchange	HFS
Vosko, Wilks, and Nusair	Local Density Approximation (emphasis on electron correlation approximation)	VWN
Becke correlation functional; Lee, Yang, Parr electron exchange functional	Gradient-corrected LDA functional	BLYP
Becke 3-term correlation functional; Lee, Yang, Parr electron exchange functional	Hybrid DFT	B3LYP

2.6.2 Evaluation of Desulfurization Mechanism Using DFT Simulation

To better understand how an IL desulfurizes, scientists first need to know how aromatic sulfur compounds in fuel interact with ILs. Understanding this process will help them design and then synthesize appropriate task-specific ILs for high-efficiency desulfurization. In DFT, the energy in an electron system is formulated in terms of its density: $E=E(\rho)$. Further, with DFT, quantum problems may be reformulated as mono-particle problems instead of multi-particle ones simply by using the electron density function rather than the wave function. This can then be measured by applying only three variables. Using this three-variable limitation rule reduces the variable number for calculations.¹²⁰

The main reason to utilize DFT is to predict bond energies that exist between atoms, which may be done by applying quantum mechanics principles.¹²⁰ The foundational work for this strategy, as mentioned previously, was published in the creation of Fermi and Thomas.¹²¹ The researchers developed a statistical model for approximating electron distribution, i.e., density, in atoms. The model was then applied in the calculation of kinetic energy. However, Fermi and Thomas's model

did not take into account any bonding between electrons, which reduced its accuracy.¹²¹ Nearly three decades later, Kohn and Hohenberg (1964) developed an approach for exploiting density in the formulation of system properties. It is worth noting that their theory was severely limited in that it did not have broad application at the time.

Several theoretical studies published in the literature focus on mechanisms underlying non-metal-based ILs interactions, such as hydrogen bond interactions, π - π interactions, and CH- π interactions.¹²¹⁻¹²³ Newly-synthesized ILs are not yet adequately explored about their characteristics or suitability in specific applications. Therefore, molecular-level studies would be helpful to better understand the chemical reactivity, geometry, and electronic states of ILs.¹¹⁴

In DFT, electron density functionals are employed to describe chemical compounds in an electronic state. The properties of these functionals may be changed by increasing theoretical computation accuracy.¹¹⁴ The following sections provide an overview of a few recent studies that use DFT-based strategies to explain the intermolecular interactions and structure of various ILs.

In work conducted by Tankov et al.¹²³, the authors looked at the chemical reactivity, electronic structure, and geometry of pyridinium hydrogen sulfate ($[\text{H-Py}][\text{HSO}_4]$) using quantum chemical DFT formulations. They employed DFT-B3LYP techniques with 6-311+G(d,p), 6-31++G (2d,2p) basis sets, aiming to optimize this particular IL's chemical reactivity, electronic structure, and geometry, while also exploring its quantum chemical characteristics, e.g., electronegativity, chemical potential, global hardness and softness, HOMO-LUMO energy gap, and electrophilicity index. The results of Tankov et al. study showed that, concerning the negative charge, the highest was located near the hydrogen sulfate anion ($[\text{HSO}_4]^-$), and that the pyridinium cation ($[\text{H-Py}]^+$) indicates high electropositive potential. The authors also applied natural bond orbital analysis to determine whether the intramolecular transfer of charge occurred between pyridinium hydrogen

sulfate's bonding and antibonding orbitals.¹²³ Wang and Chu used DFT to investigate how pyridine ILs react to various substituent lengths when at B3LYP/6-311+G** levels.¹²⁴ Their findings showed that the ILs under study had two primary configurations – CCOOH-PyCl and CCOOHPyCl – if they contained a chloride ion and pyridine. Furthermore, both anion-cation configurations featured three combinative locations. When the anion location remained in a constant state, the hydrogen bond's span between the chloride ion and the pyridine hydrogen atom increased if there was also an increase in the bond length of the acid group attached to the pyridine ring. Moreover, there is a simultaneous increase in the binding energy between the pyridine-based cations and the chloride anion when the bond length of the attached acid group likewise increases.¹²⁴

In a related work, Lin et al. used DFT to investigate interactions occurring between the ILs N-butyl-N-methylimidazolium tetrafluoroborate ([BMIM][BF₄]), N-butyl-N-methylmorpholinium tetrafluoroborate ([Bmmorpholinium][BF₄]), N-butyl-N-methyl piperidinium tetrafluoroborate ([BMPiper][BF₄]), N-butyl-N-methylpyrrolidinium tetrafluoroborate ([BMPyrro][BF₄]), and N-butyl-pyridinium tetrafluoroborate ([BPy][BF₄]) and DBT.¹²⁵ They employed the theory of atoms in molecules, natural bond orbitals analysis, and non-covalent interaction strategies to explore topological, geometric, and electronic features in DBT-IL intermolecular interactions. The research showed that interactions occurring between the studied ILs and DBT were mostly van der Waals and hydrogen bond-based types and that the IL cations/anions and DBT shared ion- π interactions. Interactions such as $\pi^+-\pi$ were, however, only present between DBT and [BPy][BF₄] and DBT and [BMIM][BF₄]. Furthermore, the authors discovered that the interactive energy between an IL and a DBT was substantially greater in cases where the IL featured an aromatic cation. Interaction energy was highest (in descending order) between DBT and

[BPy][BF₄], DBT and [BMIM][BF₄], DBT and [BMPiper][BF₄], DBT and [BMPyrro][BF₄], and DBT and [BMmorpholinum][BF₄].¹²⁵

DFT formulations have also been used together with simulation of molecular dynamics (MD) to describe pyridinium-based ILs' structural properties. Sun et al. employed DFT in work with pyridinium-based IL 1-butyl pyridinium tetrafluoroborate ([BPy]⁺[BF₄]⁻). Their study showed that electrostatic interactions and hydrogen bonding between ions that have opposite charges could synergistically measure an ion pair's configuration stability. Further, the authors showed that the IL [BPy]⁺[BF₄]⁻ features alternating anions and cations that occur within a long-range ordered structure and that pyridine rings interact in a T-shaped orientation. Sun et al. also determined that combining MD simulations and DFT calculations increases the strength of hydrogen bonds between the pyridine ring hydrogen atoms and fluorine atoms and that this strength is greater than that in hydrogen atoms on the butyl chain or hydrogen bonds between fluorine atoms.¹²⁶ Overall, DFT can be problematic in some regards, especially in choosing the most suitable method for a given circumstance. Nonetheless, DFT remains the most-used strategy for MD simulation in academia.

2.7 Summary

Sulfur present in fuels releases pollutant sulfur oxides upon combustion, making it important to reduce sulfur content in fuels. HDS is the most common method used for desulfurization of fuel oils, but it is not the most feasible one since it requires harsh reaction conditions. BDS is a highly specific desulfurization technique, but it takes a long time and is currently unable to achieve deep desulfurization. Adsorption has a high desulfurization efficiency, but is an expensive process. Meanwhile, oxidative desulfurization processes are fast gaining popularity for their inexpensiveness, efficiency and mild operating conditions. ODS with the help of ILs is an important new research area given their ‘green’ nature and substantial sulfur extractability. Additionally, theoretical approaches such as DFT have also found use in understanding how ILs achieve desulfurization at the atomic level.

References

1. Demirbas, A., Alidrisi, H., Balubaid, M.A. API gravity, sulfur content, and desulfurization of crude oil, *Petroleum Science and Technology* 33 (2015), 93-101.
2. Speight, J.G. (1999). The desulfurization of heavy oils and residua. Boca Raton: CRC Press.
3. Al-Degs, Y.S., El-Sheikh, A.H., Al Bakain, R.Z., Newman, A.P., Al-Ghouti, M.A. Conventional and upcoming sulfur-cleaning technologies for petroleum fuel: A review, *Energy Technology*, 4 (2016), 679-699.
4. Kumar, S., Srivastava, V.C., Nanoti, S.M. Extractive desulfurization of gas oils: a perspective review for use in petroleum refineries, *Separation & Purification Reviews* 46 (2017), 319-347.
5. Hernández-Maldonado, A.J., Yang, F.H., Qi, G., Yang, R.T. Desulfurization of transportation fuels by π -complexation sorbents: Cu (I)-, Ni (II)-, and Zn (II)-zeolites, *Applied Catalysis B: Environmental* 56 (2005), 111-126.
6. Hansmeier, A.R., Meindersma, G.W., de Haan, A.B. Desulfurization and denitrogenation of gasoline and diesel fuels by means of ionic liquids, *Green Chemistry* 13 (2011), 1907-1913.
7. Harrop, T.C., Mascharak, P.K. Fe (III) and Co (III) centers with carboxamido nitrogen and modified sulfur coordination: lessons learned from nitrile hydratase, *Accounts of Chemical Research* 37 (2004), 253-260.
8. Kovacs, J.A. Synthetic analogues of cysteinylated non-heme iron and non-corrinoid cobalt enzymes, *Chemical Reviews* 104 (2004), 825-848.
9. Kobayashi, M., Nagasawa, T., Yamada, H. Enzymatic synthesis of acrylamide: a success story not yet over, *Trends in Biotechnology* 10 (1992), 402-408.
10. Fox, B.R. Investigations into the oxidative desulfurization activity in a film-shear reactor, the source of enhanced reactivity, and other potential applications. Doctoral dissertation, University of Oregon, Eugene, USA, 2011.
11. Clemons, J.L. Adsorptive Desulfurization of Liquid Transportation Fuels Via Nickel-based Adsorbents for Fuel Cell Applications. Masters thesis, The Pennsylvania State University, State College, USA, 2009.
12. Cheng, S.S. Ultra clean fuels via modified UAO process with room temperature ionic liquid (RTIL) & solid catalyst polishing. Doctoral dissertation, University of Southern California, Los Angeles, USA, 2008.
13. Song, C. An overview of new approaches to deep desulfurization for ultra-clean gasoline, diesel fuel and jet fuel, *Catalysis Today* 86 (2003), 211-263.
14. Kareem, J.H. Sulfur Extraction from Oil Using Ionic Liquids. Doctoral dissertation, University of Leicester, Leicester, UK, 2017.
15. Muhammad, Y., Lu, Y., Shen, C., Li, C. Dibenzothiophene hydrodesulfurization over Ru promoted alumina-based catalysts using in situ generated hydrogen, *Energy Conversion and Management* 52 (2011), 1364-1370.
16. Lo, W-H, Yang, H-Y, Wei, G-T. One-pot desulfurization of light oils by chemical oxidation and solvent extraction with room temperature ionic liquids, *Green Chemistry* 5 (2003), 639-642.
17. He, L., Li, H., Zhu, W., Guo, J., Jiang, X., Lu, J., Yan, Y. Deep oxidative desulfurization of fuels using peroxophosphomolybdate catalysts in ionic liquids, *Industrial & Engineering Chemistry Research* 47 (2008), 6890-6895.

18. Xiao, J., Wu, L., Wu, Y., Liu, B., Dai, L., Li, Z., Xia, Q., Xi, H. Effect of gasoline composition on oxidative desulfurization using a phosphotungstic acid/activated carbon catalyst with hydrogen peroxide, *Applied Energy* 113 (2014), 78-85.
19. Robinson, P.R., Dolbear, G.E. (2006). Hydrotreating and hydrocracking: fundamentals. In *Practical Advances in Petroleum Processing*. New York: Springer, 177-218.
20. Fleck R.N., Nahin, P.G. (1950). Catalysts for conversion of hydrocarbons. USA: Union Oil Company.
21. Robinson, P.R. (2006). Petroleum processing overview. *Practical advances in petroleum processing*. New York: Springer, 1-78.
22. Jarullah, A.T., Mujtaba, I.M., Wood, A.S. Improving fuel quality by whole crude oil hydrotreating: A kinetic model for hydrodeasphaltenization in a trickle bed reactor, *Applied Energy* 94 (2012), 182-191.
23. Jantaraksa, N., Prasassarakich, P., Reubroycharoen, P., Hinchiranan, N. Cleaner alternative liquid fuels derived from the hydrodesulfurization of waste tire pyrolysis oil, *Energy Conversion and Management* 95 (2015): 424-434.
24. Babich, I.V., Moulijn, J.A. Science and technology of novel processes for deep desulfurization of oil refinery streams: a review, *Fuel* 82 (2003), 607-631.
25. El-Gendy, N.S., Speight, J.G. (2015) Handbook of refinery desulfurization: Volume 140, Boca Raton: CRC Press.
26. Zhang, S., Zhang, Q., Zhang, Z.C. Extractive desulfurization and denitrogenation of fuels using ionic liquids, *Industrial & Engineering Chemistry Research* 43 (2004), 614-622.
27. Kulkarni, P.S., Afonso, C.A.M. Deep desulfurization of diesel fuel using ionic liquids: current status and future challenges, *Green Chemistry* 12 (2010), 1139-1149.
28. Singh, R., Kunzru, D., Sivakumar, S. Monodispersed ultrasmall NiMo metal oxide nanoclusters as hydrodesulfurization catalyst, *Applied Catalysis B: Environmental* 185 (2016), 163-173.
29. Yuan, P., Cui, C., Han, W., Bao, X. The preparation of Mo/ γ -Al₂O₃ catalysts with controllable size and morphology via adjusting the metal-support interaction and their hydrodesulfurization performance, *Applied Catalysis A: General* 524 (2016), 115-125.
30. Kertesz, M.A. Riding the sulfur cycle—metabolism of sulfonates and sulfate esters in Gram-negative bacteria, *FEMS Microbiology Reviews* 24 (2000), 135-175.
31. Soleimani, M., Bassi, A., Margaritis, A. Biodesulfurization of refractory organic sulfur compounds in fossil fuels, *Biotechnology Advances* 25 (2007), 570-596.
32. Boniek, D., Figueiredo, D., dos Santos, A.F.B., de Resende Stoianoff, M.A. Bio desulfurization: a mini review about the immediate search for the future technology, *Clean Technologies and Environmental Policy* 17 (2015), 29-37.
33. Izumi, Y., Ohshiro, T., Ogino, H., Hine, Y., Shima, M. Selective desulfurization of dibenzothiophene by *Rhodococcus erythropolis* D-1, *Applied and Environmental Microbiology* 60 (1994), 223-226.
34. Chen, T.C., Shen, Y.H., Lee, W.J., Lin, C.C., Wan, M.W. An economic analysis of the continuous ultrasound-assisted oxidative desulfurization process applied to oil recovered from waste tires, *Journal of Cleaner Production* 39 (2013), 129-136.
35. Guobin, S., Huaiying, Z., Jianmin, X., Guo, C., Wangliang, L., Huizhou, L. Bio desulfurization of hydro desulfurized diesel oil with *Pseudomonas delafieldii* R-8 from high density culture, *Biochemical Engineering Journal* 27 (2006), 305-309.

36. Caro, A., Boltes, K., Letón, P., García-Calvo, E. Dibenzothiophene bio desulfurization in resting cell conditions by aerobic bacteria, *Biochemical Engineering Journal* 35 (2007), 191-197.
37. Srivastava, V.C. An evaluation of desulfurization technologies for sulfur removal from liquid fuels, *RSC Advances* 2 (2012), 759-783.
38. Li, Y.G., Gao, H.S., Li, W.L., Xing, J.M., Liu, H.Z. In situ magnetic separation and immobilization of dibenzothiophene-desulfurization bacteria, *Bioresource Technology* 100 (2009), 5092-5096.
39. Mjalli, F.S., Ahmed, O.U., Al-Wahaibi, T., Al-Wahaibi, Y., AlNashef, I.M. Deep oxidative desulfurization of liquid fuels, *Reviews in Chemical Engineering*, 30 (2014), 337-378.
40. Campos-Martin, J.M., Capel-Sanchez, M.D.C., Perez-Presas, P., Fierro, J.L.G. Oxidative processes of desulfurization of liquid fuels, *Journal of Chemical Technology & Biotechnology* 85 (2010), 879-890.
41. Abro, R., Abdeltawab, A.A., Al-Deyab, S.S., Yu, G., Qazi, A.B., Gao, S., Chen, X. A review of extractive desulfurization of fuel oils using ionic liquids, *RSC Advances* 4 (2014), 35302-35317.
42. Pawelec, B., Navarro, R.M., Campos-Martin, J.M., Fierro, J.L. Retracted article: Towards near zero-sulfur liquid fuels: a perspective review, *Catalysis Science & Technology* 1 (2011), 23-42.
43. Williams B.H. The thermal decomposition of hydrogen peroxide in aqueous solutions, *Transactions of the Faraday Society* 24 (1928), 245-255.
44. Baxendale, J.H., Evans, M.G., Park, C.S. The mechanism and kinetics of the initiation of polymerisation by systems containing hydrogen peroxide, *Transactions of the Faraday Society* 42 (1946): 155-169.
45. Tam, P.S., Kittrell, J.R., Eldridge, J.W. Desulfurization of fuel oil by oxidation and extraction. 1. Enhancement of extraction oil yield, *Industrial & Engineering Chemistry Research* 29 (1990), 321-324.
46. Ali, M.F., Al-Malki, A., El-Ali, B., Martinie, G., Siddiqui, M.N. Deep desulphurization of gasoline and diesel fuels using non-hydrogen consuming techniques, *Fuel* 85 (2006), 1354-1363.
47. Ito, E., Van Veen, J.A.R. On novel processes for removing sulphur from refinery streams, *Catalysis Today* 116 (2006), 446-460.
48. Campos-Martin, J.M., Capel-Sanchez, M.D.C., Perez-Presas, P., Fierro, J.L.G. Oxidative processes of desulfurization of liquid fuels, *Journal of Chemical Technology & Biotechnology* 85 (2010), 879-890.
49. Green, J.B., Yu, S.K.T., Pearson, C.D., Reynolds, J.W. Analysis of sulfur compound types in asphalt, *Energy & Fuels* 7 (1993), 119-126.
50. Wilkes, J.S. A short history of ionic liquids—from molten salts to neoteric solvents, *Green Chemistry* 4 (2002), 73-80.
51. Clare, B., Sirwardana, A., MacFarlane, D.R. (2009). Synthesis, purification and characterization of ionic liquids. In *Ionic Liquids*, Berlin: Springer, 1-40.
52. Singh, S.K., Savoy, A.W. Ionic liquids synthesis and applications: An overview, *Journal of Molecular Liquids*, 297 (2020), 112038.
53. McIntosh, A.J., Griffith, J., Gräsvik, J. (2016). Methods of synthesis and purification of ionic liquids. In *Application, Purification, and Recovery of Ionic Liquids*, Amsterdam: Elsevier, 59-99.

54. Singh, V., Kaur, S., Sapehiyia, V., Singh, J., Kad, G.L. Microwave accelerated preparation of [bmim][HSO₄] ionic liquid: an acid catalyst for improved synthesis of coumarins, *Catalysis Communications* 6 (2005), 57-60.
55. Varma, R.S., Namboodiri, V.V. An expeditious solvent-free route to ionic liquids using microwaves, *Chemical Communications* 7 (2001), 643-644.
56. Lévêque, J.M., Luche, J.L., Pétrier, C., Roux, R., Bonrath, W. An improved preparation of ionic liquids by ultrasound, *Green Chemistry* 4 (2002), 357-360.
57. Namboodiri, V.V., Varma, R.S. Solvent-free sonochemical preparation of ionic liquids, *Organic Letters* 4 (2002), 3161-3163.
58. Zbancioc, G., Mangalagiu, I.I. and Moldoveanu, C., 2015. Ultrasound assisted synthesis of imidazolium salts: an efficient way to ionic liquids, *Ultrasonics Sonochemistry* 23 (2015), 376-384.
59. Giernoth, R. Task-specific ionic liquids, *Angewandte Chemie International Edition* 49 (2010), 2834-2839.
60. Welton, T. Room-temperature ionic liquids. Solvents for synthesis and catalysis, *Chemical Reviews* 99 (1999), 2071-2084.
61. Noritomi, H., Minamisawa, K., Kamiya, R., Kato, S. Thermal stability of proteins in the presence of aprotic ionic liquids, *Journal of Biomedical Science and Engineering* 4 (2011), 94.
62. Elfgen, R., Hollóczki, O., Ray, P., Groh, M.F., Ruck, M., Kirchner, B. Theoretical Investigation of the Te₄Br₂ Molecule in Ionic Liquids, *Zeitschrift für anorganische und allgemeine Chemie* 643 (2017), 41-52.
63. Kim, D.W., Song, C.E., Chi, D.Y. Significantly enhanced reactivities of the nucleophilic substitution reactions in ionic liquid, *The Journal of Organic Chemistry* 68 (2003), 4281-4285.
64. Gui, J., Liu, D., Sun, Z., Liu, D., Min, D., Song, B., Peng, X. Deep oxidative desulfurization with task-specific ionic liquids: an experimental and computational study, *Journal of Molecular Catalysis A: Chemical* 331 (2010), 64-70.
65. Silva, T.P., Paixão, S.M., Teixeira, A.V., Roseiro, J.C., Alves, L. Optimization of low sulfur carob pulp liquor as carbon source for fossil fuels bio desulfurization, *Journal of Chemical Technology & Biotechnology* 88 (2013), 919-923.
66. Asikkala, J. Applications of ionic liquids and microwave activation in selected organic reactions. Doctoral dissertation, University of Oulu, Oulu, Finland, 2008.
67. Yang, H., Jiang, B., Sun, Y., Hao, L., Huang, Z., Zhang, L. Synthesis and oxidative desulfurization of novel lactam-based Brønsted-Lewis acidic ionic liquids, *Chemical Engineering Journal* 306 (2016), 131-138.
68. Salem, A.B.S.H., Hamid, H.S. Removal of sulfur compounds from naphtha solutions using solid adsorbents, *Chemical Engineering & Technology: Industrial Chemistry-Plant Equipment-Process Engineering-Biotechnology* 20 (1997), 342-347.
69. Koch, V. R., Nanjundiah, C., Carlin, R.T. (1998). US Patent 5. 872, p. 602.
70. Eßer, J., Wasserscheid, P., Jess, A. Deep desulfurization of oil refinery streams by extraction with ionic liquids, *Green Chemistry* 6 (2004), 316-322.
71. Jiang, X., Nie, Y., Li, C., Wang, Z. Imidazolium-based alkylphosphate ionic liquids—a potential solvent for extractive desulfurization of fuel, *Fuel* 87 (2008), 79-84.
72. Zhu, W., Li, H., Jiang, X., Yan, Y., Lu, J., Xia, J. Oxidative desulfurization of fuels catalyzed by peroxotungsten and peroxomolybdenum complexes in ionic liquids, *Energy & Fuels* 21 (2007), 2514-2516.

73. Zhu, W., Li, H., Jiang, X., Yan, Y., Lu, J., He, L., Xia, J. Commercially available molybdc compound-catalyzed ultra-deep desulfurization of fuels in ionic liquids, *Green Chemistry* 10 (2008), 641-646.
74. Ito, E., Van Veen, J.A.R. On novel processes for removing sulphur from refinery streams, *Catalysis Today* 116 (2006), 446-460.
75. Lu, L., Cheng, S., Gao, J., Gao, G., He, M.Y. Deep oxidative desulfurization of fuels catalyzed by ionic liquid in the presence of H₂O₂, *Energy & Fuels* 21 (2007), 383-384.
76. Liang, W., Zhang, S., Li, H., Zhang, G. Oxidative desulfurization of simulated gasoline catalyzed by acetic acid-based ionic liquids at room temperature, *Fuel Processing Technology* 109 (2013), 27-31.
77. Zhu, W., Li, H., Jiang, X., Yan, Y., Lu, J., Xia, J. Oxidative desulfurization of fuels catalyzed by peroxotungsten and peroxomolybdenum complexes in ionic liquids, *Energy & Fuels* 21 (2007), 2514-2516.
78. Ge, J., Zhou, Y., Yang, Y., Xue, M. The deep oxidative desulfurization of fuels catalyzed by surfactant-type octamolybdate in acidic ionic liquids, *Petroleum Science and Technology* 32 (2014), 116-123.
79. Shao, B., Shi, L., Meng, X. Deep desulfurization of 4, 6-dimethyldienzothiophene by an ionic liquids extraction coupled with catalytic oxidation with a molybdc compound, *Industrial & Engineering Chemistry Research* 53 (2014), 6655-6663.
80. Zhang, B., Jiang, Z., Li, J., Zhang, Y., Lin, F., Liu, Y., Li, C. Catalytic oxidation of thiophene and its derivatives via dual activation for ultra-deep desulfurization of fuels, *Journal of Catalysis* 287 (2012), 5-12.
81. Xu, J., Zhao, S., Chen, W., Wang, M., Song, Y.F. Highly efficient extraction and oxidative desulfurization system using Na₇H₂LaW₁₀O₃₆· 32 H₂O in [bmim] BF₄ at room temperature, *Chemistry—A European Journal* 18 (2012), 4775-4781.
82. Lü, H., Ren, W., Wang, H., Wang, Y., Chen, W., Suo, Z. Deep desulfurization of diesel by ionic liquid extraction coupled with catalytic oxidation using an Anderson-type catalyst [(C₄H₉)₄N] ₄NiMo₆O₂₄H₆, *Applied Catalysis A: General* 453 (2013), 376-382.
83. Asumana, C., Yu, G., Li, X., Zhao, J., Liu, G., Chen, X. Extractive desulfurization of fuel oils with low-viscosity dicyanamide-based ionic liquids, *Green Chemistry* 12 (2010), 2030-2037.
84. Gao, H., Luo, M., Xing, J., Wu, Y., Li, Y., Li, W., Liu, Q., Liu, H. Desulfurization of fuel by extraction with pyridinium-based ionic liquids, *Industrial & Engineering Chemistry Research* 47 (2008), 8384-8388.
85. Zhao, D., Wang, J., Zhou, E. Oxidative desulfurization of diesel fuel using a Brønsted acid room temperature ionic liquid in the presence of H₂O₂, *Green Chemistry* 9 (2007), 1219-1222.
86. Zhao, D., Wang, Y., Duan, E. Oxidative desulfurization of fuel oil by pyridinium-based ionic liquids, *Molecules* 14 (2009), 4351-4357.
87. Lu, L., Cheng, S., Gao, J., Gao, G., He, M.Y. Deep oxidative desulfurization of fuels catalyzed by ionic liquid in the presence of H₂O₂, *Energy & Fuels* 21 (2007), 383-384.
88. Xuemei, C., Yufeng, H., Jiguang, L., Liang, Q., Yansheng, L., Zhang, X., Xiaoming, P., Wenjia, Y. Desulfurization of diesel fuel by extraction with [BF₄]-based ionic liquids, *Chinese Journal of Chemical Engineering* 16 (2008), 881-884.
89. Dharaskar, S.A., Wasewar, K.L., Varma, M.N., Shende, D.Z., Yoo, C.K. Ionic liquids: the novel solvent for removal of dibenzothiophene from liquid fuel, *Procedia Engineering* 51 (2013), 314-317.

90. Dharaskar, S., Wasewar, K., Varma, M., Shende, D. Ionic liquids: environmentally benign solvent for extractive deep-desulfurization of liquid fuels, *Journal of Modern Chemistry & Chemical Technology* 5 (2014), 28-34.
91. Gao, H., Zeng, S., Liu, X., Nie, Y., Zhang, X., Zhang, S. Extractive desulfurization of fuel using N-butylpyridinium-based ionic liquids, *RSC Advances* 5 (2015), 30234-30238.
92. Kazmi, B., Zahoor, A., Hashmi, S., Ghouri, Z.K. Desulfurization of the dibenzothiophene (DBT) by using imidazolium-based ionic liquids (ILs), *Materials Physics and Chemistry* 1 (2018), 1-11.
93. Zhao, D.S., Sun, Z.M., Li, F.T., Shan, H.D. Optimization of oxidative desulfurization of dibenzothiophene using acidic ionic liquid as catalytic solvent, *Journal of Fuel Chemistry and Technology* 37 (2009), 194-198.
94. Zhao, D.S., Sun, Z.M., Li, F.T., Shan, H.D. Optimization of oxidative desulfurization of dibenzothiophene using acidic ionic liquid as catalytic solvent, *Journal of Fuel Chemistry and Technology* 37 (2009), 194-198.
95. Li, H., Zhu, W., Wang, Y., Zhang, J., Lu, J., Yan, Y. Deep oxidative desulfurization of fuels in redox ionic liquids based on iron chloride, *Green Chemistry* 11 (2009), 810-815.
96. Zhu, W., Wu, P., Yang, L., Chang, Y., Chao, Y., Li, H., Jiang, Y., Jiang, W., Xun, S. Pyridinium-based temperature-responsive magnetic ionic liquid for oxidative desulfurization of fuels, *Chemical Engineering Journal* 229 (2013), 250-256.
97. Liu, D., Gui, J., Park, Y.K., Yang, S., Gao, Y., Peng, X., Sun, Z. Deep removal of sulfur from real diesel by catalytic oxidation with halogen-free ionic liquid, *Korean Journal of Chemical Engineering* 29 (2012), 49-53.
98. Jiang, B., Yang, H., Zhang, L., Zhang, R., Sun, Y., Huang, Y. Efficient oxidative desulfurization of diesel fuel using amide-based ionic liquids, *Chemical Engineering Journal* 283 (2016), 89-96.
99. Chen, X., Guan, Y., Abdeltawab, A.A., Al-Deyab, S.S., Yuan, X., Wang, C., Yu, G. Using functional acidic ionic liquids as both extractant and catalyst in oxidative desulfurization of diesel fuel: An investigation of real feedstock, *Fuel* 146 (2015), 6-12.
100. Gui, J., Liu, D., Sun, Z., Liu, D., Min, D., Song, B., Peng, X. Deep oxidative desulfurization with task-specific ionic liquids: an experimental and computational study, *Journal of Molecular Catalysis A: Chemical* 331 (2010), 64-70.
101. Gao, H., Guo, C., Xing, J., Zhao, J., Liu, H. Extraction and oxidative desulfurization of diesel fuel catalyzed by a Brønsted acidic ionic liquid at room temperature, *Green Chemistry* 12 (2010), 1220-1224.
102. Chen, X., Song, D., Asumana, C., Yu, G. Deep oxidative desulfurization of diesel fuels by Lewis acidic ionic liquids based on 1-n-butyl-3-methylimidazolium metal chloride, *Journal of Molecular Catalysis A: Chemical* 359 (2012), 8-13.
103. Zhang, C., Pan, X., Wang, F., Liu, X. Extraction-oxidation desulfurization by pyridinium-based task-specific ionic liquids, *Fuel* 102 (2012), 580-584.
104. Nie, Y., Gong, X., Gao, H., Zhang, X., Zhang, S. Simultaneous desulfurization and denitrogen of liquid fuels using two functionalized group ionic liquids, *Science China Chemistry* 57 (2014), 1766-1773.
105. Nie, Y., Dong, Y., Bai, L., Dong, H., Zhang, X. Fast oxidative desulfurization of fuel oil using dialkylpyridinium tetrachloroferrates ionic liquids, *Fuel* 103 (2013), 997-1002.

106. Chen, X., Yuan, S., Abdeltawab, A.A., Al-Deyab, S.S., Zhang, J., Yu, L., Yu, G. Extractive desulfurization and denitrogenation of fuels using functional acidic ionic liquids, *Separation and Purification Technology* 133 (2014), 187-193.
107. Fang, D., Wang, Q., Liu, Y., Xia, L., Zang, S. High-efficient oxidation–extraction desulfurization process by ionic liquid 1-butyl-3-methyl-imidazolium trifluoroacetic acid, *Energy & Fuels* 28 (2014): 6677-6682.
108. Jiang, W., Zhu, W., Chang, Y., Li, H., Chao, Y., Xiong, J., Liu, H., Yin, S. Oxidation of aromatic sulfur compounds catalyzed by organic hexacyanoferrates in ionic liquids with a low concentration of H₂O₂ as an oxidant, *Energy & Fuels* 28 (2014), 2754-2760.
109. Ahmed, O.U., Mjalli, F.S., Al-Wahaibi, T., Al-Wahaibi, Y., AlNashef, I.M. Optimum performance of extractive desulfurization of liquid fuels using phosphonium and pyrrolidinium-based ionic liquids, *Industrial & Engineering Chemistry Research* 54 (2015), 6540-6550.
110. Kianpour, E., Azizian, S., Yarie, M., Zolfigol, M.A., Bayat, M. task-specific phosphonium ionic liquid as an efficient extractant for green desulfurization of liquid fuel: An experimental and computational study, *Chemical Engineering Journal* 295 (2016), 500-508.
111. Zhang, L., Wang, J., Sun, Y., Jiang, B., Yang, H. Deep oxidative desulfurization of fuels by superbase-derived Lewis acidic ionic liquids, *Chemical Engineering Journal* 328 (2017), 445-453.
112. Gao, S., Li, J., Chen, X., Abdeltawab, A.A., Yakout, S.M., Yu, G. A combination desulfurization method for diesel fuel: Oxidation by ionic liquid with extraction by solvent, *Fuel* 224 (2018), 545-551.
113. Wang, J., Zhang, L., Sun, Y., Jiang, B., Chen, Y., Gao, X., Yang, H. Deep catalytic oxidative desulfurization of fuels by novel Lewis acidic ionic liquids, *Fuel Processing Technology* 177 (2018), 81-88.
114. Yang, W. Direct calculation of electron density in density-functional theory, *Physical Review Letters* 66 (1991), 1438-1441.
115. Baker, E.B. The application of the Fermi-Thomas statistical model to the calculation of potential distribution in positive ions, *Physical Review* 36 (1930), 630-647.
116. Hohenberg, P., Kohn, W. Inhomogenous electron gas. *Physical Review* 136 (1964), B864-B871.
117. Jaramillo, J., Scuseria, G.E., Ernzerhof, M. Local hybrid functionals, *The Journal of Chemical Physics* 118 (2003), 1068-1073.
118. Jackson, K., Pederson, M.R. Accurate forces in a local-orbital approach to the local-density approximation, *Physical Review B* 42 (1990), 3276-3281.
119. Engel, E., Dreizler, R.M. (2013). Density functional theory. Berlin: Springer.
120. Imamura, Y., Otsuka, T., Nakai, H. Description of core excitations by time-dependent density functional theory with local density approximation, generalized gradient approximation, meta - generalized gradient approximation, and hybrid functionals, *Journal of Computational Chemistry* 28 (2007), 2067-22074.
121. Hunter, C.A., Sanders, J.K. The nature of π - π interactions, *Journal of American Chemical Society* 112 (1990), 5525–5534.
122. Lehn, J.-M. (1995). *Supramolecular Chemistry*, 1st ed., Weinheim: VCH.
123. Tankov, I., Yankova, R., Genieva, S., Mitkova, M., Stratiev, D. Density functional theory study on the ionic liquid pyridinium hydrogen sulfate, *Journal of Molecular Structure* 1139

- (2017), 400-406.
124. Wang, L.M., Chu, D.Q. Study on Structure Properties of Pyridine Ionic Liquids of Different Acid-Based Chain Lengths, *Advanced Materials Research* 298 (2011), 51-55.
 125. Lin, J., Lü, R., Wu, C., Xiao, Y., Liang, F., Famakinwa, T. A density functional theory study on the interactions between dibenzothiophene and tetrafluoroborate-based ionic liquids, *Journal of Molecular Modeling* 23 (2017), 145-152.
 126. Sun, H., Qiao, B., Zhang, D., Liu, C. Structure of 1-butylpyridinium tetrafluoroborate ionic liquid: quantum chemistry and molecular dynamic simulation studies, *The Journal of Physical Chemistry A* 114 (2010), 3990-3996.

Chapter 3: Oxidative Desulfurization by the Pyridinium-Based Ionic Liquid *N*-Butyl-Pyridinium Tetrafluoroborate

The following chapter has been published in a peer-reviewed journal:

Mohumed, H., Rahman, S., Imtiaz, S.A., Zhang, Y. Oxidative-extractive desulfurization of model fuels using a pyridinium ionic liquid. *ACS Omega* 5, no. 14 (2020), 8023-8031.

3.1 Introduction

Production of ultra-low-sulfur (ULSD) or sulfur-free diesel fuel has become a major task of refineries all over the world.¹ As such, deep-desulfurization and ultra-deep desulfurization have become growing research areas and have attracted increasing attention. Hydrodesulfurization (HDS), a catalytic chemical process requiring the use of hydrogen to remove sulfur-containing compounds from petroleum products, has the drawback of low efficiency in removing refractory sulfur-containing compounds such as benzothiophene (BT), dibenzothiophene (DBT), and their alkyl derivatives. Alternative desulfurization processes, namely oxidative desulfurization (ODS), extractive desulfurization (EDS), and bio-desulfurization (BDS) have recently been developed for deep desulfurization.²⁻³ One environment-friendly or ‘green’ approach to removing refractory sulfur-containing compounds that is quickly gaining popularity is the use of ionic liquids (ILs) for EDS.

ILs are low-melting salts typically with melting points below 100°C. The cations of most ILs are organic moieties such as imidazolium, *n*-alkyl-pyridinium, tetra-alkylammonium and tetra-

alkylphosphonium ions; whereas their anionic counterparts can be organic or inorganic entities, such as halides, nitrate, acetate, hexafluorophosphate ($[\text{PF}_6]$), and tetrafluoroborate ($[\text{BF}_4]$)⁴ ILs have low volatility, good thermal stability, controllable physicochemical properties and long-term stability. Due to these unique properties, ILs have attracted great attention and are increasingly being used as ‘green’ solvents for bioseparation, fuel desulfurization and chemical synthesis.⁵

Imidazolium or pyridinium-based ILs are most commonly employed for desulfurization of fuels by EDS and oxidative-extractive desulfurization (OEDS). For example, Alonso et al. used 1-octyl-3-methylimidazolium tetrafluoroborate ($[\text{Omim}][\text{BF}_4]$) as an extractant on model fuel containing different hydrocarbons and achieved DBT and thiophene removal efficiencies of 87 % and 79 %, respectively.⁶ Similarly, Chen et al. used a Lewis acidic IL, namely, 1-butyl-3-methylimidazolium chloride/ ZnCl_2 ($[\text{Bmim}][\text{Cl}]/\text{ZnCl}_2$), to extract DBT and thiophene from mixtures of hexane and octane.⁷ They achieved DBT and thiophene removal efficiencies of 95.9 % and 93.8 %, respectively at room temperature with 1:1 (w/w) ratio of IL to oil in 30 minutes.⁸ In another study, Zhu et al. prepared the temperature-responsive magnetic IL *N*-butyl-pyridinium tetrachloroferrate ($[\text{BPy}][\text{FeCl}_4]$) for the desulfurization of DBT and BT from a model oil. They observed DBT and BT removal efficiencies of 95.3 % and 75.0 %, respectively in 10 minutes of reaction time.⁹

Some of the most critical factors that determine the performance of ILs in desulfurization are their size and structure. Holbrey and co-workers used ILs with different types of cations and anions to investigate the removal of DBT from dodecane via extraction.¹⁰ An evaluation of the partition ratios of DBT with ILs revealed obvious differences between the desulfurization ability of ILs with different cation types, with the partition ratios following the sequence: dimethylpyridinium > methylpyridinium > pyridinium \approx imidazolium \approx pyrrolidinium. In another similar study, Gao et al. observed that ILs with different pyridinium cations followed the following sequence for their

efficiency of removal of aromatic sulfur-containing compounds from diesel: [OPy][BF₄] > [HPy][BF₄] > [BPy][BF₄].¹¹

In yet another study, Wlazło and co-workers investigated the extraction of thiophene and BT by ILs with 1-alkyl-cyanopyridinium bis{(trifluoromethyl) sulfonyl} imide as the cationic part.¹² This study revealed that the solubility of aromatic sulfur-containing compounds in ILs increases as the alkyl chain length of the IL cation increases.¹² This is because the induced polarity of the aromatic ring's π -electron cloud increases as the alkyl chain length becomes longer, leading to a stronger π - π interaction between aromatic sulfur-containing compounds and the imidazolium or pyridinium ring of ILs.¹² A similar result was obtained when Wang et al. utilized six *n*-alkylpyridinium-based ILs for desulfurization of gasoline. Their results indicated that *N*-butyl-pyridinium tetrafluoroborate ([BPy][BF₄]) has the highest sulfur removal efficiency under ambient conditions.⁹

A big challenge for EDS using ILs is the co-extraction of aromatic hydrocarbons. To overcome this challenge, oxidants are used along with ILs to increase the extraction selectivity of sulfur-containing compounds. Interestingly, in OEDS, ILs can act as extractants, catalysts or both. Lo. et al. and Pârvulescu and Hardacre explored the use of ILs for catalysis.^{13,14} Meanwhile, Li et al. discussed the benefits of using ILs for 'green' catalytic approaches.¹⁵ Several other studies also looked at possible improvements to desulfurization methods.^{16,17,20} These studies showed that the amount of the aromatic sulfur-containing compounds removed by simultaneous oxidation and extraction increased by approximately one order of magnitude compared to when only IL-based extraction was performed (from 10-40 % without oxidation to 90 % with oxidation). This is because ILs not only serve as extractants of sulfur-containing compounds but also provide suitable oxidation conditions for these compounds to transform into sulfones and sulfur oxides.

One of the most widely used oxidants for OEDS is hydrogen peroxide (H_2O_2) owing to its high oxygen content as well as, more recently, its ‘green’ appeal. However, studies have shown that desulfurization reactions may require excess H_2O_2 most likely due to one of two reasons: 1) excess H_2O_2 allows the oxidation-cum-desulfurization reaction to reach an equilibrium, resulting in improved process efficiency, or 2) some catalysts lead to decomposition of H_2O_2 , leading to only a small fraction of the oxidant being utilized in the desulfurization reaction.¹⁸⁻²⁰ Therefore, it is necessary to optimize the operating conditions of the OEDS process to reduce the consumption of H_2O_2 as much as possible.

Generally, employing ILs for ODS can be beneficial on several different fronts, the main ones of which are optimal energy-efficiency and ultra-low sulfur levels in the end product. Another key advantage is the simplification of the overall process, which is accomplished by combining the stages of reaction and extraction into a single stage. Despite the many benefits of extraction desulfurization, some issues still remain unaddressed. There is a lack of studies that address the issues which make ILs impractical for large-scale implementation. The three main issues include: (1) high viscosity of ILs, particularly amphiphilic (surfactant-inspired) ILs that are used to enable phase-transfer catalysis; (2) high costs due to expensive anions and cations; and (3) low efficiency in sulfur removal from real liquid fuels (10-30 %)²¹. These issues could potentially be resolved with further research and testing.^{22,23}

In the present study, $[\text{BPy}][\text{BF}_4]$ was synthesized to investigate the oxidative desulfurization of DBT, an aromatic sulfur-containing component comprising about 80% of the total sulfur content in diesel fuels. The focus of this investigation is to examine different ways to optimize EDS and OEDS of DBT from a model fuel with $[\text{BPy}][\text{BF}_4]$. To accomplish our research objective, a facile two-step synthetic process was employed to prepare $[\text{BPy}][\text{BF}_4]$, followed by an examination of

its structure by nuclear magnetic resonance (NMR) spectroscopy and Fourier-transform infrared spectroscopy (FTIR). By studying the effects of different operating parameters, such as extraction time, temperature, the volume ratio of IL to model fuel as well as the volume ratio of oxidant to model fuel, the optimal extraction conditions for [BPy][BF₄] were determined. In order to reduce the operating cost, recovery of the IL from desulfurized fuel was also investigated.

3.2 Experimental Methods

3.2.1 Chemicals and Reagents

All chemicals were obtained from commercial sources and were used without further purification. Analytical grade pyridine, acetone, 1-bromobutane, cyclohexane, ethyl acetate, potassium tetrafluoroborate, hydrogen peroxide (H₂O₂) and hexane were obtained from Fisher Scientific (Waltham, MA). Standard diesel oil was obtained from a local gas station.

3.2.2 Synthesis of *N*-butyl-pyridinium tetrafluoroborate ([BPy][BF₄])

The IL [BPy][BF₄] was synthesized as per previously reported two-step procedures.^{24,25} Briefly, in the first step, *N*-butyl-pyridinium bromide was synthesized using the following procedure (Figure 3.1). A solution of pyridine (40.27 mL, 0.50 mol) and 1-bromobutane (53.94 mL, 0.50 mol) was added into a solution of cyclohexane (50 mL) in a 250 mL round-bottom flask connected to a water-cooled reflux condenser fitted with an anhydrous calcium chloride drying tube. The reaction mixture was stirred by a magnetic stirrer at 64°C for 24 h until no more precipitate was formed. The white precipitate was filtered off, and the unreacted pyridine was subsequently removed from the resulting solid by washing with ethyl acetate (3×50 mL) solvent. The resulting solid was evaporated in a vacuum drying oven to remove the remaining ethyl acetate and yield *N*-butyl-pyridinium bromide (73.1 g, 67.7 %) as a colourless solid. In the second step (Figure 3.2), the

freshly synthesized *N*-butyl-pyridine bromide (64.8 g, 0.30 mol) was mixed with potassium tetrafluoroborate (44 g, 0.30 mol). The solid mixture was dissolved in 300 mL of acetone in a 500 mL conical flask and the reaction mixture was stirred using a magnetic stirrer at room temperature for 24 h. The solution was then placed in a refrigerator for 24 h until potassium bromide (KBr) was precipitated from the solution. The resulting precipitate was then filtered off, and the solvent was removed by rotary evaporation to yield [BPy][BF₄] IL (12.4 g) as a yellowish liquid. The IL was stored in a refrigerator until further use. The corresponding chemical reactions involved in the synthesis of [BPy][BF₄] are described in [Scheme 3.1](#).

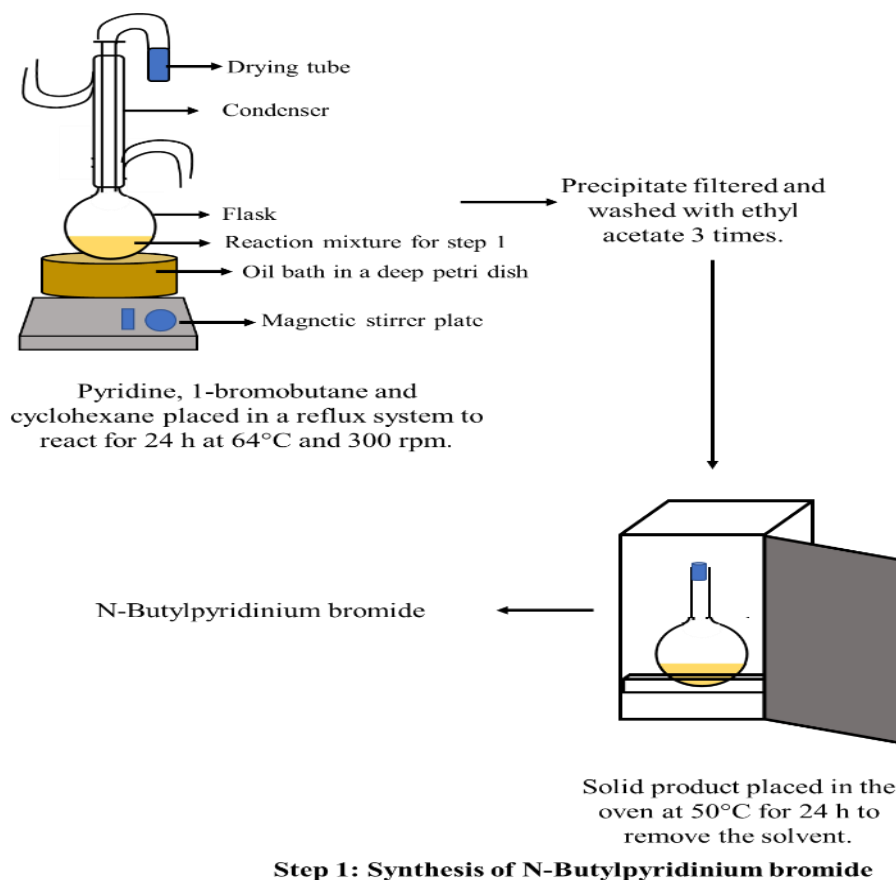
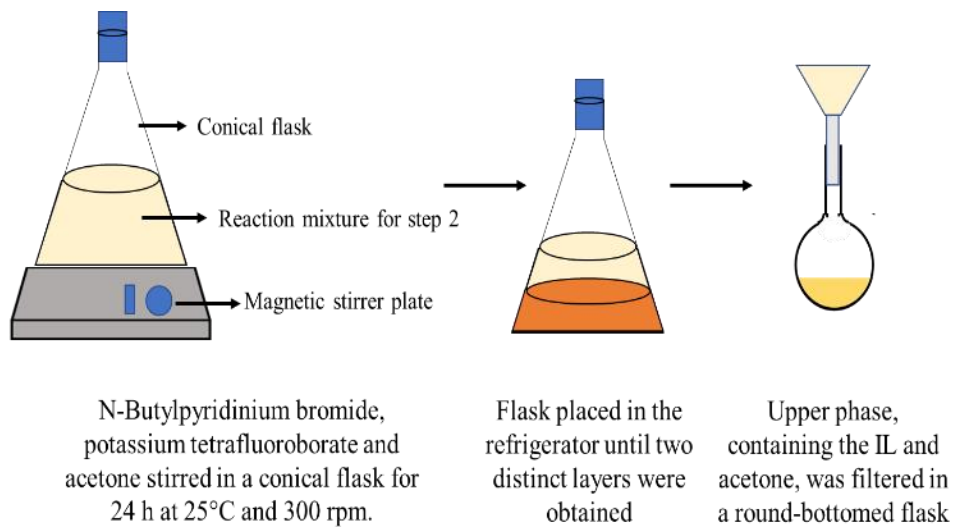


Figure 3.1: Synthesis of the IL N-Butylpyridinium tetrafluoroborate: Step 1 – Synthesis of N-Butylpyridinium bromide.



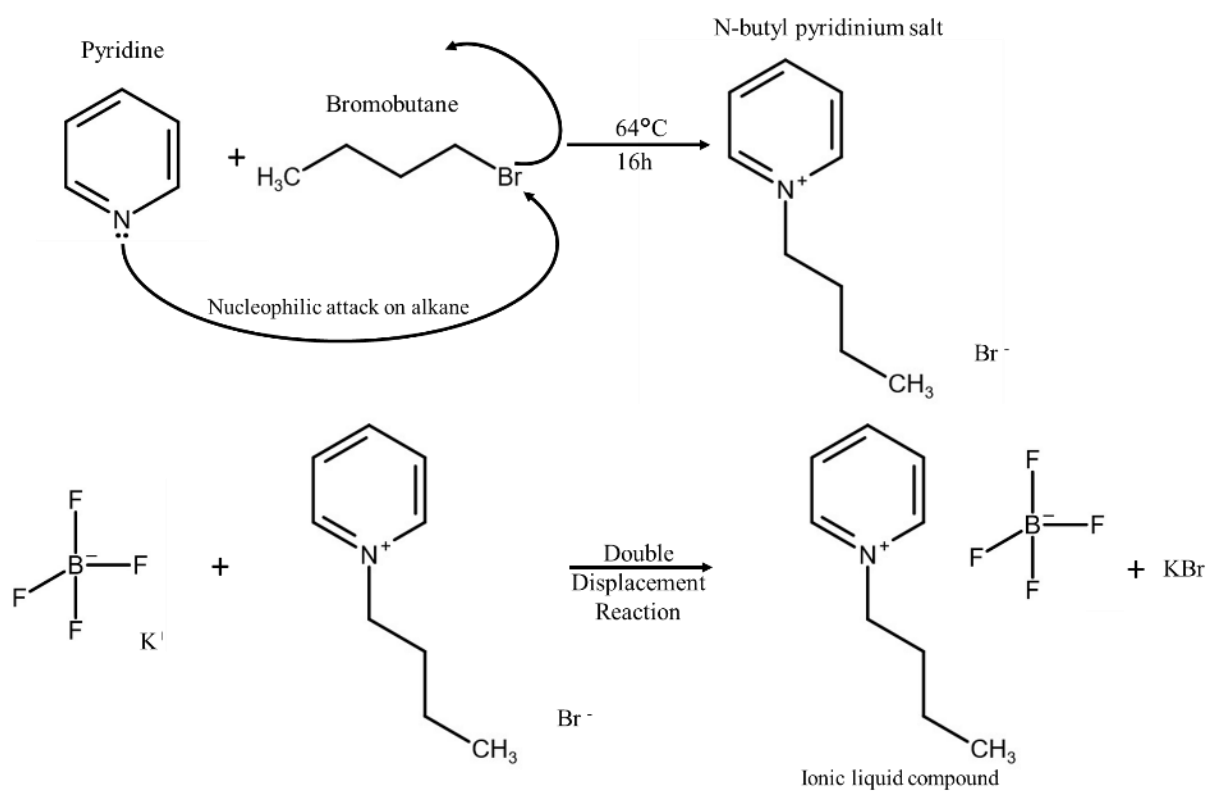
IL N-Butylpyridinium tetrafluoroborate



Acetone removed by rotary evaporation

Step 2: Synthesis of N-Butylpyridinium tetrafluoroborate

Figure 3.2: Synthesis of the IL N-Butylpyridinium tetrafluoroborate: Step 2 – Synthesis of N-Butylpyridinium from N-Butylpyridinium bromide.



Scheme 3.1: Synthetic route for [BPy][BF₄].

3.2.3 Desulfurization of Model Fuels by IL

3.2.3.1 Model Fuel Preparation

A model fuel was employed as a surrogate for real diesel fuel with an initial DBT concentration of 1000 ppm in *n*-hexane. This concentration was chosen as it is widely used in desulfurization literature.¹⁶

3.2.3.2 Extractive Desulfurization Experiments

Desulfurization experiments were conducted in 50 mL glass conical flasks. The volume ratios of the IL to the model fuel that were used for these experiments were 1:1, 1:2, 1:3 and 1:4. Different amounts of ionic liquid were added to the model fuel and the mixtures were magnetically stirred vigorously at 30 °C with various extraction times. The two layers were separated after completion of the reaction and settling of the reaction mixture. The sulfur content of the upper phase (model fuel phase) was analyzed by UV-visible spectrophotometry at λ_{max} 284 nm. UV-visible spectrophotometry was chosen over other commonly used methods for various reasons. It was preferred over High-Performance Liquid Chromatography (HPLC) because of concerns that the volatile model fuel solvent (hexane in this case) could evaporate during the HPLC runtime, potentially leading to experimental errors. UV-visible spectrophotometry, on the other hand, has the ability to handle highly volatile solvents. This technique was preferred over Inductively Coupled Plasma (ICP) – Mass Spectrometry (MS) and ICP – Optical Emission Spectrometry (OES) because it is faster, cheaper and easier to perform while yielding results that are comparable to other techniques.²⁶ Moreover, the present study only needed a single element analysis whereas ICP-MS and ICP-OES are more relevant for multielement analyses.

Finally, in the present study, the extraction desulfurization efficiency was calculated in terms of the net sulfur removal based on the initial and final sulfur content in the model fuel via the following equation:

$$\eta = \frac{[\text{DBT}]_{ini} - [\text{DBT}]_{final}}{[\text{DBT}]_{ini}} \times 100\%$$

3.2.3.3 Oxidative-Extractive Desulfurization Experiments

For the OEDS experiments, a solution of the model fuel (10.0 mL) was mixed with the IL (10.0 mL), after which a solution of H₂O₂ was added to the liquid mixture. The resulting mixtures with different volume ratios among IL, model fuel and the oxidizing agent (H₂O₂) (volume ratios of IL to model fuel use were 1:1, 1:2, 1:3 and 1:4, while volume ratios of oxidant to model fuel used were 0 %, 1 %, 10 % and 40 % v/v) were stirred under various temperatures (20°C, 30°C and 40°C) and extraction time periods (10 min, 25 min, 35 min, 45 min, 60 min, 80 min, 100 min and 120 min). The aqueous phase (IL phase) and model fuel phase were separated by using a separatory funnel. Thereafter, samples were collected from both the phases for analysis to determine the oxidation extraction desulfurization efficiency.

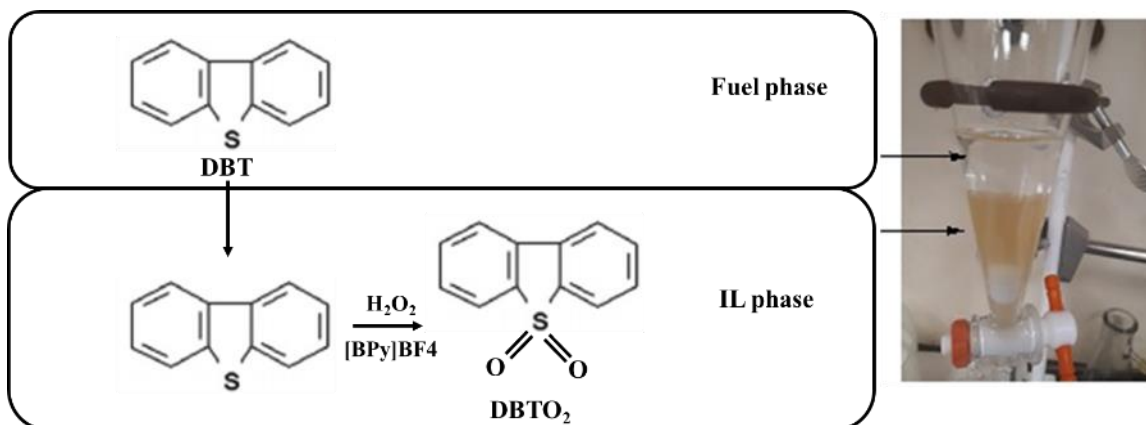


Figure 3.3: Oxidative-extractive desulfurization of sulfur compounds by using the IL.

3.2.4 Recycling of the IL

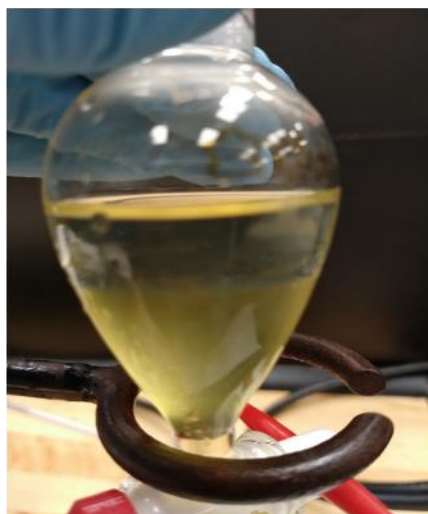
Regeneration of the sulfur-loaded IL was conducted by distillation in an oil bath at 110°C to remove H_2O_2 , followed by re-extraction using tetrachloromethane (CCl_4) at 30°C for 30 minutes by using an incubator shaker (New Brunswick Scientific, Innova 43) with the volume ratio of IL to CCl_4 being 1:1. The mixture was left to stand for 10 minutes for the phases to separate. The lower layer thus obtained was a mixture of CCl_4 and DBT and the upper layer was the regenerated IL. The two layers were separated by using a separating funnel (Figure 3.4). Subsequently, the regenerated IL was analyzed by $^1\text{H-NMR}$, $^{13}\text{C-NMR}$, and FTIR spectroscopy for its purity.



Distillation of used, sulfur-loaded IL in an oil bath at 110°C to remove H_2O_2



Re-extraction using CCl_4 at 30°C for 30 minutes in an incubator shaker



Using the separatory funnel to separate the two phases obtained after phase separation

Figure 3.4: Recycling of the IL.

3.2.5 Desulfurization of Aromatic Compounds from Diesel Fuel by IL

Real diesel fuel, containing 1000 ppm DBT, was treated with [BPy][BF₄] to test the extraction ability of the IL in real hydrocarbon feedstock. The extractions were conducted for 10, 20, 30, 35, 40, and 45 min at 40°C with a fixed volume ratio (1:1) of IL to diesel fuel.

3.3 Analytical Methods

3.3.1 Proton Nuclear Magnetic Resonance (Hydrogen-1 NMR or ¹H-NMR) and Carbon-13 NMR (¹³C-NMR)

The synthesized IL product ([BPy][BF₄]) was characterized by NMR and IR spectroscopic analyses. The ¹H-NMR and ¹³C-NMR NMR spectra of [BPy][BF₄] were recorded on Bruker Advance 300 MHz spectrometer. Dimethyl sulfoxide (DMSO) was used as the solvent.

3.3.2 Ultraviolet-Visible-Infrared (UV-Vis-IR) Spectrophotometric Analysis

For UV-Vis-IR spectrophotometric analysis, samples of DBT in model oil were measured by Agilent Cary 6000i UV-Vis-IR Spectrophotometer at the wavelength of λ_{\max} 284 nm to determine DBT concentration. Standard solutions with DBT concentrations of 100 ppm, 50 ppm, 30 ppm, 20 ppm, 15 ppm, 10 ppm, 7 ppm, 5 ppm, and 1 ppm in *n*-hexane were used to generate the calibration curve.

3.4 Results and Discussion

3.4.1 ¹H-NMR, ¹³C-NMR and FTIR Characterization of [BPy][BF₄]

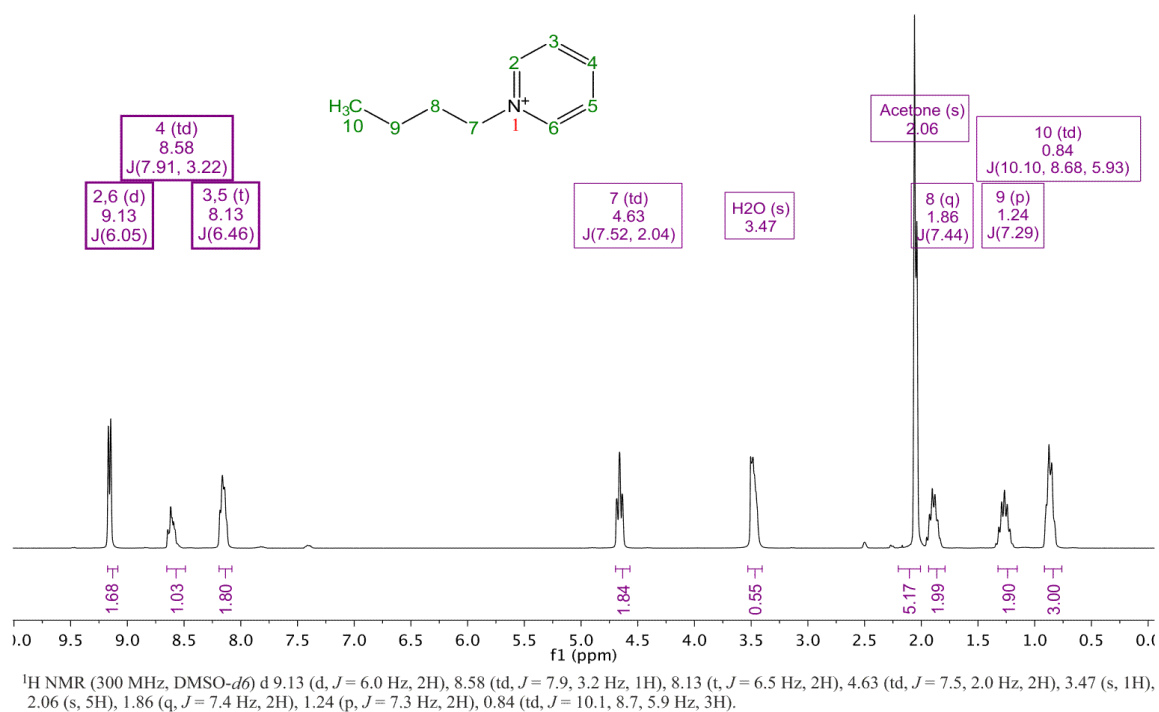
The ¹H-NMR and ¹³C-NMR spectra of the synthesized IL [BPy][BF₄] are shown in [Figure 3.5](#).

The δ values of ¹H-NMR and ¹³C-NMR of the synthesized IL [BPy][BF₄] in the present study are

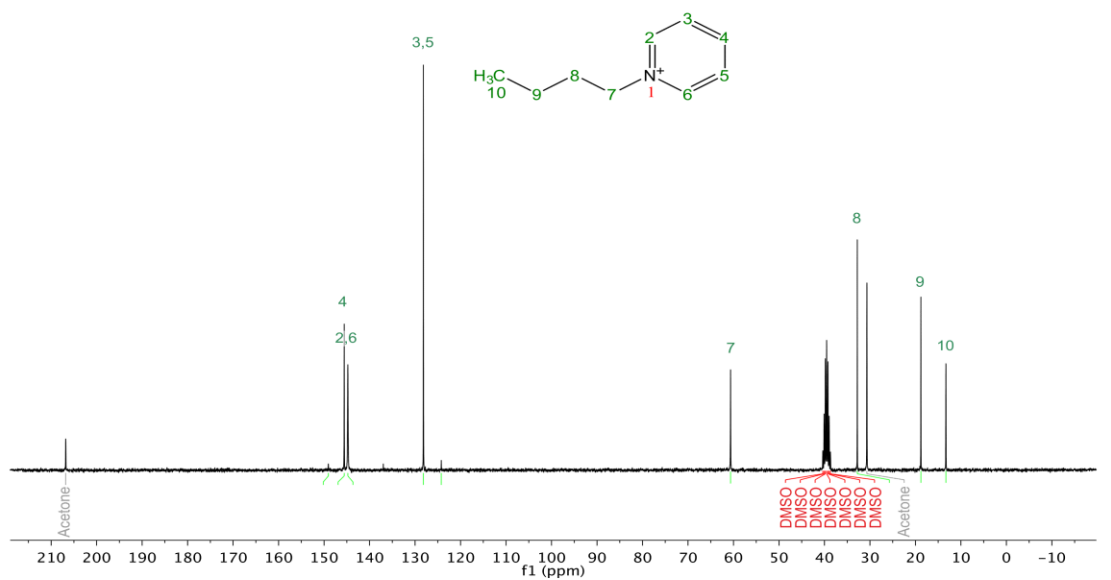
consistent with those reported in other studies.²⁴⁻²⁵ $^1\text{H-NMR}$ (300 MHz, $\text{DMSO-}d_6$): $\delta = 9.13$ (2H, d, $J=6.0$ Hz, Py- $H_{(2,6)}$), 8.58 (1H, td, $J=7.9, 3.2$ Hz, Py- H_4), 8.13 (2H, t, $J=6.5$ Hz, Py- $H_{(3,5)}$), 4.63 (2H, td, $J=7.5, 2.0$ Hz, Py- CH_2), 1.86 (2H, q, $J=7.4$, Hz, Py- $\text{CH}_2\text{-CH}_2$), 1.24 (2H, m, $J=7.3, 2.0$ Hz, $\text{CH}_3\text{-CH}_2$) and 0.84 (3H, td, $-\text{CH}_3$) ppm. ^{13}C NMR (75 MHz, $\text{DMSO-}d_6$): $\delta = 206.81, 149.06, 145.58, 144.24, 128.16, 60.64, 32.78, 30.67, 18.80$ and 13.30 ppm.

Meanwhile, the FTIR spectrum of the synthesised IL [BPy][BF₄] (Figure 3.6) shows prominent peaks at wave numbers 1035.72 and 1047.29 cm^{-1} , both in the characteristic range for C-N stretching, as expected based on the structure of this IL. Thus, both NMR and FTIR spectroscopy data helped confirm the identity of the synthesised IL as [BPy][BF₄].

^1H NMR



¹³C NMR



¹³C NMR (75 MHz, DMSO) δ = 206.81, 149.06, 145.58, 144.78, 128.16, 124.24, 60.64, 40.36, 40.08, 39.80, 39.52, 39.24, 38.96, 38.69, 32.78, 30.67, 18.80, 13.30.

Figure 3.5: (a) ¹H-NMR (300 MHz), DMSO-*d*₆), (b) ¹³C-NMR (75 MHz, DMSO-*d*₆) spectra of [BPY][BF₄].

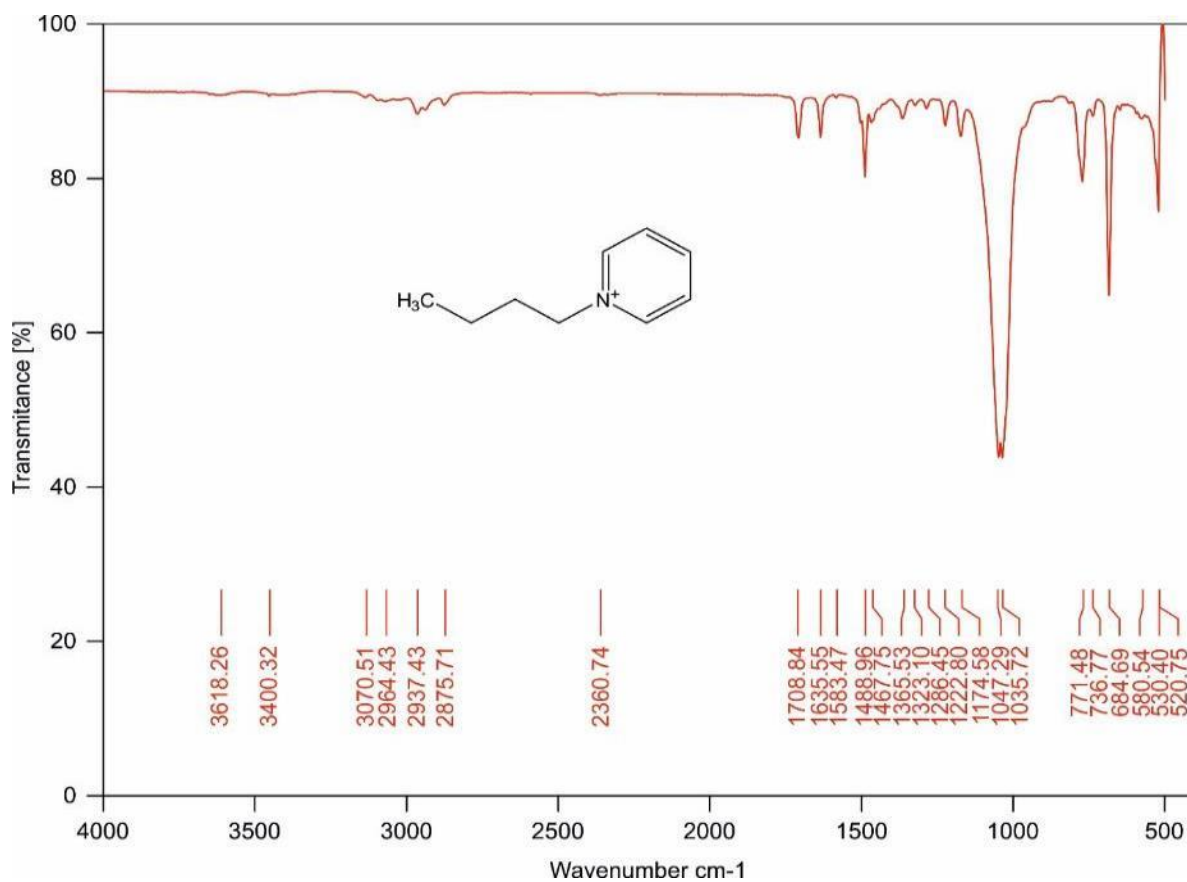


Figure 3.6: FTIR spectrum of the IL [BPY][BF₄].

3.4.2 Effect of Operating Parameters on Desulfurization Efficiency

EDS and OEDS of DBT were carried under moderate reaction conditions in this study and the effects of key operating parameters, such as extraction time, extraction temperature, IL to model fuel ratio and dosage of the oxidizing agent H_2O_2 on the desulfurization efficiency were investigated. The results of these experiments have been discussed in the forthcoming paragraphs.

3.4.2.1 Effect of Extraction Temperature

Reaction temperature plays a vital role in the OEDS process. The effect of temperature on DBT removal from the model fuel (with a DBT concentration of 1000 ppm) was examined by varying the temperature from 20°C to 40°C. Moreover, three different IL to oil volume ratios were used – 1:1, 1:2 and 1:3. The results from these experiments are illustrated in [Figure 3.7](#).

Irrespective of the volume ratio of IL to model fuel (oil) used, higher desulfurization efficiency was observed at an elevated temperature. This is because reaction temperature has a direct effect on the kinetic rate constant, thereby increasing the rate of reaction and hence the removal rate of DBT. Therefore, the highest DBT removal efficiencies were obtained at the highest temperature (40°C). The desulfurization efficiencies at this temperature were 76.0 %, 71.5 % and 68.9 % for the IL to model fuel volume ratios of 1:1, 1:2 and 1:3, respectively ([Figure 3.7](#)).

Not surprisingly, it was observed that the desulfurization efficiency decreased with a decrease in the volume ratio of IL to model fuel, since a higher amount of DBT in the reaction mixture makes the IL almost saturated. Therefore, the greatest DBT removal efficiencies were observed for the IL to model fuel volume ratio of 1:1. The desulfurization efficiencies at this IL to model fuel volume ratio were 68.3 %, 70.9 % and 76.0 % at temperatures 20°C, 30°C and 40°C, respectively.

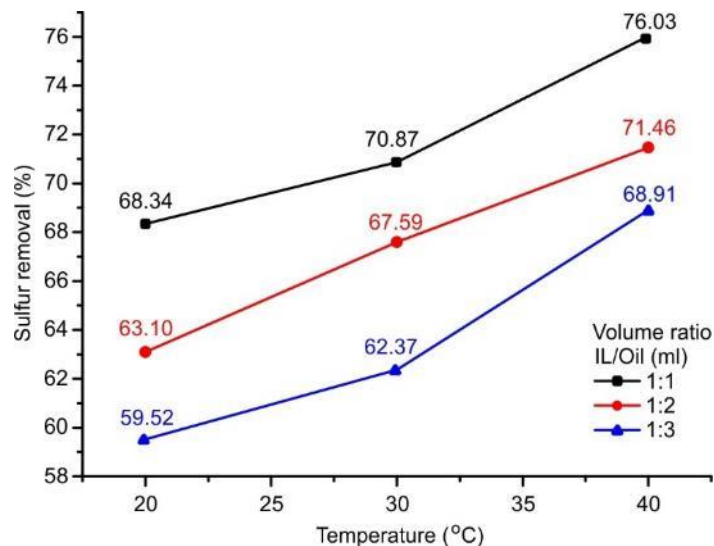


Figure 3.7: Oxidation extraction desulfurization efficiency at different temperatures and IL:Oil volume ratios. ([DBT]_{ini} = 1000 ppm; V(H₂O₂): V(model oil) = 1 %, t = 40 min)

3.4.2.2 Effect of Extraction Time

The effect of extraction time on the removal rate of DBT was studied for both EDS and OEDS processes with an initial DBT concentration of 1000 ppm at 40°C. As seen from Figure 3.8, for EDS, the efficiency of DBT removal (desulfurization efficiency) increases rapidly with time within the first 45 minutes. However, the rise in desulfurization efficiency slows down after 45 minutes and is nearly stable after 60 minutes, leading to a final DBT removal efficiency of 75.5 %.

Compared with EDS, the DBT removal rate by OEDS (with 1.0 % v/v of H₂O₂) is even higher under the same operating conditions, resulting in a nearly 75 % desulfurization rate within just 10 minutes of the reaction. The phase equilibrium was reached after 60 minutes with an enhanced desulfurization efficiency of 79.2 %.

Comparing the IL to model fuel ratios within OEDS experiments, as the volume ratio decreases from 1:1 to 1:3, desulfurization efficiency is observed to be 21% lower (75 % for 1:1 ratio, 59.3 % for 1:3) at the same contact time due to a three-fold higher DBT amount in the model fuel. The difference between the desulfurization efficiencies at the two volume ratios was observed to be gradually reduced at longer time points after phase equilibrium was reached.

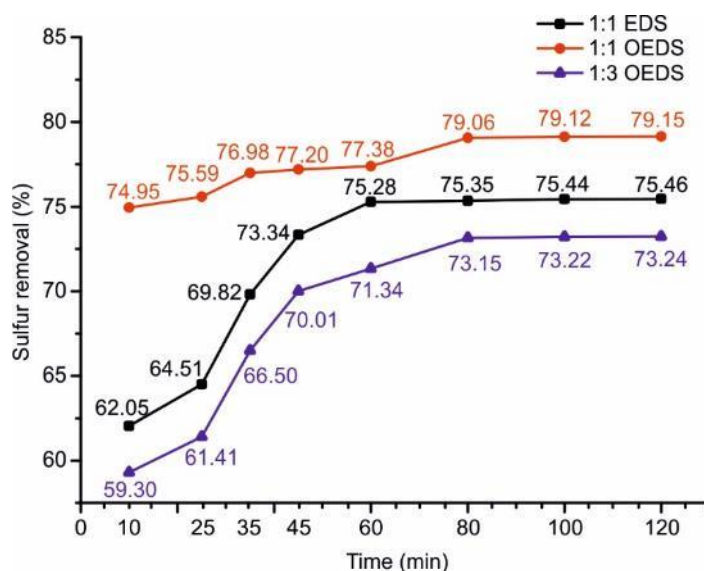


Figure 3.8: Desulfurization efficiency of EDS and OEDS at different time. ($[DBT]_{ini}=1000$ ppm; $T = 40$ °C).

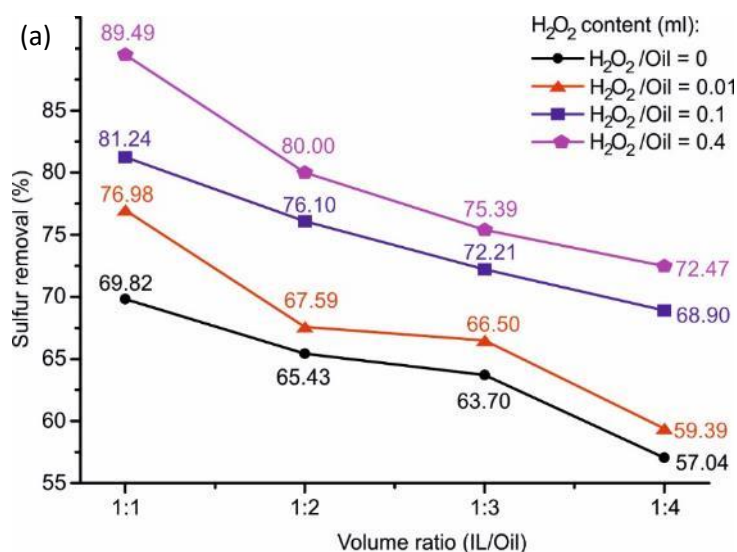
3.4.2.3 Effect of Oxidant (H_2O_2) Dosage

The effect of H_2O_2 dosage on desulfurization efficiency was studied at $T = 40^\circ C$ using four different oxidants to oil volume ratios (0 (0%), 0.01 (1.0 %), 0.1 (10 %) and 0.4 (40 %)) and four different IL to oil volume ratios (1:1, 1:2, 1:3 and 1:4). The results from this experiment are shown in [Figure 3.9](#). As expected, it was observed that desulfurization efficiency increased with an increase in the amount of H_2O_2 (characterized by volume ratio of H_2O_2 to model fuel) added to the system. Thus, for all different volume ratios of IL to model fuel studied, the maximum

desulfurization efficiency was achieved when the highest amount of H₂O₂ (40.0 % v/v) was used. This observation is corroborated by similar trends reported by Zhao et al.²⁴ Moreover, the evaluation of standard deviations revealed very small deviation from the mean values, indicating high reproducibility of the experiments (Figure 3.9).

However, the extent to which H₂O₂ dosage influenced desulfurization efficiency was found to be slightly different when different volume ratios of IL to model fuel were applied. At a high-volume ratio 1:1 of IL to model fuel, just the addition of 1.0 % v/v of H₂O₂ to the model fuel (meaning 0.01 volume ratio of H₂O₂ to oil) led to a 7.16 % increase in desulfurization efficiency from 69.82 % (without using H₂O₂) to 77.0 %. A further increase of 4.3% in desulfurization efficiency was observed from 1.0 % v/v to 10.0 % v/v of H₂O₂ being used.

On the other hand, when a low volume ratio (1:4) of IL to model fuel was used, desulfurization efficiency increased only slightly from 57.0 % (without using H₂O₂) to 59.4 % after adding 1.0 % v/v of H₂O₂. However, a remarkable increase of 9.5 % in desulfurization efficiency was achieved when the oxidant dosage was increased from 1.0 % v/v to 10.0 % v/v of H₂O₂ being used.



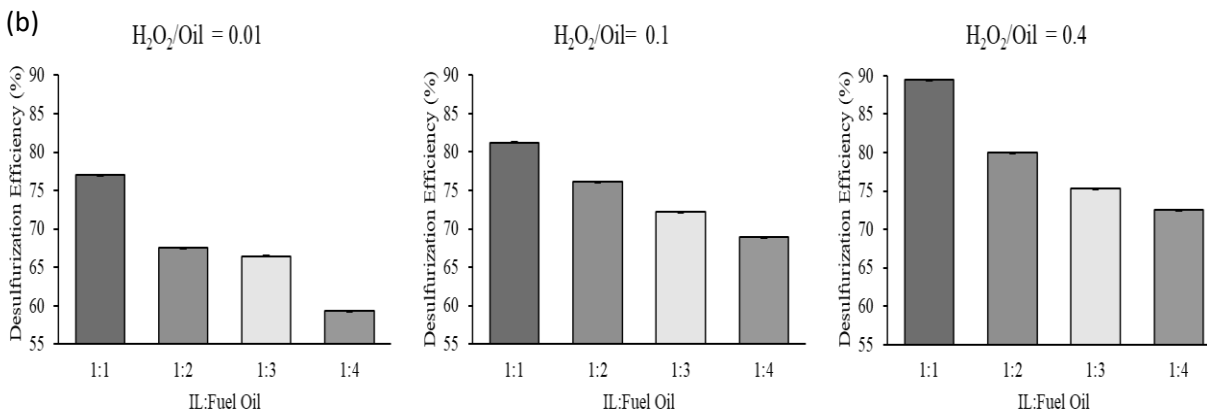


Figure 3.9: (a) Desulfurization efficiency of EDS and OEDS at different volume ratios of H₂O₂ to model fuel. ([DBT]_{ini} = 1000 ppm; T = 40 °C and t = 40 min). (b) standard deviation of desulfurization efficiency (n = 3).

3.4.2.4 Effect of the Volume Ratio of IL to Model Fuel

The effect of the IL to model fuel volume ratio on desulfurization efficiency was studied for both EDS and OEDS. Specifically, three volume ratios of IL to model fuel were tested: 1:1, 1:2 and 1:3, with T = 40°C and an O:S ratio of 40 %. The desulfurization efficiencies of EDS and OEDS for different volume ratios of IL to model fuel are depicted in Figure 3.10.

For both sets of experiments, the desulfurization efficiency decreases when a lower volume ratio of IL to model fuel is used. For OEDS, the efficiency decreases by 16% from 89.5 % to 75.4 % as the volume ratio is reduced from 1:1 to 1:3. On the other hand, with all the other operating conditions being the same, the desulfurization efficiency for EDS decreases by only 9 % (from 69.8 % to 63.7 %) as the volume ratio decreases from 1:1 to 1:3. In real-life, industrial applications, an optimum volume ratio of IL to model fuel must be selected so as to maintain a balance between the desulfurization efficiency and the production capacity.

Meanwhile, as was also noted in Figure 3.8, EDS resulted in overall lower desulfurization efficiencies when compared to OEDS. This trend held true for all the three volume ratios of IL to

model fuel tested. However, the gap between EDS and OEDS decreased with a decrease in the IL to model fuel volume ratio, from 19.67 % (89.49 % – 69.82 %) at 1:1 volume ratio of IL to model fuel, to 11.69 % (75.39 % – 63.70 %) at a volume ratio of 1:3.

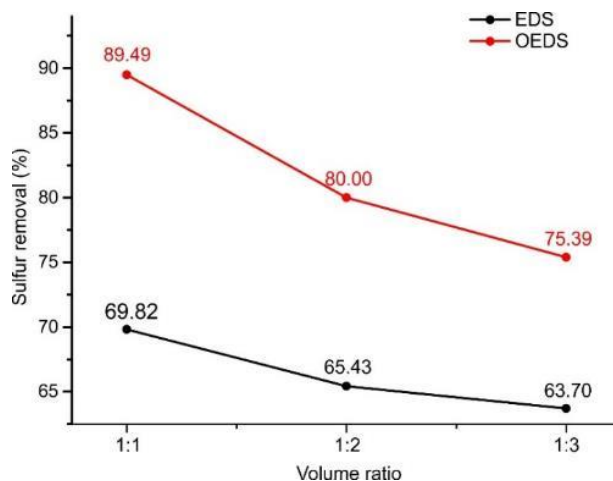


Figure 3.10: Desulfurization efficiency of EDS and OEDS at different volume ratios of IL to model fuel. ([DBT]_{ini} = 1000 ppm; V(H₂O₂): V(model oil) = 40 %, T = 40 °C and t = 40 min)

3.4.3 Interaction of Various Operating Parameters to Determine Desulfurization

Efficiency

The interplay among the key operating parameters of the desulfurization reaction on the desulfurization efficiency of EDS and OEDS was studied by changing two variables randomly while keeping the remaining two parameters constant. The effect of temperature (T) and H₂O₂ dosage on DBT removal was evaluated under constant time ($t = 35$ min) and constant volume ratio of IL to model fuel (1:1). [Figure 3.11](#) shows a linear positive effect of temperature on DBT removal.

On the contrary, a nonlinear relationship of desulfurization efficiency and H₂O₂ dosage is observed. Adding 10 % v/v of H₂O₂ to the system leads to a very dramatic increase in DBT removal

efficiency, whereas further increase in H₂O₂ dosage (from 10 % to 20 % to 30 % to 40 %) results in only gradual increases in DBT removal efficiency. Overall, although increasing temperature and H₂O₂ dosage can both be used to improve desulfurization efficiency, it is better to find the optimum combination of these two parameters so that there is no significant increase in the operating cost.

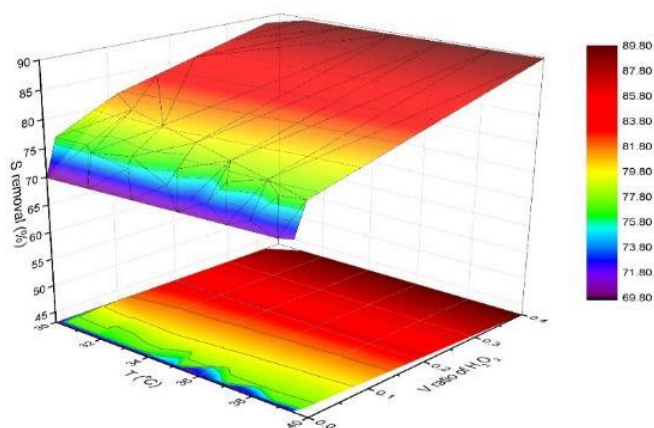


Figure 3.11: Graphic representation of temperature (T) and IL to model fuel ratio on DBT removal. Legend on the right shows colored mapping of DBT removal in %.

The interplay between H₂O₂ dosage and volume ratio of IL to model fuel on DBT removal was examined under constant reaction time ($t = 35$ min) and temperature ($T = 40$ °C). [Figure 3.12](#) depicts the different impacts of H₂O₂ dosage on DBT removal efficiency for different volume ratios of IL to model fuel. At a high-volume ratio (1:1) of IL to model fuel, the impact of H₂O₂ dosage on desulfurization efficiency is remarkably greater (steeper), as can be seen from the upper right side of the surface illustrated in [Figure 3.12](#). However, for the reduced IL to model fuel ratio of 1:4, a gradual increase of DBT removal efficiency is observed with an increase in the dosage of H₂O₂. Notably, the graph surface resembles a square with one edge bent upwards (at 40 % v/v H₂O₂ and 1:1 IL to model fuel volume ratio) and edge next to it downwards (at no H₂O₂ and 1:1 IL to model fuel volume ratio). Notably, Zhao et al. also conducted a study of desulfurization of a model fuel containing thiophene and DBT using [BPy][BF₄]. In this work, they found that a

temperature of 55°C, IL:Oil ratio of 1:1, O:S ratio of 40 % and desulfurization time of 30 min gave them the best desulfurization efficiency (84.3 %).²⁴ In the present work, a better desulfurization efficiency (89.5%) was noted at milder reaction conditions. It should, however, be noted that only DBT was used in the model fuel in the present study.

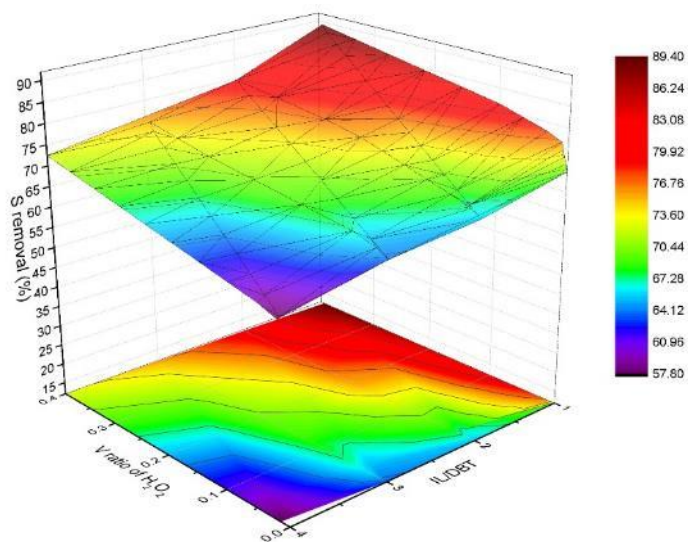


Figure 3.12: Graphic representation of H₂O₂ dosage and IL to model fuel ratio on DBT removal. Legend on the right shows colored mapping of DBT removal in %.

Figure 3.13 simultaneously depicts the effects of two parameters, namely, H₂O₂ to model fuel ratio and IL to model fuel ratio, on the desulfurization efficiency of [BPy][BF₄].

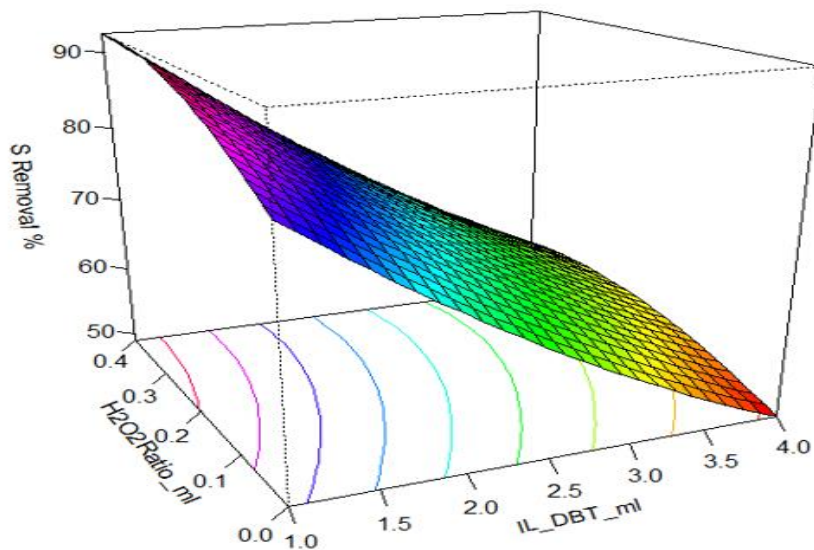


Figure 3.13: Graphic representation of the effect of H₂O₂ and IL to model fuel ratios on DBT removal. Legend on the right shows colored mapping of DBT removal in %.

Figure 3.14 simultaneously depicts the effects of two parameters, namely, H₂O₂ to model fuel ratio and temperature, on the desulfurization efficiency of [BPy][BF₄].

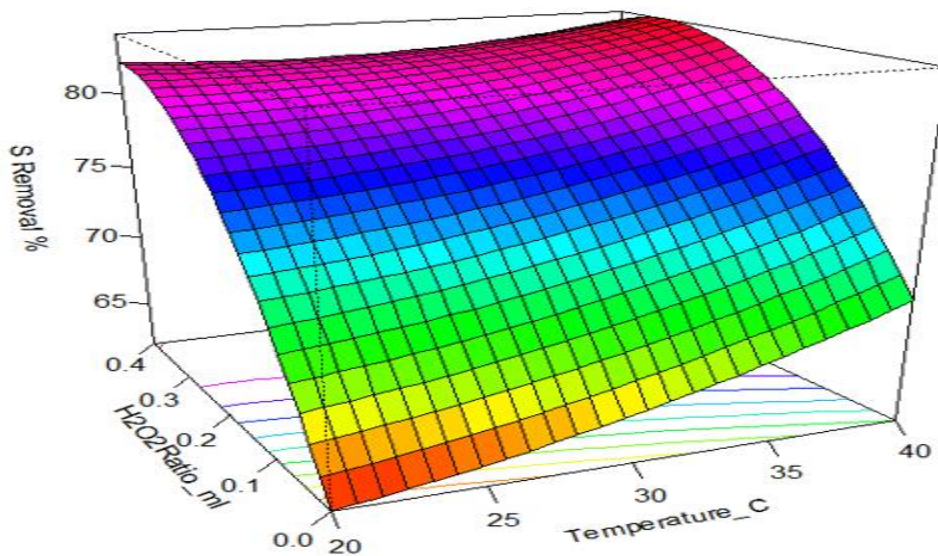


Figure 3.14: Graphic representation of the effect of temperature (T) and H₂O₂ to model fuel ratio on DBT removal. Legend on the right shows colored mapping of DBT removal in %.

Figure 3.15 simultaneously depicts the effects of two parameters, namely, IL to model fuel ratio and temperature, on the desulfurization efficiency of [BPy][BF₄].

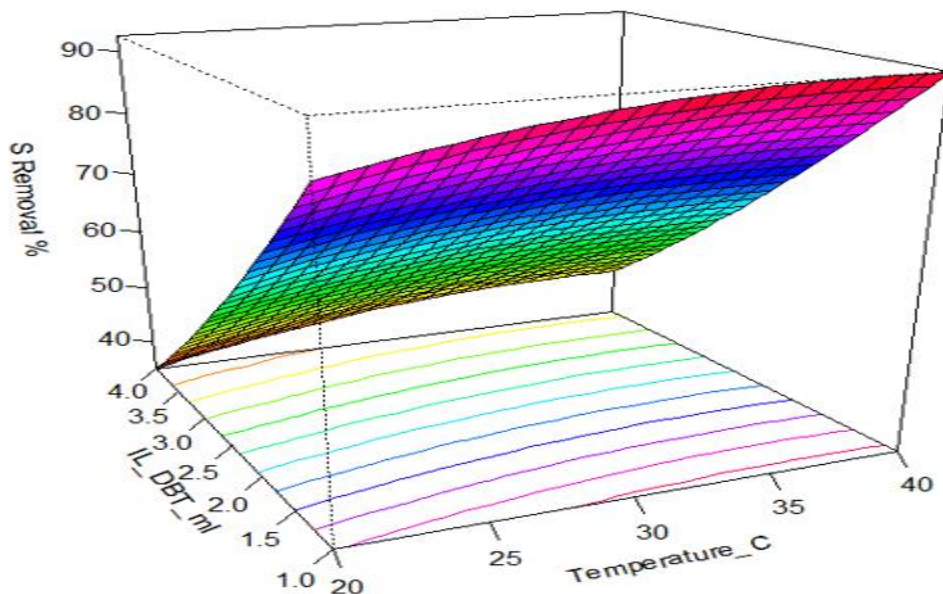


Figure 3.15: Graphic representation of temperature (T) and IL to model fuel ratio on DBT removal. Legend on the right shows colored mapping of DBT removal in %.

Figure 3.16 simultaneously depicts the effects of two parameters, namely, H₂O₂ to model fuel ratio and extraction time, on the desulfurization efficiency of [BPy][BF₄].

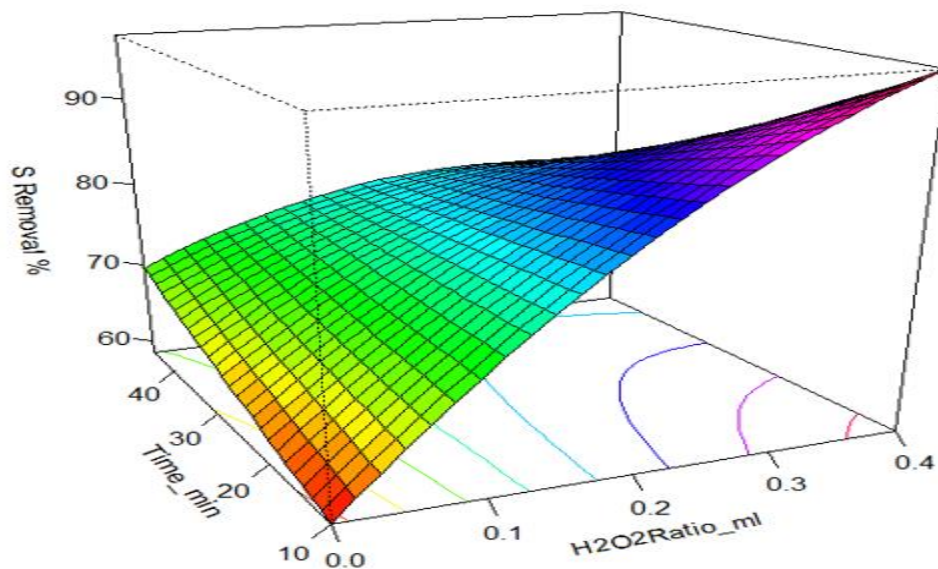


Figure 3.16: Graphic representation of time and H₂O₂ to model fuel ratio on DBT removal. Legend on the right shows colored mapping of DBT removal in %.

Figure 3.17 simultaneously depicts the effects of two parameters, namely, IL to model fuel ratio and extraction time, on the desulfurization efficiency of [BPy][BF₄].

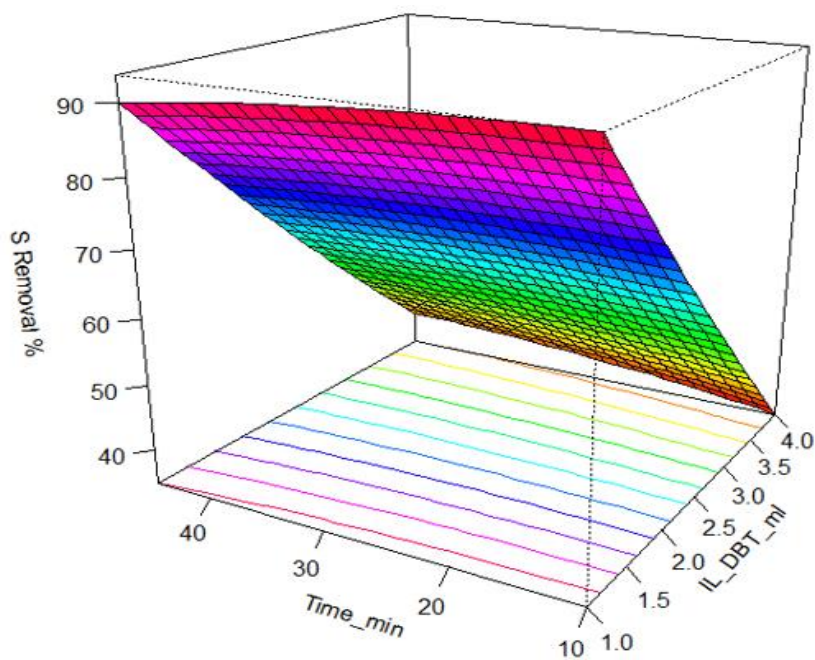


Figure 3.17: Graphic representation of extraction time and IL to model fuel ratio on DBT removal. Legend on the right shows colored mapping of DBT removal in %.

Table 3.1 and Figure 3.18 depict the magnitude and nature of interaction between different operating parameters – temperature, H₂O₂ volume and fuel volume – of the desulfurization reaction with [BPy][BF₄]. Figures 3.19 and 3.20 further elaborate this interaction. It is clear that fuel volume has the highest (negative) impact on desulfurization efficiency, meaning that an increase in fuel volume decreases the desulfurization efficiency. On the other hand, H₂O₂ volume has the highest positive impact, meaning that an increase in H₂O₂ volume leads to an increase in desulfurization efficiency of the IL.

Table 3.1: Magnitude and nature of interaction between different operating parameters of the desulfurization reaction.

Factor (Parameter)	Effect size (coefficient)
T (Temperature)	0.43
H (H ₂ O ₂ volume)	5.04
F (Fuel volume)	-5.80
T:H (Temperature and H ₂ O ₂ volume)	-0.31
T:F (Temperature and fuel volume)	0.35
H:F (H ₂ O ₂ volume and fuel volume)	-1.23
T:H:F (Temperature, H ₂ O ₂ volume and fuel volume)	-0.38

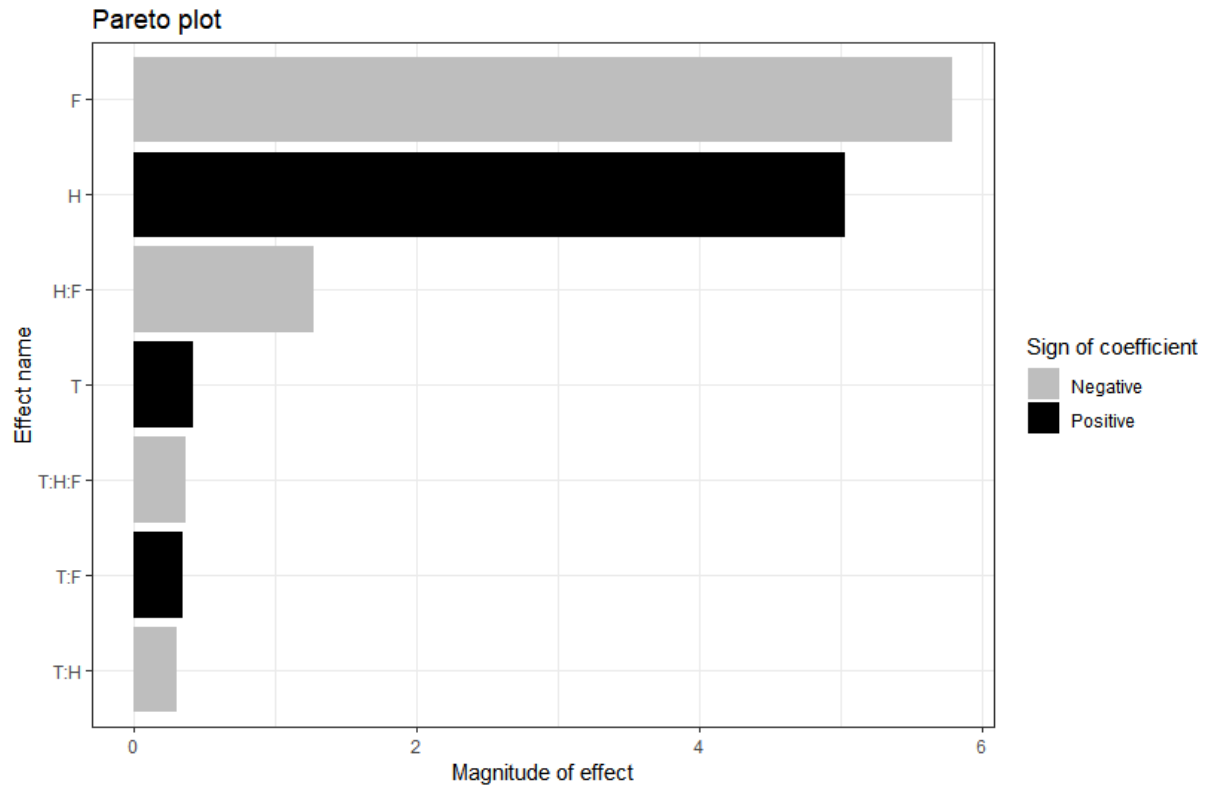


Figure 3.18: Magnitude and nature of interaction between different operating parameters of the desulfurization reaction.

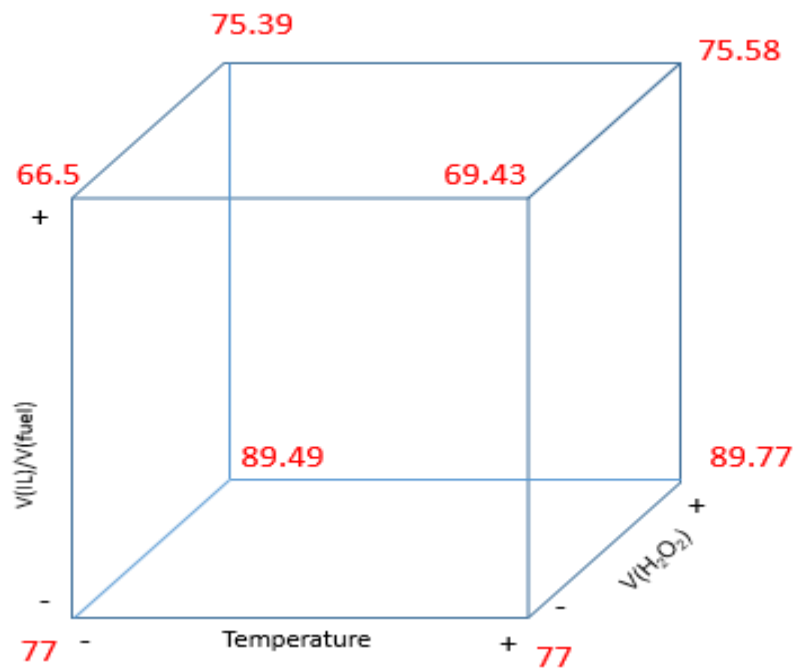


Figure 3.19: Interaction of 3 variables – H₂O₂ to model fuel ratio, IL to model fuel ratio and temperature on the desulfurization efficiency of the IL.

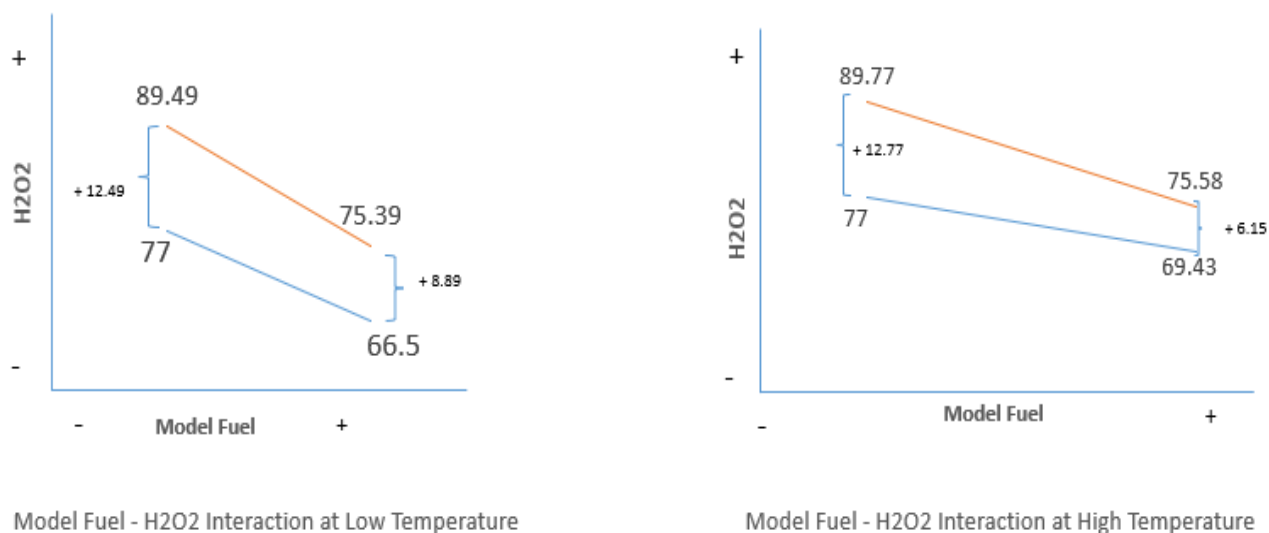


Figure 3.20: Interaction of model fuel and H₂O₂ volumes at low and high temperatures in the desulfurization reaction.

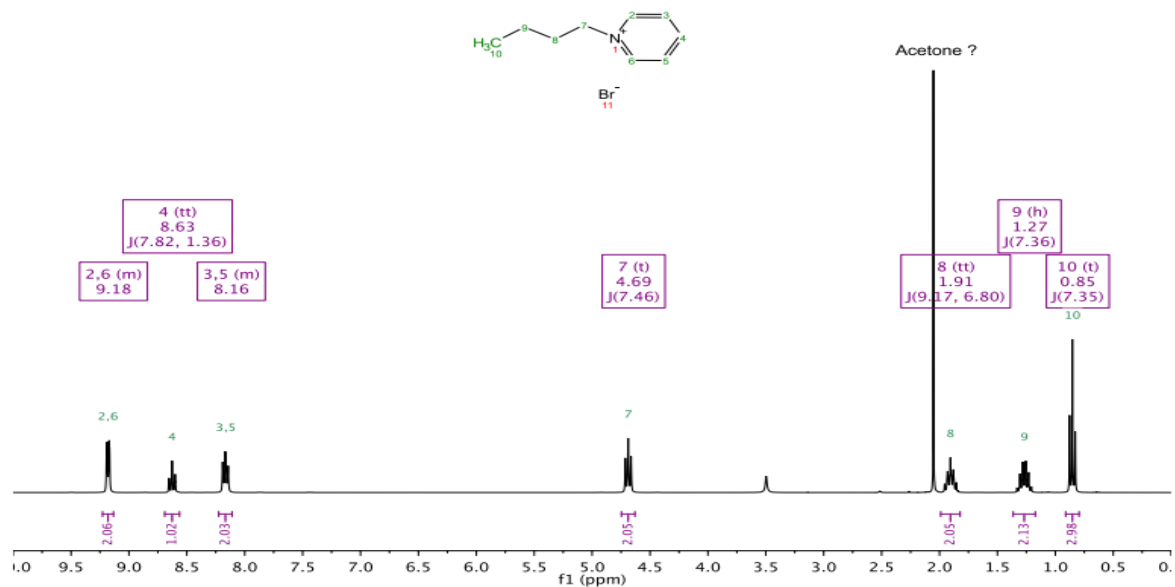
3.4.4 Regeneration of the IL

Regeneration and subsequent recycling of ILs are crucial steps in their industrial applications. In the present study, the sulfur-loaded IL was regenerated by first conducting distillation to remove water and H₂O₂, and subsequently performing re-extraction using CCl₄. The regenerated IL was analyzed by ¹H-NMR & ¹³C-NMR (Figure 3.21) and the comparison between the original ionic liquid spectra and the recycled ionic liquid (Figures 3.22 and 3.23) spectroscopy, which indicated that there was no change in the structure of the regenerated [BPy][BF₄].

To test the extent of reusability of the regenerated IL, it was reused for OEDS of DBT at the optimized reaction conditions for eight consecutive cycles. The results of DBT removal efficiency of the regenerated IL are shown in Figure 3.24. Although the desulfurization efficiency of the

regenerated IL is slightly reduced after each cycle (overall decrease between the 1st and 8th cycles was 12 %, from 80.87 % to 71.05 %), the efficiency is still quite high after the 8th cycle (71.05 %). A similar observation was reported by Zhao et al. using the same IL, but only up to 4 cycles.²⁴ Moreover, Zhao et al. used a solution of thiophene and DBT in *n*-octane as the model fuel in their study, compared to DBT in *n*-hexane used in the present study.²⁴ However, it should be noted that due to the high energy cost for distillation, this method is only suitable for laboratory scale. Alternative low-energy-cost regeneration techniques need to be investigated for large-scale applications.

¹H NMR



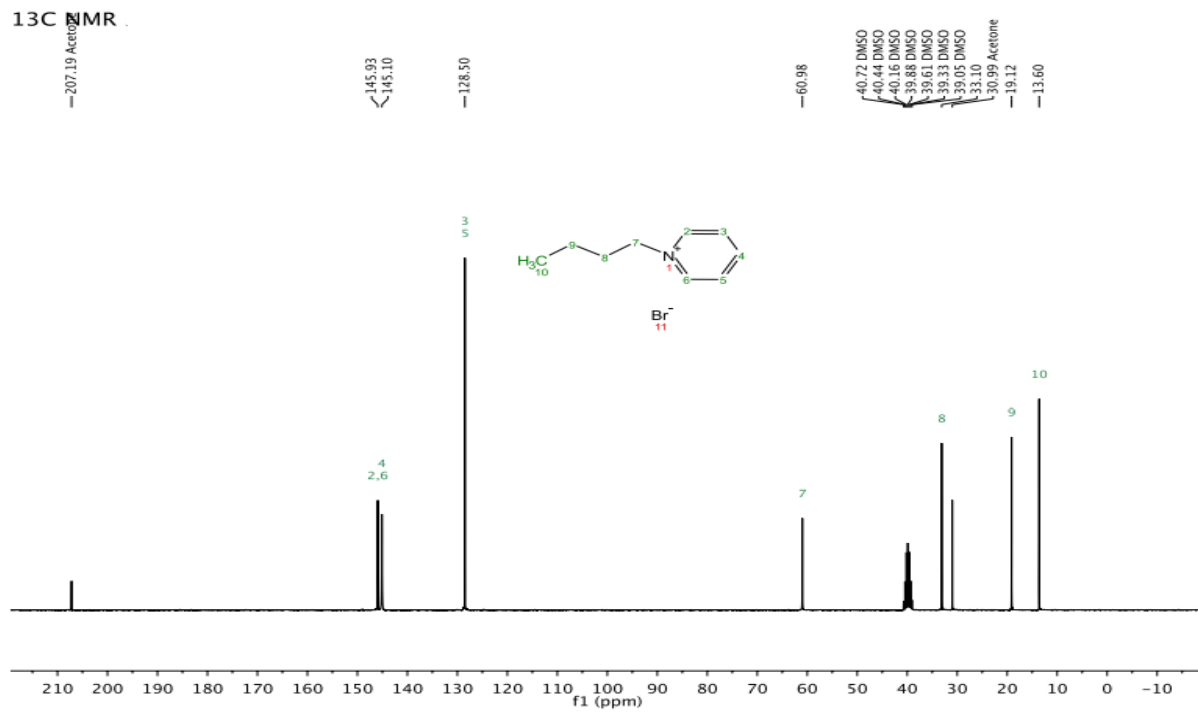


Figure 3.21: (a) ¹H-NMR (300 MHz), DMSO-*d*₆, (b) ¹³C-NMR (75 MHz, DMSO-*d*₆) spectra of [BPy][BF₄].

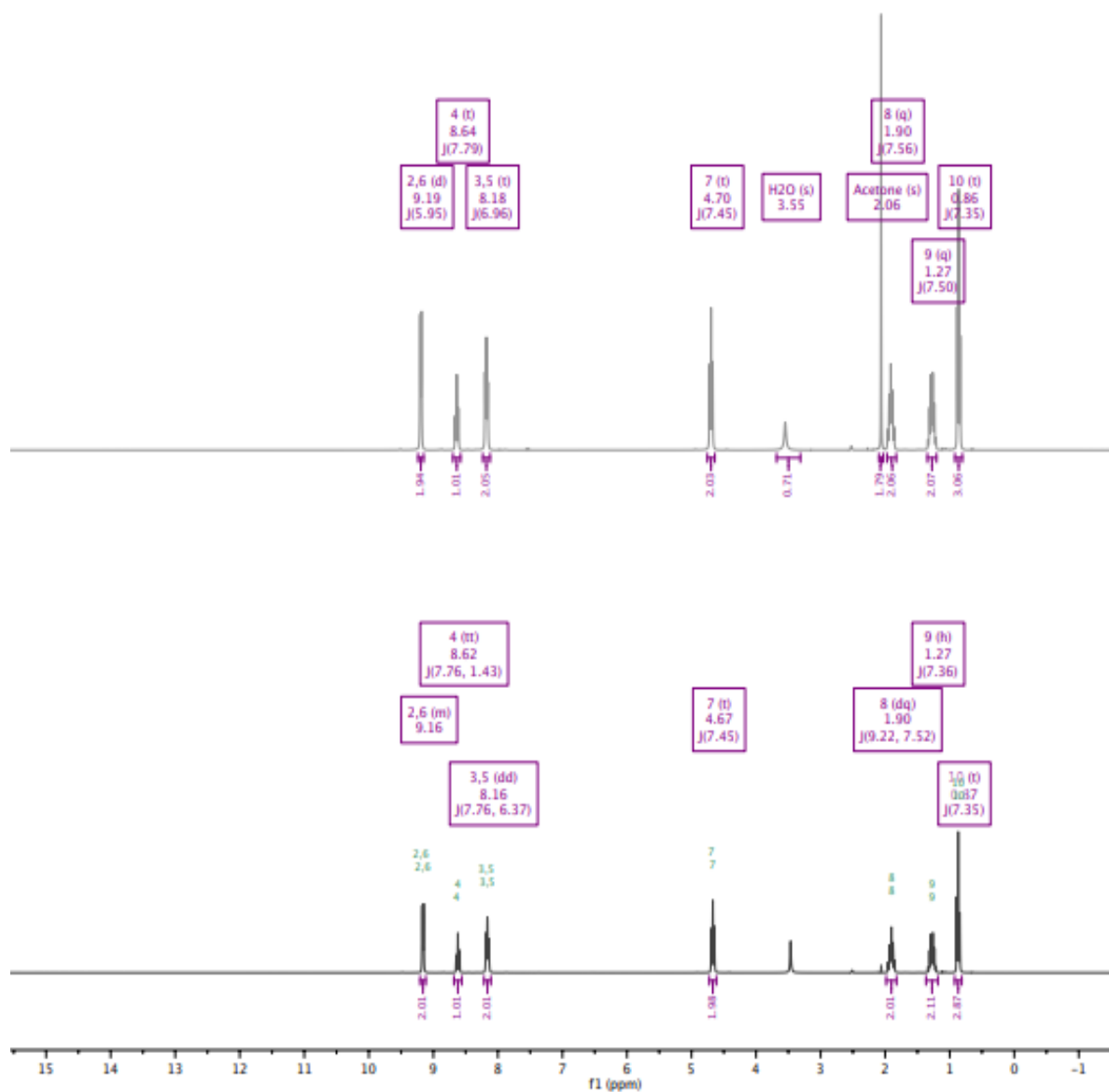


Figure 3.22: ¹H-NMR spectra of regenerated IL.

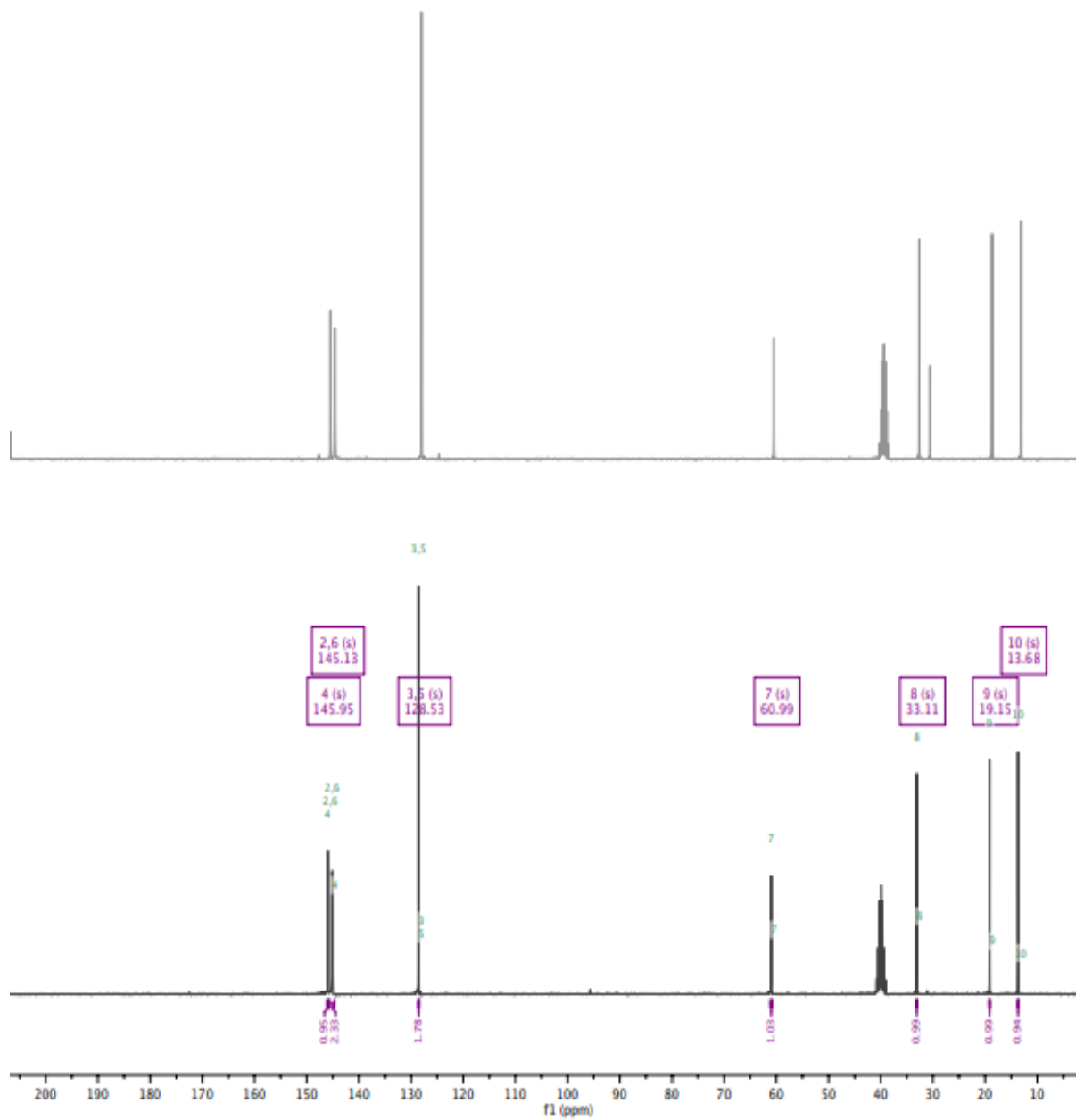


Figure 3.23: ^{13}C -NMR spectra of regenerated IL.

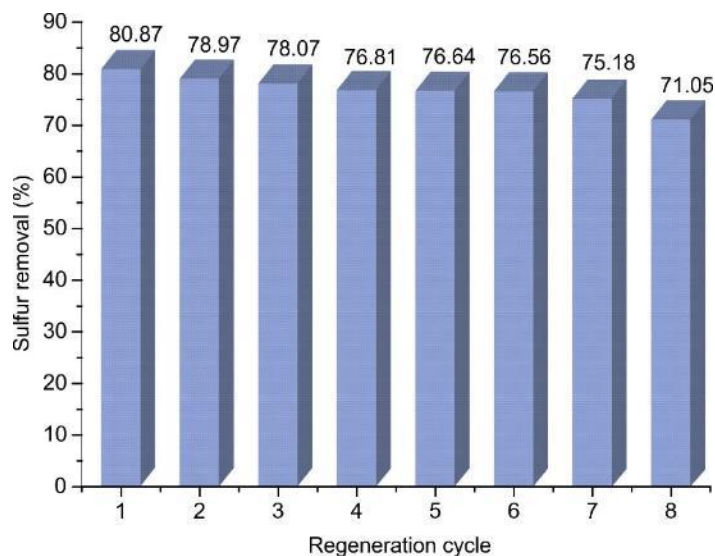


Figure 3.24: OEDS of DBT by regenerated [BPy][BF₄]. ([DBT]_{ini} = 1000 ppm, V(IL): V(model oil) = 1:1, V(H₂O₂): V(model oil) = 40 %, T = 40 °C)

3.4.5 Desulfurization of DBT from Diesel Fuel with [BPy][BF₄]

In the present study, diesel fuel containing 1000 ppm DBT was treated with [BPy][BF₄] to test its extraction ability on real hydrocarbon feedstock. The extraction reactions were conducted for 10 min, 20 min, 30 min, 35 min, 40 min, and 45 min at 40°C with a fixed volume ratio (1:1) of IL to diesel fuel. [Figure 3.25](#) shows the results for desulfurization of DBT from real diesel fuel.

It can be seen from [Figure 3.25](#) that the amount of DBT extracted by [BPy][BF₄] from diesel fuel is considerably lower than that extracted from the model oil (at 40 min under the same reaction conditions, the desulfurization efficiency of the IL on model fuel was 89.49 %, whereas for real diesel, the corresponding desulfurization efficiency is 59.38 %). This could be because real diesel fuel contains a mixture of components, including paraffinic, aromatic, alkyl-aromatic and a range of polyaromatic hydrocarbons. These components may be partially miscible in the IL and could thus reduce the selectivity of [BPy][BF₄] towards DBT.

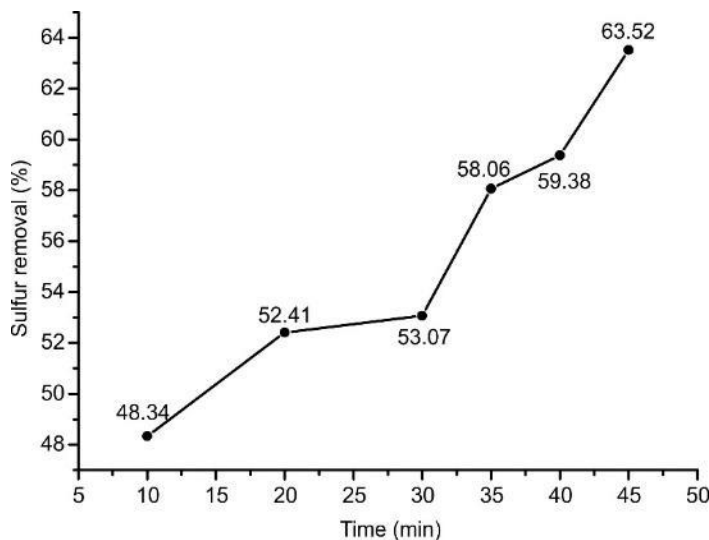


Figure 3.25: Desulfurization efficiency of DBT in diesel fuel. ($[\text{DBT}]_{\text{ini}} = 1000$ ppm, $V(\text{IL}): V(\text{model oil}) = 1:1$, $V(\text{H}_2\text{O}_2): V(\text{model oil}) = 40\%$, $T = 40$ °C)

3.5 Conclusion

In the present study, a pyridinium-based IL $[\text{BPy}][\text{BF}_4]$ was synthesized via a two-step method and was characterized by $^1\text{H-NMR}$, $^{13}\text{C-NMR}$, and FTIR spectroscopy. The NMR and FTIR spectra confirmed the molecular structure and configuration of $[\text{BPy}][\text{BF}_4]$. Thereafter, the synthesized IL was used as an extractant to remove DBT from a model fuel under different experimental conditions. $[\text{BPy}][\text{BF}_4]$ was found to be effective in the extraction of DBT from the model fuel as both EDS and OEDS reactions reached equilibrium within 1 h. The results indicate that H_2O_2 dosage and volume ratio of IL to model fuel also have significant impact on desulfurization efficiency. Desulfurization efficiency increased remarkably with an increase in the amount of H_2O_2 when a high-volume ratio (1:1) of IL to model fuel is used. On the other hand, only a gradual increase of DBT removal efficiency is observed with increasing dosage of H_2O_2 when a low volume ratio of IL to model fuel (1:4) is applied. In addition, our experimental results confirmed that $[\text{BPy}][\text{BF}_4]$ can be regenerated and reused for at least 8 times without a significant

decline in desulfurization efficiency. Lastly, the amount of DBT extracted by [BPy][BF₄] from diesel fuel was found to be considerably lower than that extracted from the model oil, possibly due to reduced selectivity of [BPy][BF₄] towards DBT in the presence of other hydrocarbons of similar chemical structures present in diesel oil.

References

1. Kulkarni, P.S., Afonso, C.A.M. Deep desulfurization of diesel fuel using ionic liquids: current status and future challenges, *Green Chemistry* 12 (2010), 1139–1149.
2. Dharaskar, S.A., Wasewar, K.L., Varma, M.N., Shende, D.Z., Yoo, C.K. Synthesis, characterization and application of 1-butyl-3-methylimidazolium tetrafluoroborate for extractive desulfurization of liquid fuel, *Arabian Journal of Chemistry* 9 (2016), 578–587.
3. Ibrahim, M.H., Hayyan, M., Hashim, M.A., Hayyan, A. The role of ionic liquids in desulfurization of fuels: A review, *Renewable and Sustainable Energy Reviews*, 76 (2017), 1534–1549.
4. Plechkova, N.V., Seddon, K.R. Applications of ionic liquids in the chemical industry, *Chemical Society Reviews*, 37 (2008), 123–150.
5. Vekariya, R.L. A review of ionic liquids: Applications towards catalytic organic transformations, *Journal of Molecular Liquids* 227 (2017), 44-60.
6. Alonso, L., Arce, A., Francisco, M., Rodriguez, O., Soto, A. Gasoline desulfurization using extraction with [C₈mim][BF₄] ionic liquid, *AIChE Journal* 53 (2007), 3108-3115.
7. Chen, X., Yuan, S., Abdeltawab, A.A., Al-Deyab, S.S., Zhang, J., Yu, L., Yu, G. Extractive desulfurization and denitrogenation of fuels using functional acidic ionic liquids, *Separation and Purification Technology* 133 (2014), 187-193.
8. Zhu, W., Wu, P., Yang, L., Chang, Y., Chao, Y., Li, H., Jiang, Y., Jiang, W., Xun, S. Pyridinium-based temperature-responsive magnetic ionic liquid for oxidative desulfurization of fuels, *Chemical Engineering Journal* 229 (2013), 250-256.
9. Wang, J., Zhao, D., Zhou, E., Dong, Z. Desulfurization of gasoline by extraction with N-alkyl-pyridinium-based ionic liquids, *Journal of Fuel Chemistry and Technology* 35 (2007), 293-296.
10. Holbrey, J.D., López-Martin, I., Rothenberg, G., Seddon, K.R., Silveroc, G., Zheng, X. Desulfurization of oils using ionic liquids: selection of cationic and anionic components to enhance extraction efficiency, *Green Chemistry* 10 (2008), 87-92.
11. Gao, H., Luo, M., Xing, J., Wu, Y., Li, Y., Li, W., Liu, Q., Liu, H. Desulfurization of fuel by extraction with pyridinium-based ionic liquids, *Industrial and Engineering Chemical Research* 47 (2008), 8384-8388.
12. Wlazło, M., Ramjugernath, D., Naidoo, P., Domańska, U. Effect of the alkyl side chain of the 1-alkylpiperidinium-based ionic liquids on desulfurization of fuels, *The Journal of Chemical Thermodynamics* 72 (2014), 31–36.
13. Lo, W.-H., Yang, H.-Y., Wei, G.-T. One-pot desulfurization of light oil by chemical oxidation and solvent extraction with room temperature ionic liquids, *Green Chemistry* 5 (2003), 639–

642.

14. Pârvolescu, V.I., Hardacre, C. Catalysis in ionic liquids, *Chemical Reviews* 107 (2007), 2615–2665.
15. Li, F.-T., Wu, B., Liu, R.-H., Wang, X.-J., Chen, L.-J., Zhao, D.-S. An inexpensive N-methyl-2-pyrrolidone-based ionic liquid as efficient extractant and catalyst for desulfurization of dibenzothiophene, *Chemical Engineering Journal* 274 (2015), 192–199.
16. Elwan, H.A., Zaky, M.T., Faray, A.S., Soliman, F.S., Hassan, M.E.D. A coupled extractive-oxidative process for desulfurization of gasoline and diesel fuels using a bifunctional ionic liquid, *Journal of Molecular Liquids* 248 (2017), 549–555.
17. Choi, A.E.S., Roces, S., Dugos, N., Wan, M.W. Oxidation by H₂O₂ of bezothiophene and dibenzothiophene over different polyoxometalate catalysts in the frame of ultrasound and mixing assisted oxidative desulfurization, *Fuel* 180 (2016), 127–136.
18. Jiang, W., Jia, H., Li, H., Zhu, L., Tao, R., Zhu, W., Li, H., Dai, S. Boric acid-based ternary deep eutectic solvent for extraction and oxidative desulfurization of diesel fuel, *Green Chemistry* 21 (2019), 3074–3080.
19. Gao, S., Li, J., Chen, X., Abdeltawab, A.A., Yakout, S.M., Yu, G. A combination desulfurization method for diesel fuel: Oxidation by ionic liquid with extraction by solvent, *Fuel* 224 (2018), 545–551.
20. Zhang, C., Pan, X., Wang, F., Liu, X. Extraction-oxidation desulfurization by pyridinium-based task-specific ionic liquids, *Fuel* 102 (2012), 580–584.
21. Syntyhaki, E., Karonis, D. Oxidative and extractive desulfurization of petroleum middle distillates, using imidazole ionic liquids. *Fuel Communications* 7 (2021), 100011.
22. Verdía, P., González, E.J., Rodríguez-Cabo, B., Tojo, E. Synthesis and characterization of new polysubstituted pyridinium-based ionic liquids: Application as solvents on desulfurization of fuel oils, *Green Chemistry* 13 (2011), 2768–2776.
23. Francisco, M., Arce, A., Soto, A. Ionic liquids on desulfurization of fuel oils, *Fluid Phase Equilibrium* 294 (2010), 39–48.
24. Zhao, D., Wang, Y., Duan, E. Oxidative desulfurization of fuel oil by pyridinium-based ionic liquids, *Molecules* 14 (2009), 4351–4357.
25. Enayati, M., Faghihian, H. N-butyl-pyridinium tetrafluoroborate as a highly efficient ionic liquid for removal of dibenzothiophene from organic solutions, *Journal of Fuel Chemistry and Technology* 43 (2015), 195–201.
26. Della Fonte, A.R., de Araújo Freitas, V., Barthus, R.C. Comparison of development methods based on UV/VIS spectrophotometry and ICP OES for the determination of iodine in pharmaceuticals. *Journal of Applied Pharmaceutical Science* 6, no. 04 (2016), 22-27.

Chapter 4: Oxidative-Extractive Desulfurization by the Acidic Ionic Liquid N-Carboxymethyl Pyridinium Hydrogen Sulfate

4.1 Introduction

As ultra-low-sulfur diesel (ULSD) production ramps up around the world, the negative effects of sulfur compounds on the environment are also becoming better known. For example, during combustion, S-bearing compounds convert to SO_x , which not only causes acid rain,^{1, 2} but also reduces the efficiency of catalytic converters in vehicles.³ To mitigate the impacts of S-compounds on the environment, regulations have recently been introduced. For instance, the American Environmental Protection Agency (EPA) lowered the limit in the U.S. to 15 ppm, and the European Union (EU) set a limit of 10 ppm for diesel fuel sulfur content.⁴ To comply with these regulations, industry is developing and adopting deep desulfurization methods to produce cleaner fuels.^{5, 6}

Producing ULSD without relying on hydrogen is difficult.⁷ To overcome the difficulties, a new desulfurization process that uses ionic liquids (ILs) is emerging. Ionic liquids are molten salts that are thermally stable, moisture-tolerant, and have only negligible vapor pressure.⁸ ILs were firstly used in deep desulfurization in 2001 by Wasserschied and Jess.⁹⁻¹⁰ Since then extensive research studies have been carried out for desulfurization by various ILs.

The solubility of ILs in fuel oil is an important parameter, which determines the desulfurization effectiveness and the quality of the processed fuels. Miscibility of ILs in fuels may contaminate

the fuel and increase consumption of ILs for the extraction process. This can be overcome by manipulating the cationic and anionic structures to reduce the solubility of ILs in hydrocarbons at room temperature. In a recent study, it was reported that an IL cation's structure and size determined its extractive abilities, with performance improving in pyridinium-based ILs as cation size increases, such that: ([BPy][BF₄] < [HPy][BF₄] < [OPy][BF₄]).¹¹ In a related work, acidic ILs served as both catalysts and extraction agents, which are able to extract DBT from oil phase to IL phase and to decompose H₂O₂ (in IL phase) into hydroxyl radicals that further oxidize DBT into DBT oxidests.¹² The major limitation of this approach is the need for a significant amount of ILs under high temperature conditions. An additional challenge is that BF₄ is the anion in these ILs, and that the fluoroboric acid used to prepare the acidic ILs is quite corrosive and toxic. Moreover, substances that contain fluorine have been found to be environmentally harmful.¹²⁻¹⁵ Therefore, developing cost-effective, non-toxic, and 'green' acidic ILs for ODS is still a work in progress.

For desulfurization of diesel fuels, Brønsted acidic ILs used as both extraction agents and catalysts were recently reported.^{11, 16, 17} Gao and co-workers prepared the carboxylic acid (-COOH) group-included pyridinium-based acidic ILs, which demonstrated enhanced desulfurization efficiency due to the inclusion of carboxyl groups in ILs.¹¹ Because acids are widely used as the catalysts of oxidative desulfurization process, Brønsted acidic ILs serve as both extraction solvent and catalysts for the oxidation of S-compounds at the presence of H₂O₂.

The synthetic methods of acidic ILs have significant influences on desulfurization efficacy. Zhang et al. reported that ILs exposed to ultrasound for mixing resulted in higher levels of desulfurization at lower temperatures and shorter reaction times.^{16,17} Employing an ultrasonic irradiation strategy, the authors synthesized IL N-carboxymethyl pyridine hydrogen sulfate ([CH₂COOHPy] [HSO₄]). They then used IL as catalyst and extractant in the desulfurization of the model oil DBT in n-

octane. The results were a sulfur removal rate of 99.7%, achieved at a temperature of 50°C and a 40 min reaction time. The authors also reported that the IL was recyclable 5 times at the same sulfur removal ability.¹⁶ Zhang and colleagues continued their research in another study published a year later, again investigating IL [CH₂COOHPy] [HSO₄] to desulfurize the same model oil as the earlier work.¹⁷ The authors' results were even more impressive than the previous study. Using temperature of 30°C and a 60-min reaction time, sulfur removal was nearly complete, at 99.9%. Furthermore, the IL could be recycled 9 times and still show the same or similar sulfur removal abilities.¹⁷ In addition, the acid strength, viscosity and density of the as-prepared ILs on desulfurization were investigated as well.^{16,17} Their results indicated that [CH₂COOHPy] [HSO₄] gave better results for DBT removal in n-octane using an oxidation/extraction combination. Sulfur removal peaked at 99.9% when $V_{oil} = 20$ mL, $V_{IL} = 1.2$ mL, $T = 30$ °C, and H₂O₂/S molar ratio (O/S) = 6. Under the same conditions, the removal rates of 4,6-dimethyldibenzothiophene (4,6-DMDBT) and benzothiophene (BT) by [CH₂COOHPy] [HSO₄] were 89.1% and 82.5%, respectively.

The major objective of this work is to evaluate desulfurization efficacy of acidic IL [CH₂COOHPy] [HSO₄] from both diesel and model fuels. Different parameters were tested to gauge the desulfurization abilities for the IL under study. The desulfurization efficiency by different operation modes, namely oxidative, extractive, and oxidative-extractive desulfurization was investigated and compared firstly, followed by the effects of phase ratio, oxidant (H₂O₂) dosage and extraction time.

4.2 Experimental Methods

4.2.1 Chemicals and Reagents

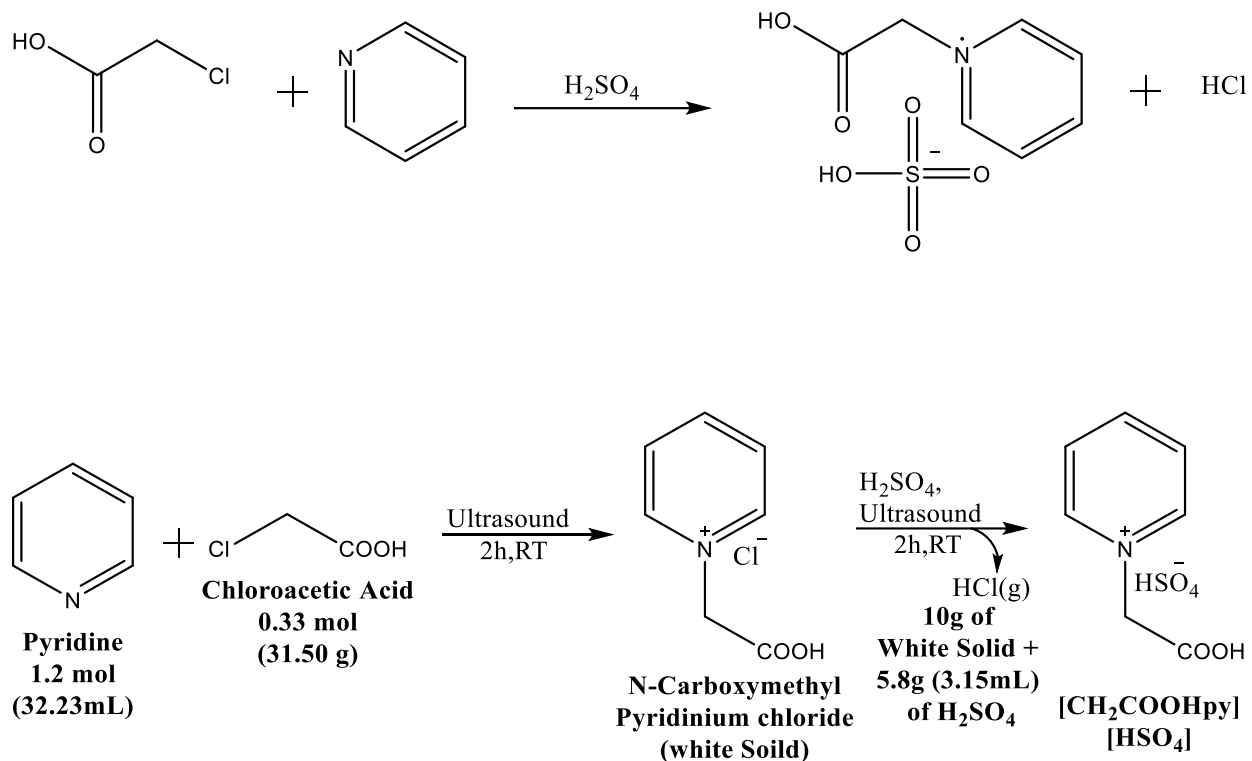
All chemicals were obtained from commercial sources and were used without further purification. Analytical grade pyridine, chloroacetic acid, dichloromethane, deionized (DI) water, sodium hydroxide solution, sulfuric acid, H₂O₂ and hexadecane were obtained from Fisher Scientific (Waltham, MA, USA). Standard diesel oil was obtained from a local gas station.

4.2.2 Synthesis of the Acidic IL N-Carboxymethyl Pyridinium Hydrogen Sulfate

The ionic liquid ([CH₂COOHPy] [HSO₄]) was synthesized according to the reported two-step procedures.^{16, 17} Briefly, N-carboxymethyl pyridinium chloride was synthesized in the first step by adding 32.23 mL of pyridine (0.39 mol) and 31.5 g of chloroacetic acid (0.33 mol) into 5.0 mL of DI water in a 250 mL round-bottom flask connected to a water-cooled reflux condenser fitted with an anhydrous calcium chloride drying tube (Figure 4.1 A-C; Scheme 4.1). The reaction mixture was homogenized using an ultrasound instrument at room temperature for 2 h until no more precipitate was formed (Figure 4.1 D). The white precipitate was filtered off, and the unreacted pyridine was subsequently removed from the resulting solid by washing with dichloromethane (three times with 50.0 mL each) solvent (Figure 4.1 E). The resulting solid was dried in a vacuum oven to remove the remaining dichloromethane and obtain N-carboxymethyl pyridinium chloride (73.1 g) as a colorless solid.

In the second step, the freshly synthesized 1-carboxymethyl pyridinium chloride (10 g, 0.058 mol) was mixed with 3.15 mL sulfuric acid (0.30 mol) in a conical flask. The reaction mixture was subsequently homogenized using ultrasound instrument at room temperature for 2 h. The resulting product was a heavy, white-coloured liquid N-carboxymethyl pyridinium hydrogen sulfate ionic

liquid (12.4 g). The ionic liquid was stored at 4°C until further use. The detailed synthetic route of ([CH₂COOHpy] [HSO₄]) is described in [Scheme 4.1](#).



Scheme 4.1: Synthetic route for [CH₂COOHpy] [HSO₄].

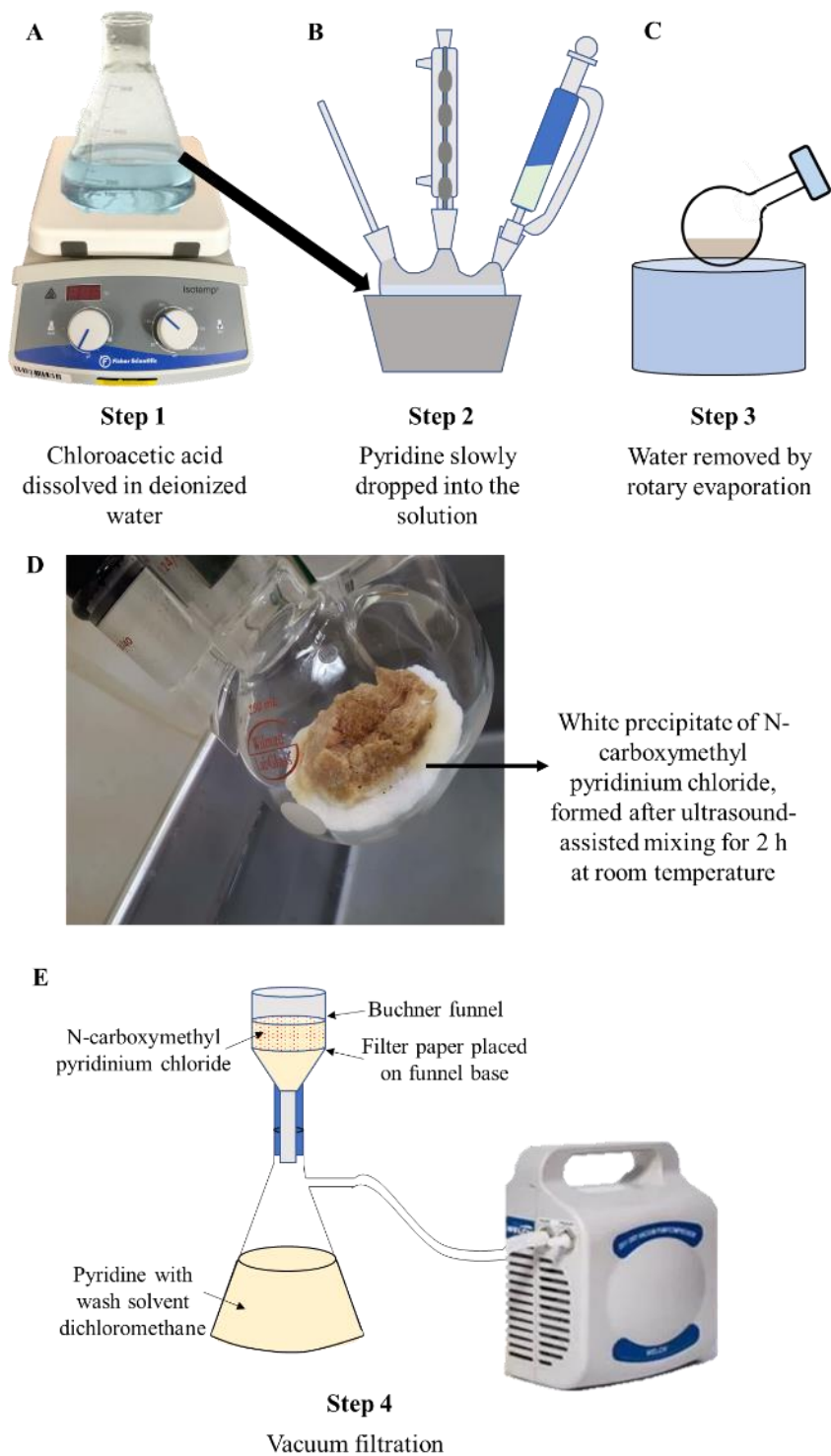


Figure 4.1: Laboratory synthetic set-up for $[\text{CH}_2\text{COOHPy}] [\text{HSO}_4]$.

4.2.3 Desulfurization of Model Fuel by the Synthesized IL

4.2.3.1 Model Fuel Preparation

Model fuel generally contains different initial concentrations of sulfur compounds such as DBT and 4,6-DMDBT, amounting to an overall sulfur concentration of 1000 ppm, a concentration that has prevalently been used in desulfurization literature.¹⁶ In the present study, a model fuel (1000 ppm) was prepared by dissolving DBT in *n*-hexadecane, to be employed as a surrogate for real diesel fuel. For one experiment, where the effect of sulfur species on desulfurization efficiency was evaluated, both DBT and 4,6-DMDBT were mixed with *n*-hexadecane (1000 ppm). Finally, real diesel fuel was also used to check the desulfurization efficiency of the IL in a real scenario.

4.2.3.2 Extractive Desulfurization Experiments (EDS)

The extractive desulfurization (EDS) experiments were conducted in a 50 mL glass conical flask by mixing the sulfur-containing model fuel with the synthesized IL (volume ratio of the IL to model fuel (DBT) was 1:1) and the mixture was stirred vigorously at 25 °C. Approximately 0.5 ml by using glass Pipette as a sample volume was collected from the conical flask every 15 min for 2 h. These time points have hitherto been referred to as ‘extraction time’. After the completion of the reaction, the reaction mixture was allowed to settle, which led to a phase separation between the oil phase and the IL phase. Thereafter, the two layers were separated using a separatory funnel [Figure 4.2](#). The sulfur content of the upper phase (model fuel phase) was analyzed by using HPLC-UV-Vis at a wavelength (λ_{\max}) of 284 nm. Thereafter, the extraction/desulfurization efficiency (η , in %) was calculated in terms of the overall sulfur removal based on the initial and final sulfur content (equivalent to the concentration of S-compounds) in the model fuel, using the following equation:

$$\text{Removal \%} = \frac{c_0 - c_e}{c_0} \times 100$$

where, c_0 is the initial concentration of sulfur compound in model fuel, and c_e is the concentration of remaining S-containing compounds in the oil phase after the reaction began for a certain amount of time.

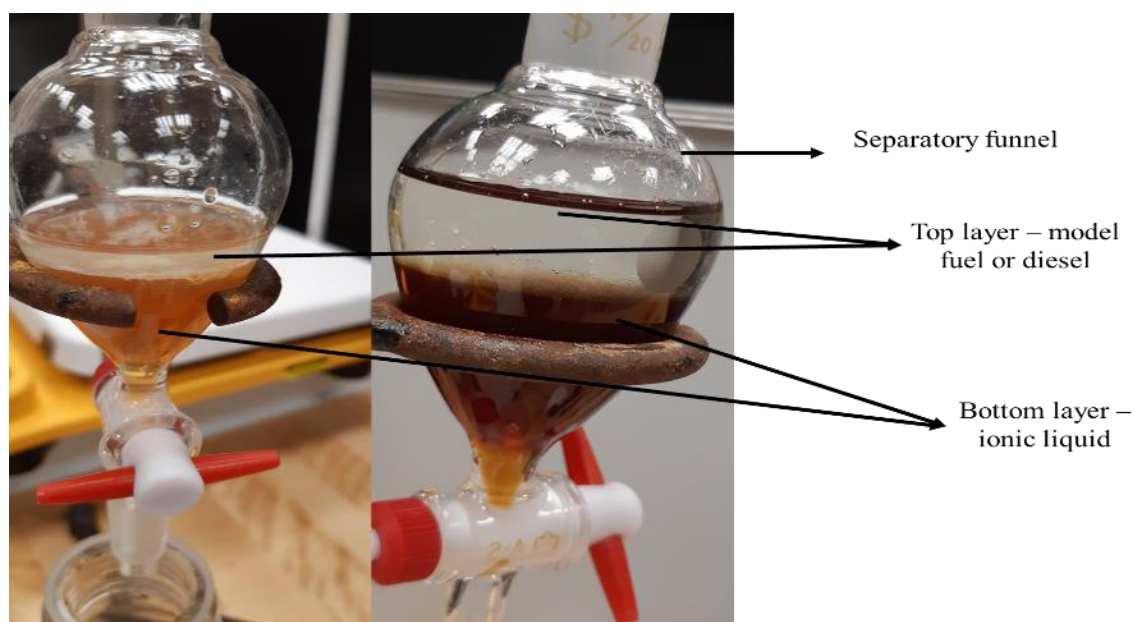


Figure 4.2: Using a separatory funnel to separate the ionic liquid phase from the model fuel or diesel phase after desulfurization.

4.2.3.3 Oxidative Desulfurization Experiments (ODS)

Similar to EDS experiments, the oxidative desulfurization (ODS) experiments were also conducted in a 50 mL glass conical flask. In these experiments, 0.4 mL of H_2O_2 (oxidising agent) was added to 10 mL of model fuel (volume ratio O/S of the H_2O_2 to the model fuel was 1:25, where O is the volume of the oxidant and S is the total volume of the model fuel, equal to the total volume of S-compounds used in the experiment). Thereafter, 10 mL of IL was added (volume ratio of IL to

model fuel = 1:1) and the mixture was stirred vigorously at 25 °C using a magnetic stir plate. Similar to EDS experiments, a sample volume was collected every 15 min for 2 h. After phase separation the sulfur content of the upper phase (model fuel phase) was analyzed by HPLC.

4.2.3.4 Oxidation-Extraction Desulfurization Experiments (OEDS)

For the oxidation-extraction desulfurization (OEDS) experiments, a solution of the model fuel (containing DBT and 4,6-DMDBT) (15.0 mL) was mixed with the IL (15.0 mL) (volume ratio of model fuel and IL was 1:1). Thereafter, a solution of H₂O₂ was added to the liquid mixture (0.4 mL) (O/S volume ratio = 2:75, where O is the volume of H₂O₂ and S is the total volume of DBT and 4,6-DMDBT). The resulting mixture was stirred at 25°C. A sample was collected every 15 min for 2 h (extraction time periods). As described previously, the IL phase and model fuel phase were subsequently separated by using a separatory funnel. Samples were collected from both the phases for analysis to define the oxidation extraction desulfurization efficiency. OEDS experiments were conducted under different operating conditions to maximize the sulfur removal efficiency.

OEDS of DBT and 4,6-DMDBT at $T=25^{\circ}\text{C}$ and volume ratio H₂O₂ to model fuel = 1/37.5 were triplicated to test the repeatability of the experimental results. Results indicated that extremely good repeatability was obtained with the errors of the desulfurization efficiency less than $\pm 1.0\%$ for both DBT and 4,6-DMDBT.

4.2.4 Recycling of the IL

After the all the desulfurization experiments, the ionic liquid separated from the model oil phase is regenerated for recycling by employing two paths of purification. At first, the ionic liquid placed into the distillation system in an oil bath at 160°C for 4 h to remove H₂O₂ [Figure 4.3](#). This was

followed by re-extraction using tetrachloromethane at 30°C for 30 minutes in an incubator shaker (New Brunswick Scientific, Innova 43), with the volume ratio of IL to tetrachloromethane (or carbon tetrachloride; CCl₄) being 1:1. The mixture was left still for 10 minutes for the phases to separate. The regenerated IL was collected after phase separation and subsequently analysed for its purity using ¹H-NMR, and ¹³C-NMR.

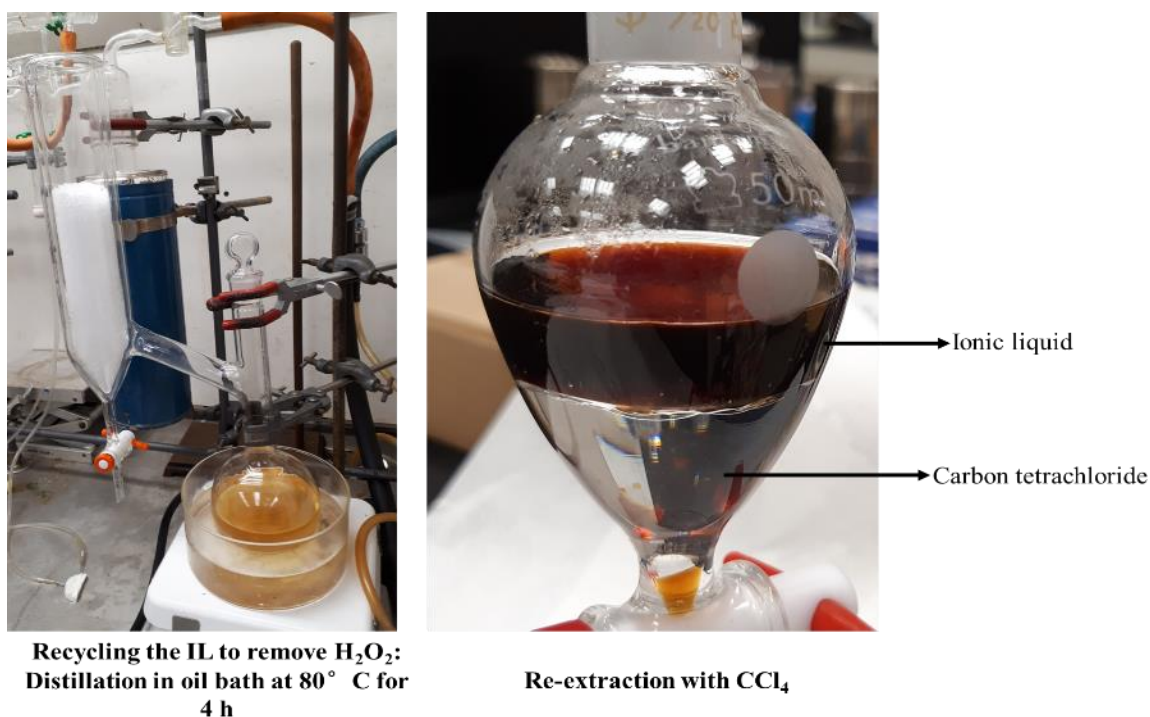


Figure 4.3: Laboratory set-up for recycling ILs.

4.2.5 Desulfurization of Aromatic Compounds from Diesel Fuel by IL

Real diesel fuel, containing 1000 ppm DBT, was treated with ([CH₂COOHPy] [HSO₄]) to test extraction ability of the IL in real hydrocarbon feedstock. The extractions were conducted for 2, 4, 6, 8, 10, 15, 20, 25, 30, 35, 40, 45, 50, and 60 min at 25 °C with a fixed volume ratio (0.6:10)

of IL to diesel fuel (1.2 mL: 20 mL) and a H₂O₂ (0.066 mL) to diesel fuel (20 mL) volume ratio (O/S) of 1:300.

4.3 Analytical Methods

4.3.1 Proton Nuclear Magnetic Resonance (hydrogen-1 NMR, or ¹H-NMR) and Carbon-13 NMR (¹³C-NMR)

The synthesized ionic liquid product ([CH₂COOH] [HSO₄]) was characterized by NMR and IR analyses. The ¹H-NMR and ¹³C-NMR spectra of ([CH₂COOH] [HSO₄]) were recorded on Bruker Advance 300 MHz spectrometer. Deuterium oxide (D₂O) was used as the solvent.

4.3.2 Agilent 1260 High Performance Liquid Chromatography-UV Spectroscopy

Agilent 1260 HPLC-UV, together with UV-vis detector was used for measuring S-compound concentrations in oil. Analysis was conducted on the aromatic hydrocarbon compounds while in the oil phase using a Zorbax Eclipse Plus C18 Rapid Resolution 4.6 × 100 mm, 3.5 micron. Solvent composition was H₂O w 0.1% is 15.0% formic acid, with Acetonitrile (ACN) of 85.0%. Flow rate was 1.0 mL/min, injection volume was 10.00 μL, and stop time was 15.00 min. Further, the spectrum range WL was between 190.0 nm and 460.0 nm.

The S-compound quantities in the model fuel were measured based on peak areas that corresponded with the HPLC chromatography sulfur species. As presented in Index A, in order to obtain a calibration curve, HPLC setup and multi-standard solution with BT, DBT and 4,6 DMDBT concentrations of 200.0 ppm, 150.0 ppm, 100.0 ppm, 75.0 ppm, 50.0 ppm, and 25.0 ppm in n-hexadecane were utilized. Retention time chromatograms measuring BT, DBT and 4,6 DMDBT were 1.674, 2.465 and 4.485 minutes, respectively. Different wavelengths were used to

quantify the S-compound concentrations in both model and diesel fuel. The optimal wavelength was found to be 284 nm.

4.4 Results and Discussion

4.4.1 $^1\text{H-NMR}$ and $^{13}\text{C-NMR}$ Characterization of $[\text{CH}_2\text{COOHPy}][\text{HSO}_4]$

The synthesized ($[\text{CH}_2\text{COOHPy}][\text{HSO}_4]$) ionic liquid was analyzed by $^1\text{H-NMR}$ and $^{13}\text{C-NMR}$ techniques and the spectra are shown in [Figure 4.4 A](#) and [B](#), respectively. The δ values of $^1\text{H-NMR}$ and $^{13}\text{C-NMR}$ of the synthesized ionic liquid ($[\text{CH}_2\text{COOHPy}][\text{HSO}_4]$) in this work are consistent with those reported.^{16, 17} $^1\text{H-NMR}$ (300 MHz, Deuterium Oxide) δ 8.41 (dd, $J = 6.6, 1.6$ Hz, 2H), 8.23 (td, $J = 7.9, 1.5$ Hz, 1H), 7.78 – 7.62 (m, 2H), 5.13 (d, $J = 5.6$ Hz, 2H) ppm. $^{13}\text{C-NMR}$ (75 MHz, Deuterium Oxide) δ 168.42, 146.62, 145.40, 127.85, 60.50 ppm. From the $^1\text{H-NMR}$ of the compound, we can see that there is a signal at 5.13 ppm for $-\text{CH}_2\text{COOH}$ proton. Generally, $>\text{CH}_2$ protons are observed at 1.2-1.3 ppm but the high electron withdrawing effect of the carboxylic acid group increases their chemical shift value towards a higher range. In pyridine, nitrogen withdraws electron from the ring through resonance, as a result of which, positive charge is generated on 2, 4, and 6 carbons. The hydrogens attached to these carbons are highly de-shielded. This de-shielding is greater than that for the benzene ring protons. The protons attached to 2, 6 carbons have a shift of 8.41 ppm and the proton attached to 4 carbons has a shift of 8.23 ppm. The resonance of the benzene ring is shown below. Again, the protons attached to 3 and 5 carbons protons are also more de-shielded than those on the benzene ring because of the electron withdrawal. However, they are slightly more shielded than the protons attached to carbons 2, 4, and 6 since positive charge is not developed directly on these carbons because of resonance. Hence, we get the observed pattern for the $^1\text{H-NMR}$.

In the ^{13}C NMR spectrum [Figure 4.4 B](#), a similar pattern can be observed. The CH_2COOH carbon comes at 60.50 ppm which is shifted to high field values because of electron withdrawal. The resonance of the pyridine ring again plays a major role in determining the NMR spectra. The 2 and 6 carbons come at 145.40 and the 4 carbon comes at 146.62 ppm. Meanwhile, the 3 and 5 carbons come at a slightly lower value than the other carbons at 127.85 ppm. Normal benzene ring carbons come between 122–123 ppm but because of the nitrogen atom in the pyridine ring the chemical shifts change to the observed values. Now, the carbonyl group of carboxylic acid group comes at 168.42 ppm, which is consistent with the expected shift value for carboxylic acid.

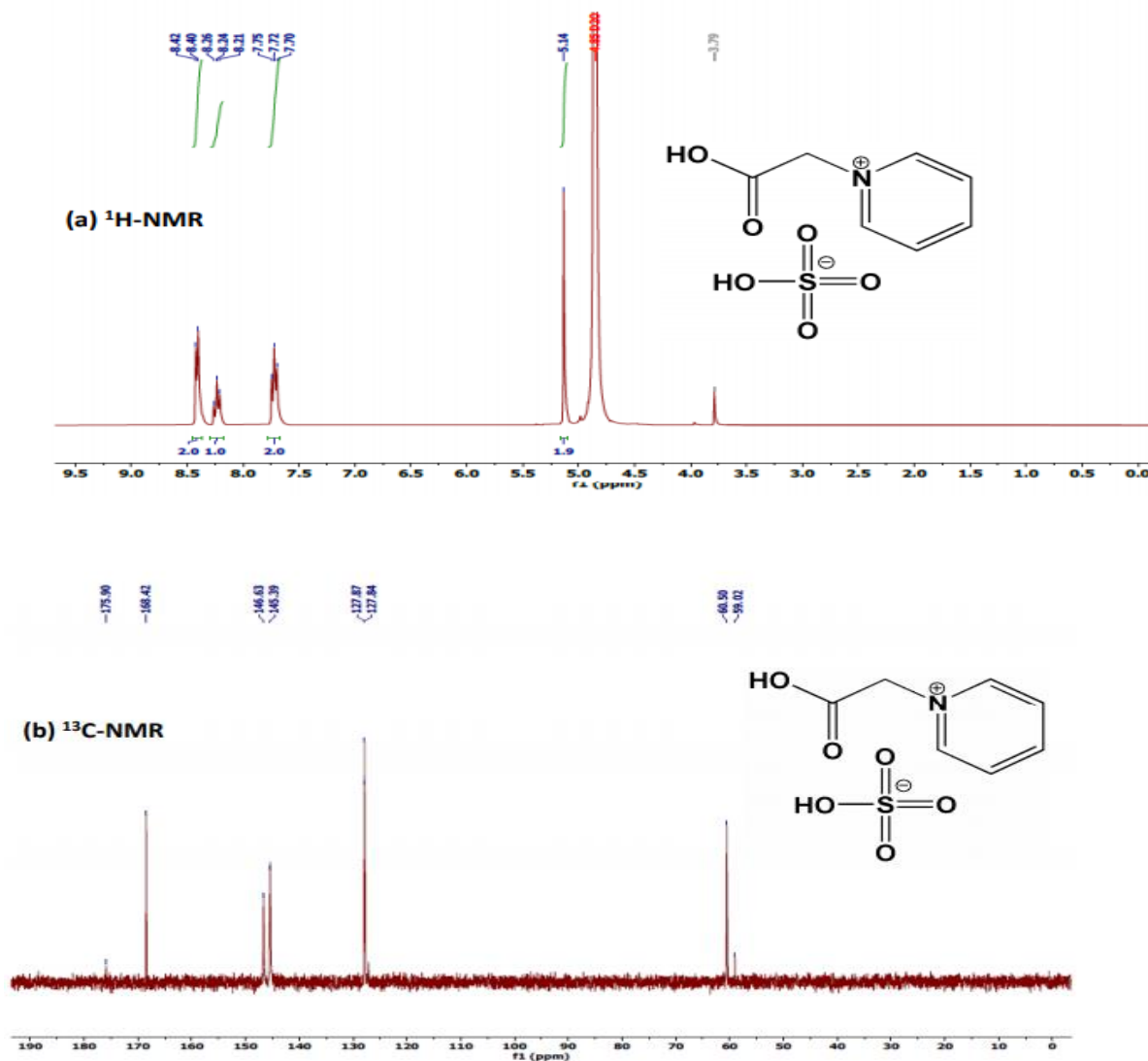


Figure 4.4: (a) ^1H -NMR (300 MHz, Deuterium Oxide), (b) ^{13}C -NMR (75 MHz, Deuterium Oxide)) spectra of $[\text{CH}_2\text{COOHPy}] [\text{HSO}_4]$.

4.4.2 Effect of Operating Parameters on Desulfurization Efficiency

EDS, ODS and OEDS of DBT were carried out at moderate conditions in this study. The effects of key operating parameters, such as extraction time, extraction temperature, IL to model fuel ratio and dosage of H_2O_2 on the desulfurization efficiency were investigated and are discussed in the following sections.

4.4.2.1 Effect of Extraction Mode

The removal rates of DBT by different extraction modes via the ODS, EDS, and OEDS desulfurization methods were investigated and compared in the present study. The initial DBT concentration was 1,000 ppm under ambient (room) temperature. [Figure 4.5](#) shows that $[\text{CH}_2\text{COOHPy}] [\text{HSO}_4]$ is effective for DBT removal from model fuels, with the highest removal (desulfurization) efficiency in the OEDS process, reaching a plateau (equilibrium) in 20 min at ambient temperature. Nonetheless, both EDS and ODS are not able to completely remove DBT removal from model fuels. Extraction of DBT by $[\text{CH}_2\text{COOHPy}] [\text{HSO}_4]$ in EDS process is very fast, with a final removal efficiency of 40%. On the contrary, ODS was not effective in removing DBT, leading to a maximum desulfurization efficiency of only around 2.7%. In this regard, OEDS was adopted in the following study to remove DBT and 4,6-DMDBT from model fuel and diesel.

From these trends as displayed in [Figure 4.5](#), it is clear that both IL and H_2O_2 were necessary for complete desulfurization in the present study. Moreover, the sequence of exposure to IL and the oxidant also matters – IL must be added to the fuel first, followed by H_2O_2 . In EDS experiments, no oxidant was added; in ODS experiments, the IL was added after the oxidant; and finally, in OEDS experiments, the IL was added first, followed by the oxidant. Thus, in EDS, the desulfurization observed was only enabled by extraction of DBT by the IL. There was no oxidation

involved, which is why the efficiency was much lower 40% compared to OEDS, nearly 100% [Figure 4.5](#). In ODS, initially, there was no catalyst present to help oxidize the DBT in the fuel phase, nor was there an extractant that can sequester the DBT molecules. Therefore, when the IL is added afterwards, it begins to be oxidized before it can complete the extraction of DBT molecules into the IL phase. Thus, both the IL phase and fuel phase are likely to have oxidized DBT residues when ODS is used. This is why the desulfurization efficiency was the poorest in this case, less than 3%.

Finally, in OEDS, both the IL and the oxidant are present. The $[\text{CH}_2\text{COOHPy}][\text{HSO}_4]$ acts as both a catalyst and an extractant. Since the IL is added first, it acts as an extractant and sequesters the DBT from the fuel phase into the interface of the fuel and IL phases. Upon the subsequent addition of H_2O_2 , the IL also acts as a catalyst for the oxidation reaction. The IL's cationic carboxyl groups are oxidized into peroxy-carboxyl groups which then bring about the oxidation of DBT to DBTO and DBTO_2 . This achieves a high desulfurization efficiency of close to 100% [Figure 4.5](#).

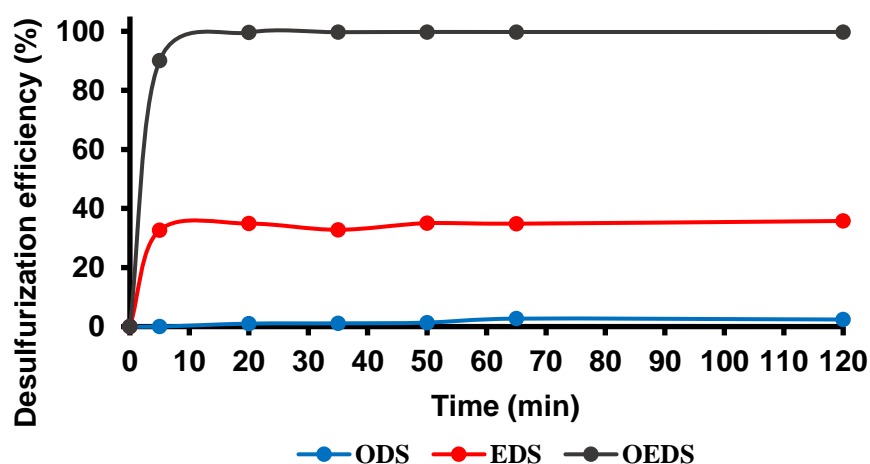


Figure 4.5: Desulfurization of model fuel by $([\text{CH}_2\text{COOHPy}][\text{HSO}_4])$ at different extraction times. Reaction conditions: volume ratio (IL: DBT): 1:1, T: 30 °C, (V) H_2O_2 : 0.4mL.

4.4.2.2 Effect of IL to Model Fuel Volume Ratios

It is evident from the previous study that the volume ratios of the IL to the model fuel as well as H₂O₂ to the model fuel strongly affect desulfurization efficiency. The first set of data that support this point is shown in [Figure 4.5](#). In contrast to EDS (for which the volume ratio of H₂O₂ to the model fuel was 0 as it did not have H₂O₂ and IL to model fuel was 1:1; 15 ml of both IL and model were used), the DBT removal rate for OEDS (for which the volume ratio of H₂O₂ to the model fuel was 2:75; 0.4 ml of H₂O₂ and 15 ml of model fuel was added, and IL to model fuel was 1:1; 15 ml of both IL and model fuel was used) is significantly higher at the same operating parameters. Phase equilibrium is achieved after just 20 min and desulfurization efficiency is 99.7%. Moreover, both EDS and OEDS have significantly higher desulfurization rates than ODS, which has an H₂O₂ to model fuel volume ratio of 1:25; 0.4 ml of H₂O₂ and 15 ml of model fuel was added, and IL to model fuel ratio of 1:1).

4.4.2.3 Effect of Oxidant Dosage on the Sulfur Removal Efficiency

In OEDS processes, H₂O₂ is used as an oxidant. the dosage of H₂O₂ affects both the oxidization reaction and the level of peroxy-carboxyl in the system, which consequently impacts desulfurization efficiency.¹⁴ Thus, the H₂O₂ dosage needs to be optimized to achieve a high sulfur removal rate and lower desulfurization costs. In this study, the impact of oxidant dosage on sulfur removal (DBT) was determined using different H₂O₂/model fuel (sulfur) volume ratio (O/S).¹⁴ At lower O/S ratio (1:300), a desulfurization efficiency of approximately 99.9% was reached within 50 min [Figure 4.6](#). At a much (8-fold) higher O/S ratio (8:300), a desulfurization efficiency of 99.91% was reached within 5 min of reaction time [Figure 4.7](#).

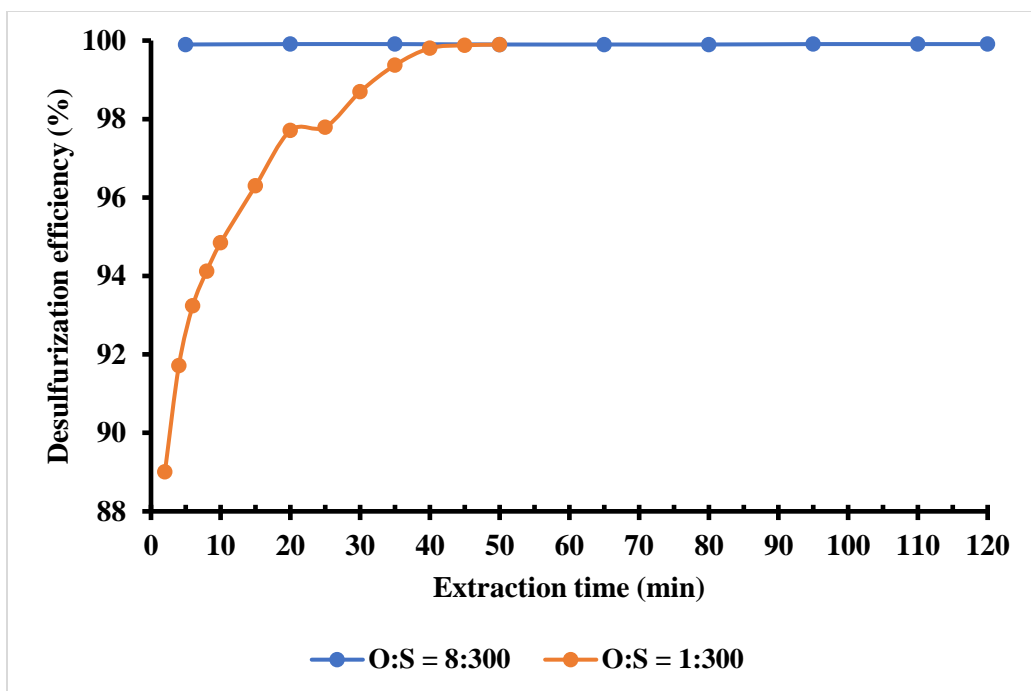


Figure 4.6: Desulfurization efficiency of OEDS at H₂O₂: model fuel (O:S) volume ratio of 1:300; temperature = 25°C at different extraction times.

4.4.2.4 Effect of Sulfur Species on Sulfur Removal

To examine the desulfurization efficiency of [CH₂COOHPy] [HSO₄], a range of sulfur compounds, including DBT, and 4,6-DMDBT, were used as substrates. Desulfurization efficiency data for DBT and 4,6-DMDBT are shown in Figure 4.7. These data exhibit the same trend in both the sulfur compounds, where the model oil's sulfur removal initially experiences a sharp rise, followed by a slow decline. Note that triplicate data was obtained only for three time points (20 min, 35 min and 50 min) and standard deviations were found to be low (below 0.5 % of the mean values), indicating high reproducibility of experimental conditions. When combined with catalytic oxidation, sulfur removal decreased as follows: 4,6-DMDBT ≥ DBT. While sulfur removal efficiency for DBT and 4,6-DMDBT reached nearly 100% (99.9%) within 20 min, this very close difference could be caused by the sulfur compounds' aromatic π -electron density.¹⁶ Overall, the

results show that [CH₂COOHPy] [HSO₄] are capable of removing both DBT and 4,6-DMDBT from model fuel.

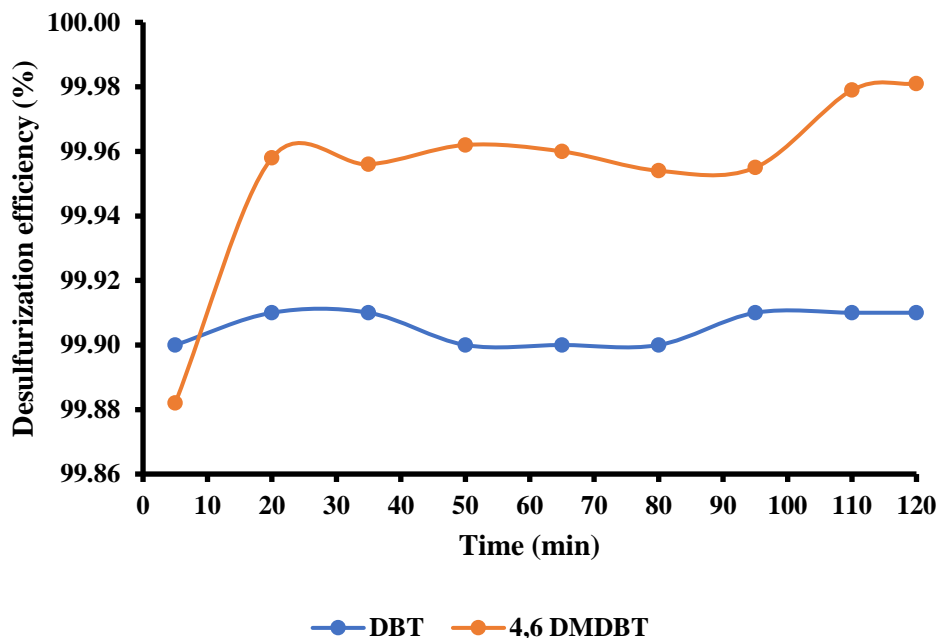


Figure 4.7: Desulfurization efficiency of OEDS at volume ratio of H₂O₂ to model fuel = 2:75, temperature = 25 °C at different extraction times.

4.4.3 Desulfurization of DBT from Diesel Fuel by Using Acidic IL

As can be noted from [Figure 4.8](#), the desulfurization efficiency for DBT reached 88.7% by the extraction time of 2 min and increased further to 91.3% by 8 min. Thereafter, this efficiency remained stable around 89% until it rose to 92% at the extraction time of 40 min. Finally, the sulfur removal became stable around 89% until the end of the experiment at 60 min.

[Figure 4.8](#) shows that the amount of DBT extracted by using the IL [CH₂COOHPy] [HSO₄] is significantly lower for real diesel fuel (peak desulfurization 90.3%) when compared to that extracted from the model oil (n-hexadecane; peak at 99.9%) under the same conditions. A similar trend was also observed in Chapter 3 with the IL [BPy][BF₄]. It should be noted that real diesel

fuel contains a mixture of components, including paraffinic, aromatic, alkyl aromatic and a range of polyaromatic hydrocarbons, which may be partially miscible in IL. This may reduce the selectivity of ([CH₂COOHPy] [HSO₄]) towards DBT, similar to [BPy][BF₄].

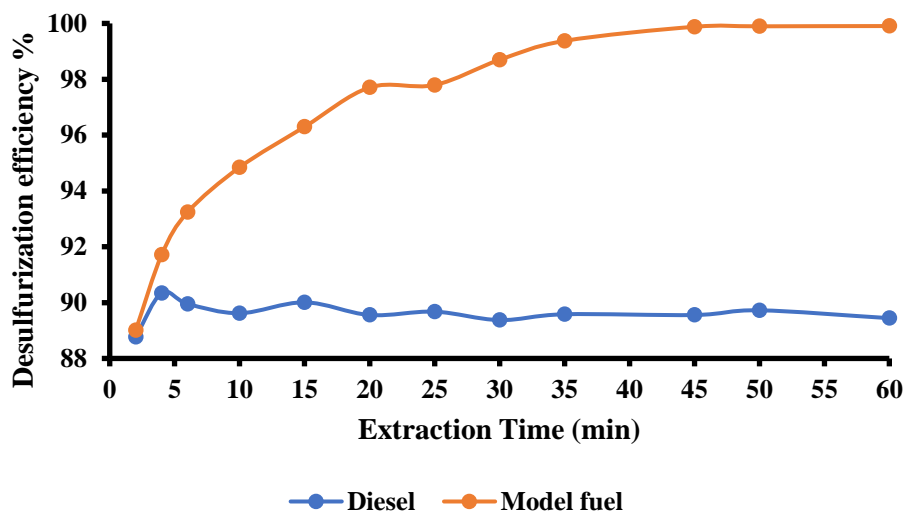


Figure 4.8: Desulfurization of DBT in model fuel and real diesel as a function of extraction time. Reaction conditions: V DBT= 20ml; V(IL)=1.2 ml, T= 25 °C; O/S=6. Standard deviation bars present only for three time points (t = 10 min, 15 min and 20 min); n = 3.

4.4.4 Recycling of Used IL

Figures 4.9 and 4.10 respectively show the ¹H-NMR and ¹³C-NMR spectra of the IL recycled after completion of the extraction cycles. These spectra highlight the purity of the recycled IL. The IL regenerated after the first desulfurization cycle was reused to remove DBT from the model fuel (hexadecane) and real diesel fuel under the same reaction parameters in the next oxidation-extraction desulfurization cycle and so on, until 10 regeneration cycles. NMR spectra of the recycled IL obtained at the end of each desulfurization cycle revealed that there was no significant change in the structure of the IL. This is consistent with the observations reported in previous studies.^{16,17} Zhang et al. reported maintenance of desulfurization efficiency of [CH₂COOHPy] [HSO₄] for up to 6 regeneration cycles.¹⁶ It should be noted that this study had used DBT dissolved

in *n*-octane as the model oil, and the optimum reaction temperature was found to be 50°C, which is significantly higher than 25°C temperature used in the present study.¹⁶

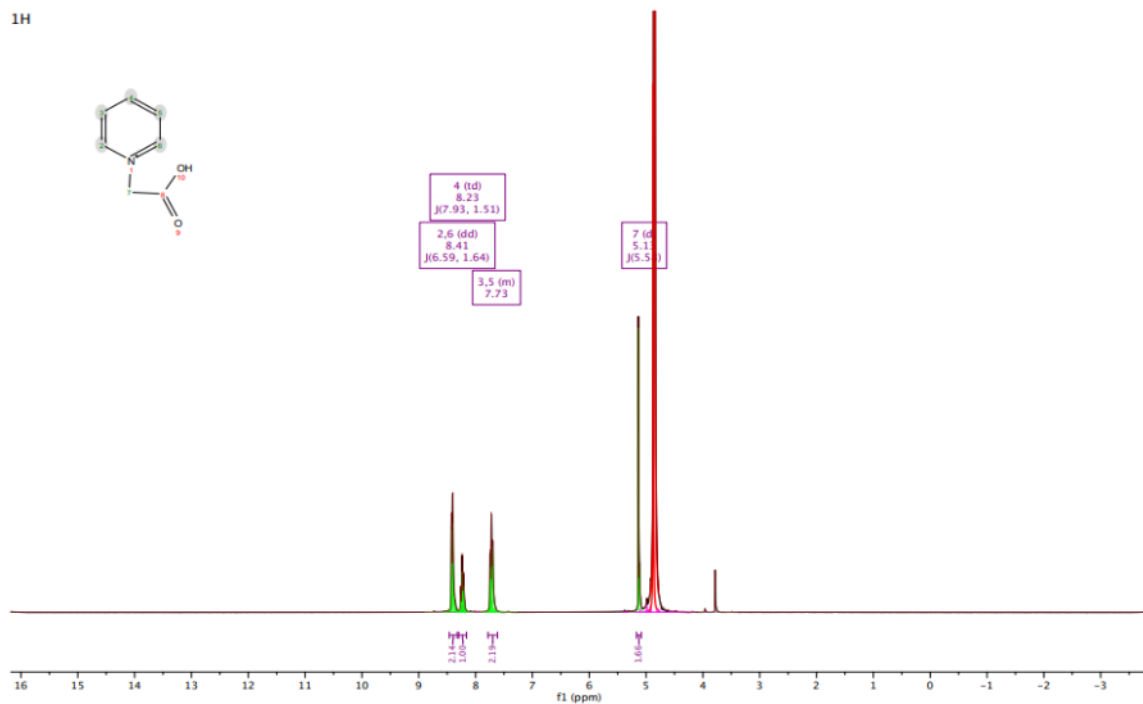


Figure 4.9: ¹H-NMR spectrum of the recycled IL.

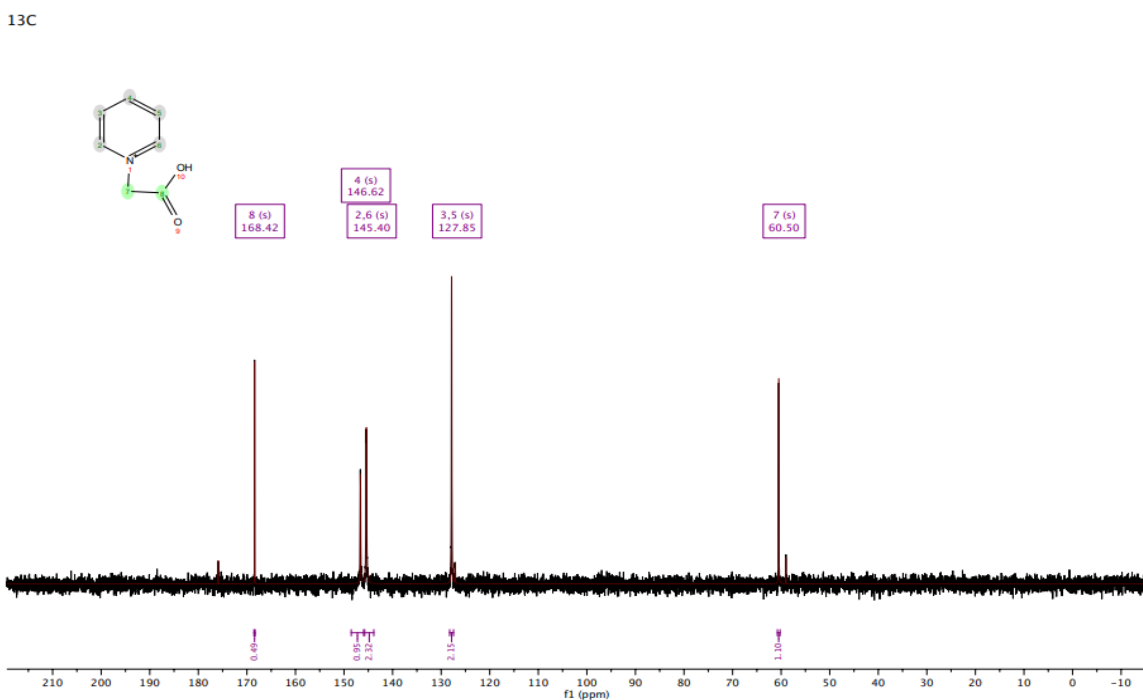


Figure 4.10: ^{13}C -NMR spectrum of the recycled IL.

In the present study, the IL $[\text{CH}_2\text{COOHPy}][\text{HSO}_4]$ was recycled 10 times and after each recycling step, it was tested for its desulfurization efficiency using a model fuel. [Figure 4.11](#) shows the variation in desulfurization efficiency with each recycling step. It can be observed that recycling did not significantly affect the ability of the IL to remove sulfur from the model fuel since desulfurization efficiency varied only minimally within the tight range of 98.2 % - 99.5 % over the 10 cycles. This result is consistent with previous one reported by Zhang and co-workers.¹⁷

However, recycling did have an impact on the IL's ability to remove sulfur from real diesel fuel, as can be seen in [Figure 4.11](#). DBT removal from the model fuel was significantly higher and near-constant during the 10 cycles at an extraction time of 40 min. However, the efficiency of DBT removal from the diesel fuel at the first recycle was already lower (92.7 %) than that noted for the model fuel (99.2 %). As the number of recycling and reuse cycles increased, the desulfurization efficiency (for DBT removal from real diesel) decreased, reducing to 76.6 % at the 10th cycle. This could be because, as also noted earlier, real diesel fuel contains a mixture of components, including paraffinic, aromatic, alkyl aromatic and a range of polyaromatic hydrocarbons, which may be partially miscible in IL and may not be removed during IL recycling via rotary evaporation and CCl_4 -based re-extraction. Consequently, as more impurities will keep getting added to the IL at each stage of reuse, there is likely to be a progressive reduction in the selectivity of $[\text{CH}_2\text{COOHPy}][\text{HSO}_4]$ towards DBT.

Previous studies have followed different re-extraction protocols to recycle the used IL $[\text{CH}_2\text{COOHPy}][\text{HSO}_4]$. Typically, water and H_2O_2 can be removed from the used ILs via rotary evaporation, followed by a re-extraction using CCl_4 .¹³ In the present study, exhausted IL was recycled by two different methods: (1) a two-step recycling which involved distillation to remove

residual H_2O_2 and followed by re-extraction by CCl_4 to remove residual DBT; and (2) only re-extraction by CCl_4 to remove the DBT. The desulfurization efficiency of the IL recycled by the two methods was measured for up to 10 cycles of desulfurization and re-extraction using real diesel fuel [Figure 4.12](#). IL recycled using only a single-step re-extraction exhibited a higher desulfurization efficiency that was maintained across the 10 cycles of recycling and reuse (range: 97.4 % to 98.8 %). However, IL recycled using the two-step method (of H_2O_2 removal followed by re-extraction) showed a relatively lower desulfurization efficiency (92.7 %) in the first cycle, and this efficiency continued to decrease as the cycle number increased, reducing to 76.7 % by the 10th cycle. This is most likely there could be some amount (however small) of residual H_2O_2 in the single-step recycled IL, which may increase desulfurization efficiency [Figure 4.13](#). Indeed, as shown previously in [Figures 4.6 and 4.7](#), a higher oxidant dosage can result in a near 100 % desulfurization within 5 min, while lower amounts of H_2O_2 achieve this desulfurization efficiency in longer times (50 min in the present study). On the other hand, in the two-step recycling method, residual oxidant is removed and thus cannot contribute to this higher efficiency of desulfurization.

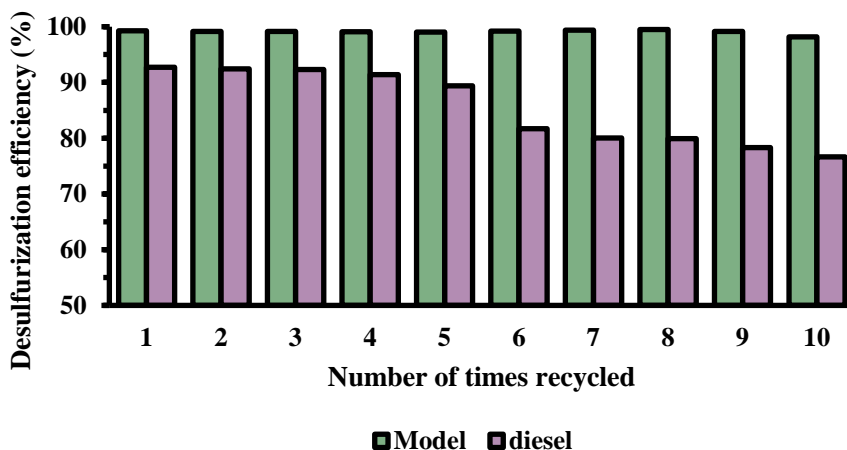


Figure 4.11: Desulfurization efficiency of OEDS of DBT under the following reaction conditions: volume ratio of H_2O_2 to oil fuel = 2:75, IL= 1.2 mL, temperature = 25 °C at extraction time 40 min.

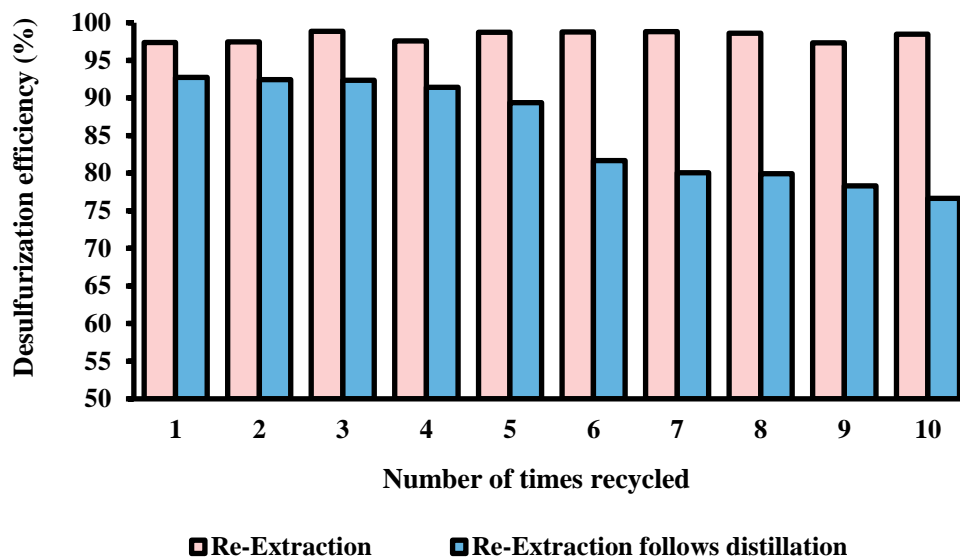


Figure 4.12: Desulfurization efficiency of OEDS of DBT under the following reaction conditions: volume ratio of H₂O₂ to real diesel fuel = 2:75, IL= 1.2 mL, temperature = 25°C at extraction times 40 min.

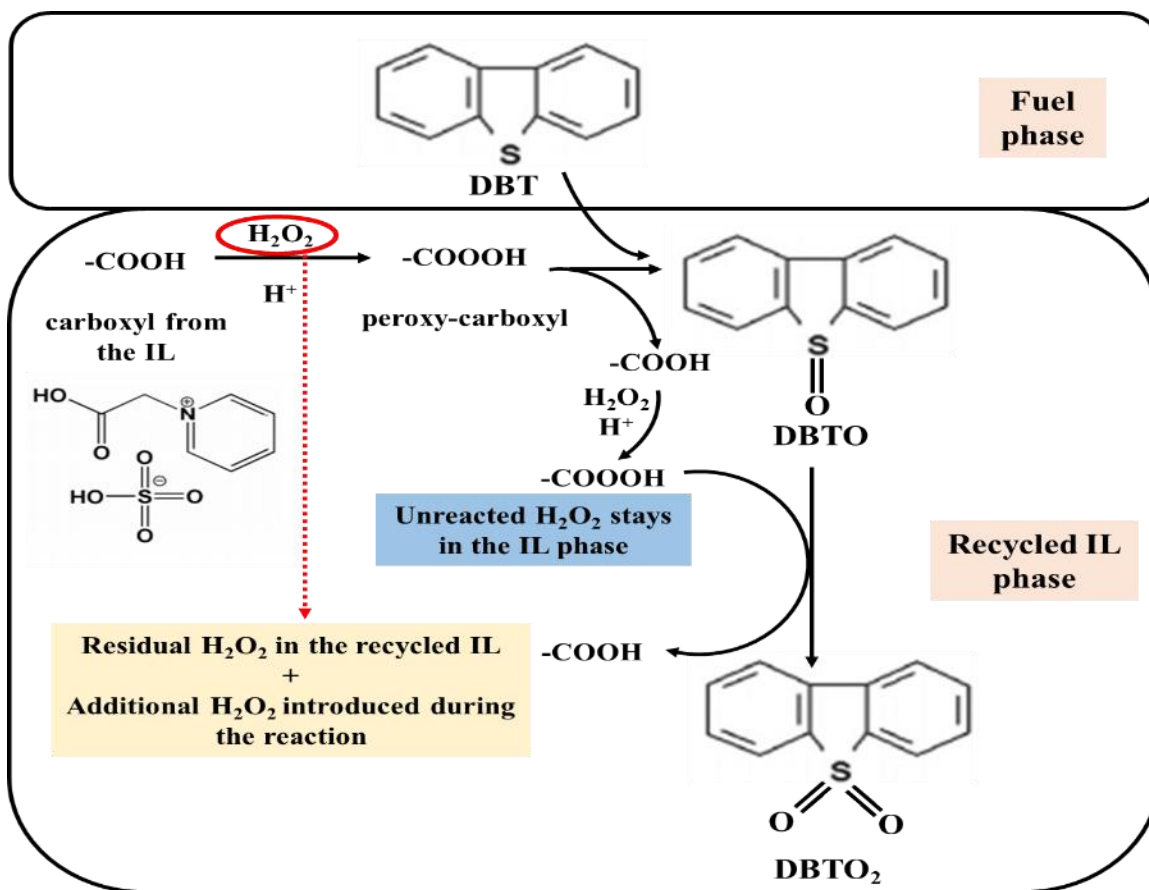


Figure 4.13: Desulfurization of DBT using recycled IL that has residual H₂O₂.

4.5 Conclusion

This study investigated the desulfurization efficiency of the IL [CH₂COOHpy] [HSO₄], using both a model fuel (DBT in n-hexadecane) and real diesel as substrates. The effect of various reaction parameters was studied, including the nature of IL application (ODS, EDS and OEDS processes), the extraction time, the type of sulfur-containing compound extracted DBT and 4,6-DMDBT, the concentration of oxidant (H₂O₂) used, and the phase ratios of IL, sulfur-containing compounds and H₂O₂. It was found that the OEDS technique results in the highest and the quickest removal of sulfur from the model fuel. An extraction time of 40 min was found to be the optimal desulfurization time for OEDS, resulting in DBT the highest sulfur removal by the desulfurization process, followed closely by 4,6-DMDBT (99.9% for both). Moreover, desulfurization was significantly higher in the model fuel compared to the real diesel fuel, probably owing to the other contaminants found in diesel that may affect the selectivity of IL towards DBT. It was also found that recycling of the IL resulted in a significant drop in desulfurization efficiency after 4 regeneration cycles in the case of real diesel fuel, while the efficiency was maintained for at least 10 cycles in the case of model fuel. Furthermore, two-step recycling, which involved distillation to remove residual H₂O₂ followed by re-extraction by CCl₄ to remove residual DBT, resulted in lower desulfurization efficiency than one-step recycling where no distillation was involved. This was most likely due to the presence of residual H₂O₂ after one-step recycling.

References

1. The European Parliament and the Council of the European Union. Directive 2003/17/EC of the European Parliament and of the Council of 3 March 2003 amending Directive 98/70/EC relating to the quality of petrol and diesel fuels. *Official Journal of the European Union* L76 (2003), 10-19.
2. Yongming, A.G.Z.T.C., Chenguang, Z.J.L.Y.L. Nonhydrodesulfurization technologies of light oil, *Progress in Chemistry* 19 (2007), 1331.
3. Babich, I.V., Moulijn, L.A. Science and technology of novel processes for deep desulfurization of oil refinery streams: a review, *Fuel* 82 (2003), 607-631.
4. <http://www.epa.gov/otaq/regs/fuels/diesel/diesel.htm>, accessed: April 2020
5. <http://www.dieselnet.com/standards/eu/fuel.php>, accessed: April 2020
6. Zhang, J.C., Song, L.F., Hu, J.Y., Ong, S.L., Ng, W.J., Lee, L.Y., Wang, Y.H., Zhao, J.G., Ma, R.Y. Investigation on gasoline deep desulfurization for fuel cell applications, *Energy Conversion and Management* 46 (2005), 1-9.
7. Holbrey, J.D., López-Martin, I., Rothenberg, G., Seddon, K.R., Silvero, G., Zheng, X. Desulfurization of oils using ionic liquids: selection of cationic and anionic components to enhance extraction efficiency, *Green Chemistry* 10 (2008), 87-92.
8. Bösmann, A., Datsevich, L., Jess, A., Lauter, A., Schmitz, C., Wasserscheid, P. Deep desulfurization of diesel fuel by extraction with ionic liquids, *Chemical Communications* 23 (2001), 2494-2495.
9. Kulkarni, P.S., Branco, L.C., Crespo, J.G., Nunes, M.C., Raymundo, A., Afonso, C.A. Comparison of physicochemical properties of new ionic liquids based on imidazolium, quaternary ammonium, and guanidinium cations, *Chemistry – A European Journal* 13 (2007), 8478-8488.
10. Kulkarni, P.S., Afonso, C.A.M. Deep desulfurization of diesel fuel using ionic liquids: current status and future challenges, *Green Chemistry* 12 (2010), 1139–1149.
11. Gao, H., Li, Y., Wu, Y., Luo, M., Li, Q., Xing, J., Liu, H. Extractive desulfurization of fuel using 3-methylpyridinium-based ionic liquids, *Energy & Fuels* 23 (2009), 2690-2694.
12. Holbrey, J.D., Reichert, W.M., Nieuwenhuyzen, M., Sheppard, O., Hardacre, C., Rogers, R.D. Liquid clathrate formation in ionic liquid–aromatic mixtures. *Chemical Communications* 4 (2003), 476-477.
13. Holbrey, J.D., López-Martin, I., Rothenberg, G., Seddon, K.R., Silvero, G., Zheng, X. Desulfurization of oils using ionic liquids: selection of cationic and anionic components to enhance extraction efficiency, *Green Chemistry* 10 (2008), 87-92.

14. Su, B.-M., Zhang, S., Zhang, Z.C. Structural elucidation of thiophene interaction with ionic liquids by multinuclear NMR spectroscopy, *The Journal of Physical Chemistry B* 108 (2004), 19510-19517.
15. Lo, W.-H., Yang, H.-Y., Wei, G.-T. One-pot desulfurization of light oils by chemical oxidation and solvent extraction with room temperature ionic liquids. *Green Chemistry* 5 (2003), 639-642.
16. Zhang, C., Feng, W., Pan, X.Y., Liu, X.Q. Study of extraction-oxidation desulfurization of model oil by acidic ionic liquid, *Journal of Fuel Chemistry and Technology* 39 (2011), 689-693.
17. Zhang, C., Pan, X., Wang, F., Liu, X. Extraction-oxidation desulfurization by pyridinium-based task-specific ionic liquids. *Fuel* 102 (2012), 580-584.

Chapter 5: Molecular Simulation Using Density

Functional Theory

5.1 Introduction

To better understand the process of desulfurization by an IL, it is important to study the interaction of aromatic sulfur compounds in fuel with ILs. As discussed in Chapter 2, DFT is an important and effective means to conduct such studies. In DFT, the energy in an electron system is formulated in terms of its density: $E=E(\rho)$.¹ Further, with DFT, quantum problems may be reformulated as mono-particle problems instead of multi-particle ones simply by using the electron density function rather than the wave function.² This makes it easier to understand inter-atomic interactions. Indeed, the main reason to utilize DFT for IL-fuel interaction analysis in the context of desulfurization is to predict bond energies (or interaction energies) between atoms by applying quantum mechanics principles.^{3,4}

5.2 A DFT Study on Oxidative and Extractive Desulfurization by ILs

5.2.1 N-Butyl-Pyridinium Tetrafluoroborate ([BPy][BF₄]) IL

5.2.1.1 DFT Calculations

To better understand the interaction action between sulfur-containing compounds dibenzothiophene (DBT) and dibenzothiophene sulfone (DBTO₂) with N-butyl-pyridinium tetrafluoroborate ionic liquid ([BPy][BF₄]), a quantum chemical DFT calculation was carried out. Our primary purpose in this work is to evaluate the experimental extraction efficiency results with calculated DFT interaction energies of the DBT/DBTO₂ by [BPy][BF₄]. All the DFT calculations

were carried out with *Gaussian 09*.⁵ The geometries of all the structures were fully optimized at the B3LYP/6-311++G(d,2p) level of theory in gas phase, hexane and CCl₄ solvent system using the polarized continuum model (PCM). The structures of *N*-butyl-pyridinium cation ion [BPy] interacting with tetrafluoroborate anion [BF₄] at different binding sites were first optimized and the most stable structure of the [BPy][BF₄] was selected. The stable optimized structure of [BPy][BF₄] were further optimized with DBT and DBTO₂ at different binding sites. The interaction energy between the ILs and DBT/DBTO₂ were defined by [Equations 5.1](#) and [5.2](#):

$$\Delta IE = E_{([BPy] \supset [BF_4])} - (E_{([BPy])} + E_{[BF_4]}) \quad (5.1)$$

$$\Delta IE = E_{([BPy][BF_4] \supset DBT/DBTO_2)} - (E_{([BPy][BF_4])} + E_{DBT/DBTO_2}) \quad (5.2)$$

5.2.1.2 Quantitative Results from the DFT Study

The energetically most stable optimized structures of the ([BPy][BF₄], DBT, DBTO₂ and their corresponding complexes ([BPy][BF₄) \supset DBT and ([BPy][BF₄) \supset DBTO₂ are shown in [Figure 5.1](#). The calculated interaction energies are summarized in [Table 5.1](#).

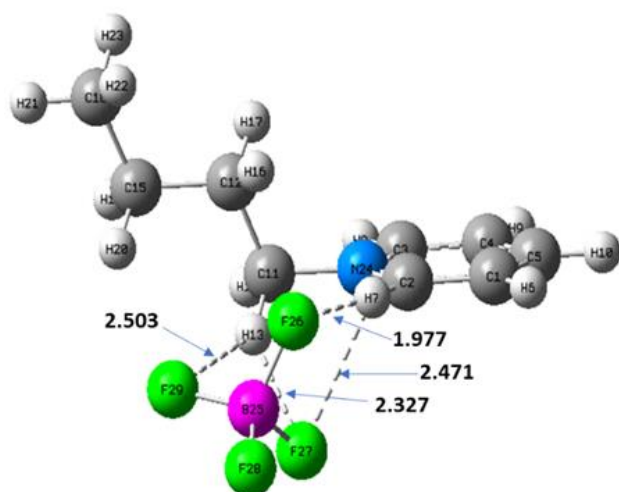
Table 5.1: Calculated interaction energies (Δ IE kJ/mol) for the ionic liquid [BPy][BF₄] with DBT and DBTO₂ sulfur-containing compounds in model fuel (hexane) and CCl₄ solvent system.

	Δ IE, kJ/mol		
	Gas phase	Hexane	CCl ₄
[BPy] \supset [B F ₄]	-336.97	-175.78	-148.43
[BPy][BF ₄] \supset DBT <i>Face to face parallel sandwich</i>	-28.98	-16.48	-14.37
[BPy][BF ₄] \supset DBTO ₂ <i>Face to face parallel-displaced</i>	-50.26	-31.16	-29.07
[BPy][BF ₄] \supset DBT <i>Edge tilted-T-shaped</i>	-27.66	-16.15	-14.69
[BPy][BF ₄] \supset DBTO ₂ <i>Edge tilted-T-shaped</i>	-51.63	-32.67	-28.91

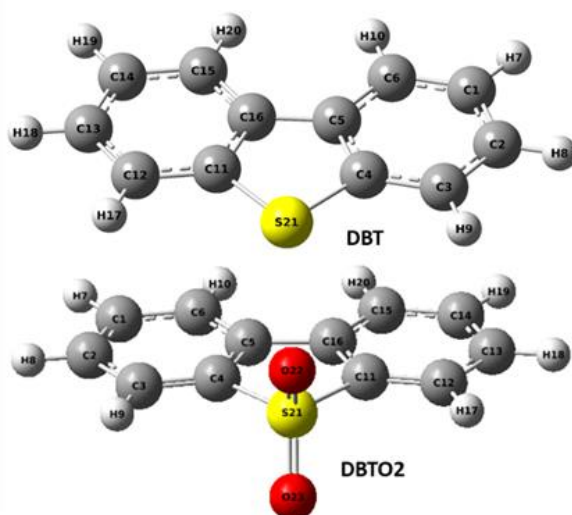
As illustrated in [Figure 5.1](#), the ionic liquid [BPY][BF₄] contains a pyridine ring which has π - π interactions with both DBT and DBTO₂. Non-covalent weak interactions such as π - π interactions, electrostatic interactions, weak hydrogen bonding and hydrophobic lipophilic interactions, play important roles in supramolecular chemistry.⁶ Non-covalent interactions could be the best possible mechanisms for the extraction of the sulfur-containing compounds from the model fuel by the pyridinium-based IL. This is because non-covalent interactions are specific yet non-rigid, allowing recycling of the sulfur-extracting compounds. Aromatic-aromatic interactions (π - π stacking) are generally defined as the attractive noncovalent interactions that occur between the-electronic clouds of aromatic systems in parallel, *face-to-face* or *edge-to-face* orientation interactions.⁴ Hohenstein and Sherrill investigated the effects of heterocyclic aromatic atoms in various configurations of a pyrimidine-benzene complex for their π - π stacking interactions.⁷ They reported that the presence of an electronegative nitrogen heteroatom into an aromatic ring has large effects on similar *stacked*, *parallel-displaced*, and *T-shaped* dimers. [Figure 5.1](#) shows the most stable optimized structures of the ([BPy][BF₄]) \supset DBT/DBTO₂ complexes. There are two types of possible π - π interactions found between [BPy][BF₄] and DBT, resulting in the formation of complexes with *face-to-face parallel-sandwich* [Figure 5.1c](#), and *edge-tilted-T-shaped* [Figure 5.1e](#) geometries. On the other hand, the π - π interactions between [BPy][BF₄] and DBTO₂, lead to *face-to-face parallel-displaced* [Figure 5.1d](#) and *edge-tilted-T-shaped* [Figure 5.1f](#) structures.

The nitrogen atom of the pyridine ring in the ionic liquid draws electrons away from the ring carbon atoms inductively, thereby increasing the positive charges of the pyridinium hydrogen atoms, thus making the pyridine moiety more effective as a “ π -hydrogen bond” donor. In the *face-to-face parallel-sandwich* type interaction ([BPY][BF₄]) \supset DBT as shown in [Figure 5.1c](#), the pyridinium hydrogens form three hydrogen bonds (C2-H7 \cdots F26, C2-H7 \cdots F27 and C11-H13 \cdots F29),

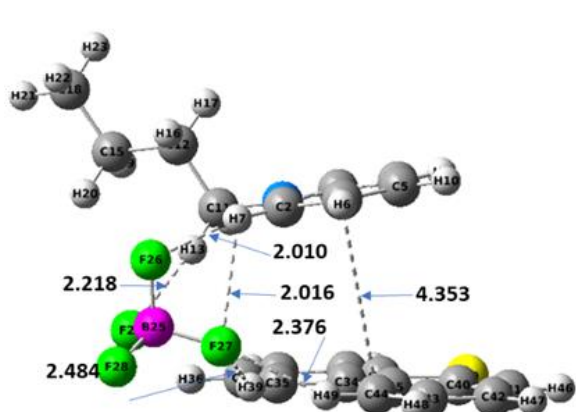
and their bond distances are 2.010 Å, 2.616 Å, and 2.218 Å, respectively. One of the other pyridinium C-H \cdots π -interactions with DBT, particularly PyC1-H6 \cdots C44 (DBT) has 4.353 Å and is almost parallel to the DBT plane, making it possible to form the “sandwich” type arrangement. While the anion [BF₄]⁻ and DBT form weak hydrogen bonding, the bond distances of DBT-C34-H39 \cdots F27 and DBT-C44-H49 \cdots F27 are 2.484 Å and 2.376 Å, respectively.



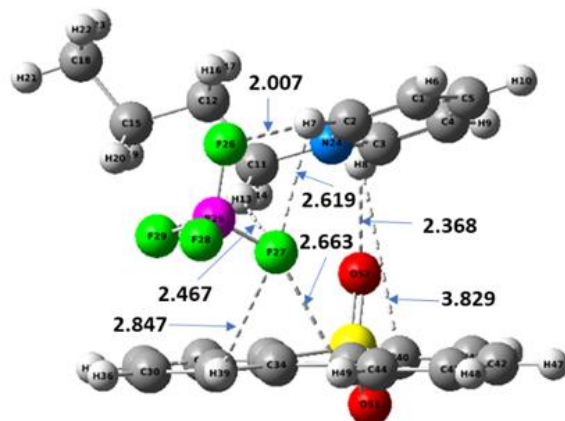
(a) [BPY][BF₄] ionic liquid in hexane



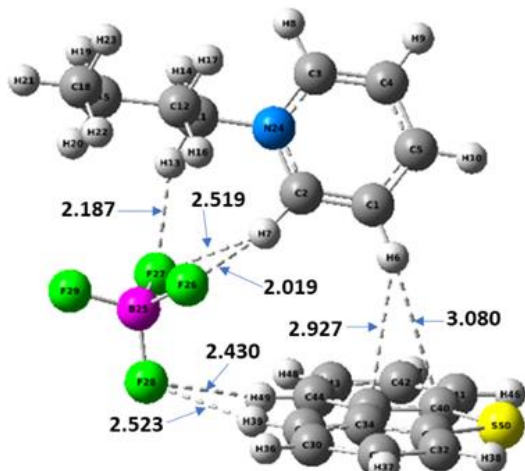
(b) DBT and DBTO₂ in hexane



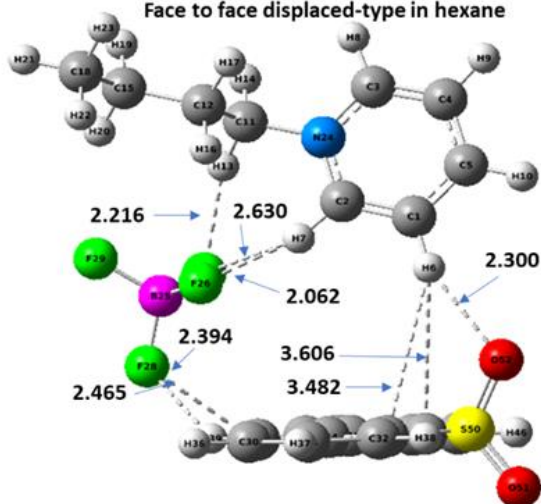
(c) [BPY][BF₄]⊃DBT-complex
Face to face sandwich-type in hexane



(d) [BPY][BF₄]⊃DBTO₂-complex
Face to face displaced-type in hexane



(e) [BPY][BF₄]⊃DBT-complex
Edge tilted-T-shaped geometry in hexane



(f) [BPY][BF₄]⊃DBTO₂-complex
Edge tilted-T-shaped geometry in hexane

Figure 5.1: The geometry optimized structures of [BPY][BF₄], dibenzothiophene (DBT), dibenzothiophene sulfone (DBTO₂), ([BPY][BF₄] ⊃ DBT and ([BPY][BF₄] ⊃ DBTO₂) in hexane solvent system. Color code: carbon = grey; hydrogen= white; nitrogen= blue; oxygen = red; sulfur = yellow, boron = magenta and fluorine = green.

In the *edge-tilted-T-shaped* structure shown in [Figure 5.1e](#), the pyridinium hydrogens form three hydrogen bonds (C2-H7...F26, C2-H7...F27 and C11-H13...F27), with bond distances of 2.019 Å, 2.519 Å and 2.187 Å, respectively. One of the other pyridinium C-H... π interactions with DBT, particularly PyC1-H6, which is almost perpendicular to the DBT plane, makes it possible to form the “T-shaped” type arrangement. The PyC1-H6...C33-DBT and PyC1-H6...C34-DBT bond distances are 2.927 Å and 3.080 Å, respectively. The BF₄⁻ anion and DBT form weak hydrogen bonding, with bond distances of DBT-C34-H39...F28 and DBT-C44-H49...F28 are 2.523 Å and 2.430 Å, respectively. The position of the BF₄⁻ anion is above the side of the pyridinium and DBT plane in the [BPy][BF₄] \supset DBT complex, which therefore creates less steric inhibition between the pyridinium and DBT for both sandwich and T-shaped type arrangements. The interaction energies of [Bpy][BF₄] \supset DBT for *sandwich* and *T-shaped* geometries are -28.99 kJ·mol⁻¹ and -27.66 kJ·mol⁻¹ in the gas phase calculations, -16.48 kJ·mol⁻¹ and -16.15 kJ·mol⁻¹, in the hexane solvent system, and -14.37 kJ·mol⁻¹ and -14.69 kJ·mol⁻¹, in the CCl₄ solvent system, respectively.

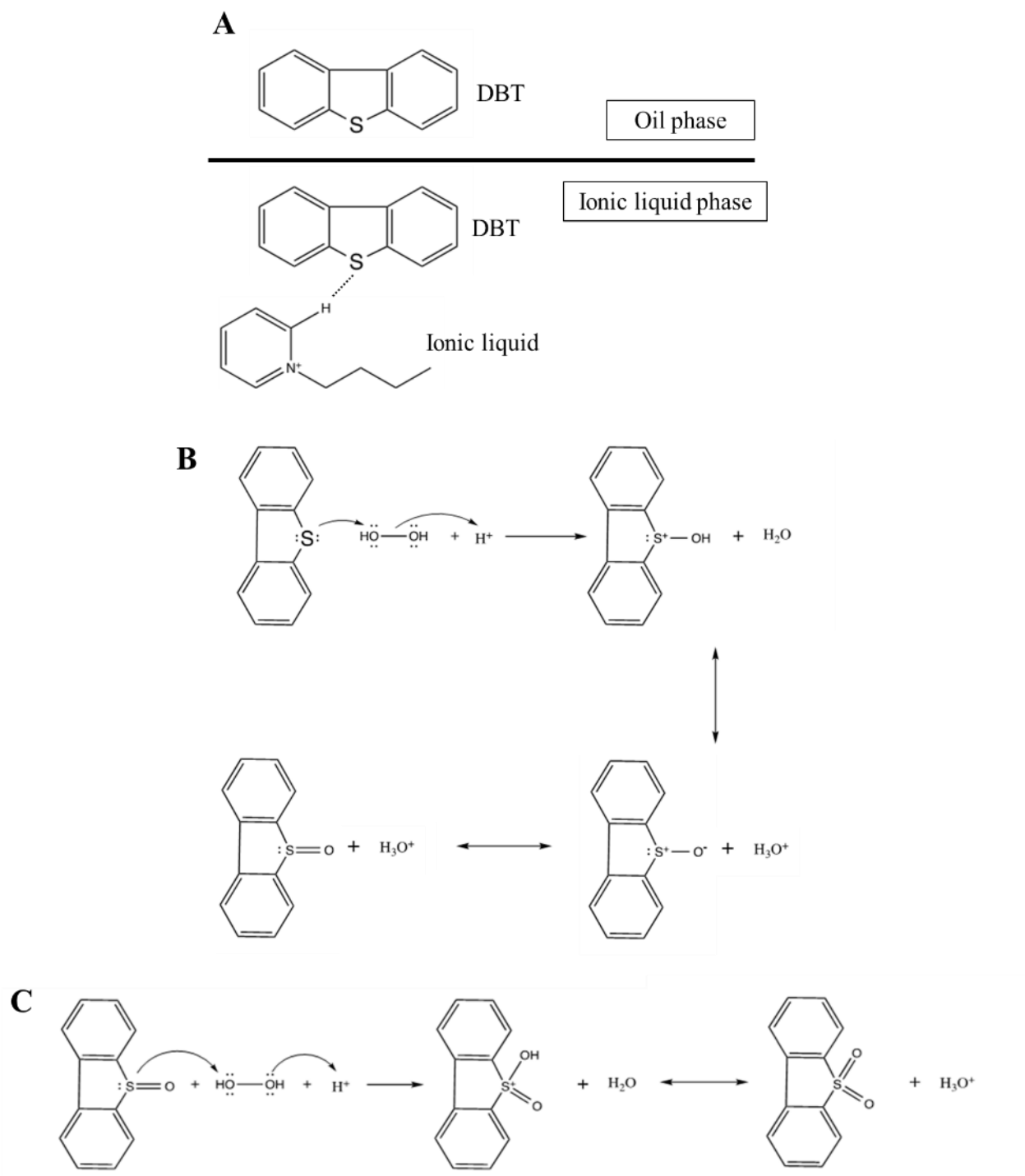
The π - π interactions between [BPy][BF₄] and DBTO₂, namely *face-to-face parallel-displaced* and *edge-tilted-T-shaped* can be seen in [Figures 5.1d](#) and [5.1f](#), respectively. In the *face-to-face parallel-displaced* interaction for [BPy][BF₄] \supset DBTO₂ [Figure 5.1d](#), the pyridinium hydrogens form four hydrogen bonds (C2-H7...F26, C2-H7...F27, C11-H13...F29 and C3-H8...O52), and the bond distances are 2.007 Å, 2.619 Å, 2.467 Å and 2.514 Å, respectively. For one of the other pyridinium C-H... π interactions with DBTO₂, i.e., PyC3-H8...C40(DBTO₂), the bond distance is 3.829 Å, which is almost parallel to the DBTO₂ plane, making it possible to form the *face-to-face parallel-displaced*-type arrangement. The anion [BF₄] and DBTO₂ form weak hydrogen bonding, the distances of DBTO₂-C34-H39...F27 and DBTO₂-C44-H49...F27 being 2.847 Å and 2.663 Å, respectively.

In the *edge-tilted-T-shaped* interaction for ([BPY][BF₄]) ⊃DBTO₂ [Figure 5.1f](#), pyridinium hydrogens form four hydrogen bonds (C2-H7···F26, C2-H7···F27, C11-H13···F27 and C3-H8···O52), and the distances are 2.062 Å, 2.630 Å, 2.216 Å and 2.300 Å, respectively. The other pyridinium C-H···π interactions with DBTO₂, particularly C1-H6···C33 and C1-H6···C40 interaction, which are almost perpendicular to the DBTO₂ plane, make it possible to form the “*T-shaped*” arrangement. The PyC1-H6···C33-DBTO₂ and PyC1-H6···C40-DBT bond distances are 3.606 Å and 3.482 Å, respectively. The anion BF₄⁻ and DBTO₂ show weak hydrogen bonding, distances of 2.465 Å and 2.349 Å, respectively for DBT-C44-H39···F28 and DBTO₂-C35-H49···F28. The position of the [BF₄]⁻ anion is above one side of the pyridinium and DBTO₂ plane in the [BPY][BF₄] ⊃DBTO₂, which thus creates less steric inhibition between the pyridinium and DBTO₂ for both the *parallel-displaced* and *T-shaped* geometry structures. The interaction energies of [BPY][BF₄] ⊃DBTO₂ for *sandwich* and *T-shaped* geometries are -50.26 kJ·mol⁻¹ and -51.63 kJ·mol⁻¹ in the gas phase calculations, -31.16 kJ·mol⁻¹ and -32.767 kJ·mol⁻¹ in the hexane solvent system, -29.07 kJ·mol⁻¹ and -28.91 kJ·mol⁻¹, in the CCl₄ solvent system, respectively. The hydrogen bonding between the oxygen atom (S=O) of the DBTO₂ with the pyridinium hydrogen (C1-H6···O52, 2.300 Å) and higher polarity of the DBTO₂ could be the possible reason for the higher interaction energies of [Bpy][BF₄] ⊃DBTO₂ versus those of [Bpy][BF₄] ⊃DBT.

The dipole moments of DBTO₂ and DBT are 6.699 and 0.869 D, respectively in hexane solvent system. Due to the higher polarity of the DBTO₂, it is more likely to be solubilized in the ionic liquid phase rather than the model fuel phase based upon these calculations. The interaction energies of the [BPY][BF₄] complexes with DBT and DBTO₂ decrease in the hexane and CCl₄ solvents system compared with gas phase calculations.

5.2.1.3 Insight into the Mechanism of Tuned Extractive Desulfurization by Pyridine Ionic Liquid

Normally, when DBT are present in oil phase, we use H_2O_2 as an oxidant to make it soluble in aqueous solution by extracting and catalyzing with ionic liquid (IL). The final product is DBTO_2 , which is water soluble. [Scheme 5.1](#) illustrates how $[\text{BPy}][\text{BF}_4]$ and DBT attract each other, moving DBT from oil phase to the interface phase, where interaction with H_2O_2 causes it to oxidize to DBTO_2 , which is water soluble. With the introduction of ionic liquid in DBT, where it makes sulfur compound switch from oil phase into interface where oxidation occurs, as depicted in [Scheme 5.1a](#). At the interface, DBT turned into DBTO through oxidation. During this time, sulfur atoms form lone pair, which causes the hydrogen to break off of H_2O_2 , which then attach the OH group, which is then removed by H_2O , which removes the hydroxyl group from the sulfur atom. As shown in [Scheme 5.1b](#), the final product formed is DBTO. Finally, in [Scheme 5.1c](#), DBTO is further oxidized with H_2O_2 to yield water-soluble DBTO_2 , the mechanism for this period is like that for stage 2. With the aid of water, DBTO_2 can easily be removed.



Scheme 5.1: Desulfurization mechanism reaction by pyridine-based ionic liquid to remove DBT.

5.2.2 N-Carboxymethyl Pyridinium Hydrogen Sulfate ([CH₂COOHPy] [HSO₄])

5.2.2.1 DFT Calculations

Objective of this study to compare experimental extraction with calculated DFT interaction energies of DBT/DBTO₂ by [(CH₂COOHPy] [HSO₄]. Through this DFT study a better understanding of the reactions of sulfur-containing compounds dibenzothiophene (DBT) and dibenzothiophene sulfone (DBTO₂) with (N-carboxyethyl)-pyridine ionic liquid [CH₂COOHPy] [HSO₄] be developed.

Throughout this work, all of the structure geometries were analyzed, analyzed at B3LYP/6.311.311++G(d,2p) level of theory in gas phase, hexane and hexadecane solvent systems using the polarized continuum model (PCM). The structure of N-carboxy (methyl/ethyl)-pyridine [CH₂COOHPy], combines with the anion HSO₄ were optimized at different binding sites, and the most stable structure [CH₂COOHPy] [HSO₄] was chosen. An optimized stable structure [CH₂COOHPy] [HSO₄], was further optimized at different binding sites using DBT and DBTO₂. In order to determine the interaction energies between DBT/DBTO₂ and the ILs, we define the following:

First, the sites were optimized. In terms of interaction energies with DBT/DBTO₂ the following equations apply:

$$\Delta IE = E_{[(CH_2COOHPy) \Rightarrow [HSO_4]]} - (E_{[(CH_2COOHPy)]} + E_{(HSO_4)}) \quad (5.3)$$

$$\Delta IE = E_{[(CH_2COOHPy)[HSO_4] \Rightarrow DBT/DBTO_2]} - (E_{[(CH_2COOHPy)[HSO_4]]} + E_{(DBT/DBTO_2)}) \quad (5.4)$$

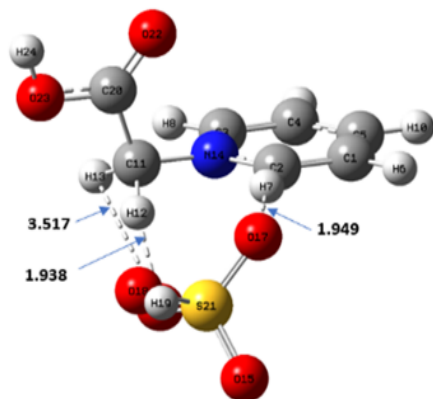
Table 5.2: Calculated interaction energies (ΔIE kJ/mol) for the ionic liquid $[\text{CH}_2\text{COOHPy}][\text{HSO}_4]$ when interacting with DBT and DBTO₂ sulfur-containing compounds in a model fuel gas phase and various solvents.

Compound	Gas phase	Hexane	Hexadecane	CCl ₄
$[\text{CH}_2\text{COOHPy}]\supset[\text{HSO}_4]$	-360.54	-195.44	-181.22	-166.93
$[\text{CH}_2\text{COOHPy}][\text{HSO}_4] \supset \text{DBT}$ face to face parallel sandwich	-35.62	-20.03	-18.67	-17.28
$[\text{CH}_2\text{COOHPy}][\text{HSO}_4] \supset \text{DBTO}_2$ complex edge tilted-T	-58.41	-36.70	-34.58	-32.38

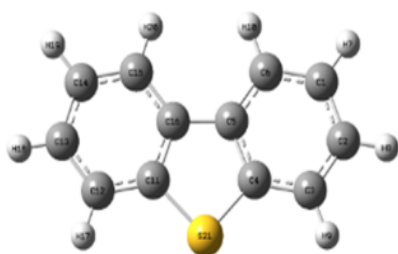
The interaction energies between $[\text{CH}_2\text{COOHPy}][\text{HSO}_4]$ and DBT for the face parallel sandwich geometries are -35.62 kJ/mol, -20.03 kJ/mol, -18.67 kJ/mol, and -17.28 kJ/mol for gas phase, hexane, hexadecane and CCl₄, respectively. The interaction energies of $[\text{CH}_2\text{COOHPy}][\text{HSO}_4] \supset \text{DBTO}_2$ for T-shaped geometries are -58.41 kJ/mol in the gas-phase calculations, -36.69 kJ/mol in hexane, -34.58 kJ/mol in hexadecane, and -32.38 kJ/mol in CCl₄, respectively. The DFT calculation results demonstrate that complexes formed between IL to DBTO₂ are energetically favored.

5.2.2.2 Quantitative Results from the DFT Study

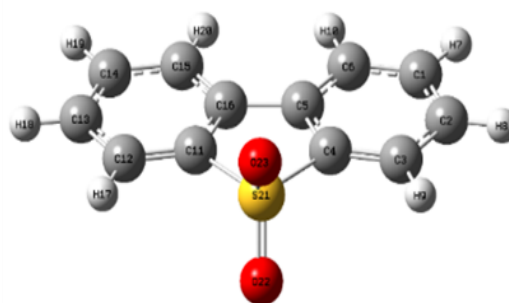
Figure 5.2 illustrates the optimized structures of $[\text{CH}_2\text{COOHPy}][\text{HSO}_4]$, DBT, DBTO₂ and the complexes formed between $[\text{CH}_2\text{COOHPy}][\text{HSO}_4]$ and DBT/DBTO₂ in gas phase. As shown in Figure 5.2, the acidic IL $[\text{CH}_2\text{COOHPy}][\text{HSO}_4]$ features pyridine rings that have π - π interactions with DBT and/or DBTO₂. Moreover, hydrogen bonds are also formed (Figure 5.2d and e) between IL and DBT/DBTO₂ that have the most potential for extracting sulfur-containing compounds from model fuels.



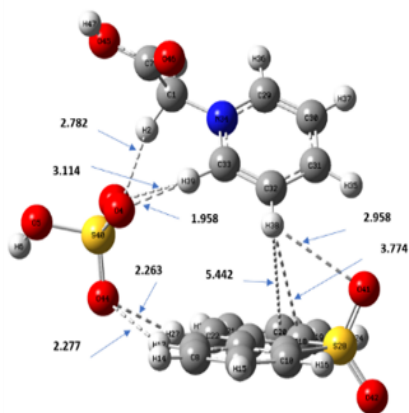
(a) $[\text{CH}_2\text{COOHpy}][\text{HSO}_4]$



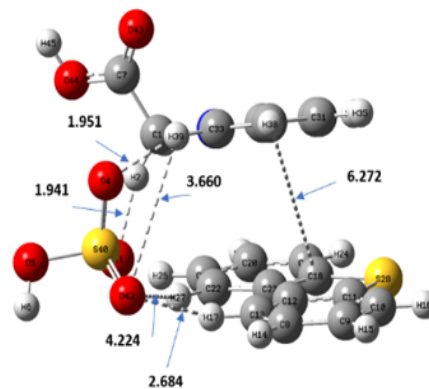
(b) DBT



(c) DBTO_2



(d) $[(\text{CH}_2)_2\text{COOHpy}][\text{HSO}_4] \supset \text{DBTO}_2$ – complex
Edge-tilted-T-shaped in gas phase



(e) $[(\text{CH}_2)_1\text{COOHpy}][\text{HSO}_4] \supset \text{DBT}$ – face
Face parallel Sandwich type in gas phase

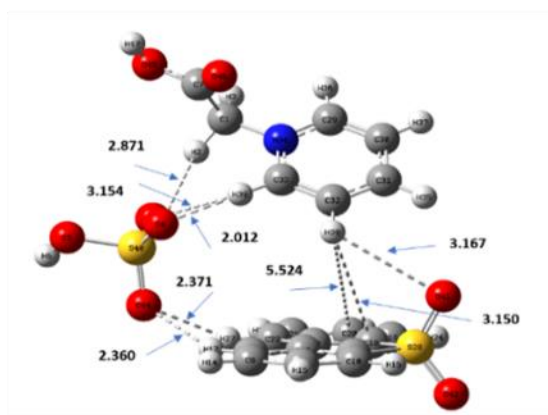
Figure 5.2: The geometry optimized structures of (a) $[\text{CH}_2\text{COOHpy}][\text{HSO}_4]$, (b) DBT, (c) DBTO_2 , (d) $[(\text{CH}_2)_2\text{COOHpy}][\text{HSO}_4] \supset \text{DBTO}_2$ in gas phase, and (e) $[(\text{CH}_2)_1\text{COOHpy}][\text{HSO}_4] \supset \text{DBT}$ in gas phase. Color code: carbon = grey; hydrogen= white; nitrogen= blue; oxygen = red; sulphur = yellow.

Different interaction modes between [CH₂COOHPy][HSO₄] with DBT/DBTO₂ depict different structures of the generated complexes. As can be seen from [Figure 5.3b, d and f](#), π - π stacking interactions between [CH₂COOHPy][HSO₄] and DBT led to the formation of *face-to-face parallel-sandwich* complexes, whereas π -hydrogen bonds between [CH₂COOHPy][HSO₄] with DBTO₂ as presented in [Figures 5.3a, c and e](#), have resulted in *edge-tilted T-shaped* complexes.

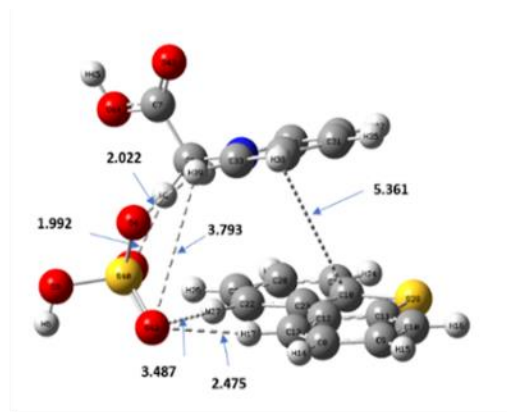
Edge-tilted T-shaped π - π interactions between [CH₂COOHPy][HSO₄] and DBTO₂ in different solvent systems have been illustrated in [Figures 5.3a, c and e](#), respectively. In CCl₄ ([Figure 5.3a](#)), three hydrogen bonds (C33-H39 \cdots O4, C33-H39 \cdots O43, and C1-H2 \cdots O43) are formed from the pyridinium hydrogen at the *edge-tilted T-shaped* structure [CH₂COOHPy][HSO₄] \supset DBTO₂, giving bond distances of 2.012 Å, 3.154 Å, and 2.871 Å, respectively. Other pyridinium C-H \cdots π interactions with DBTO₂, especially PyC32-H38 \cdots O41- DBTO₂, PyC32-H38 \cdots C20 and PyC35-H38 \cdots C18- DBTO₂, give bond distances of 3.167 Å, 5.524 Å and 3.150 Å, respectively. Because these distances are nearly parallel with the DBTO₂ plane, the *T-shaped* formation occurs. Weak hydrogen bonding forms between the anion [HSO₄]⁻ and DBTO₂, with DBTO₂-C22-H27 \cdots O44 and DBTO₂-C22-H17 \cdots O44 giving bond distances of 2.371 Å and 2.360 Å, respectively. The bond distances for the complexes formed in hexane and hexadecane can be found in [Figures 5.3c and e](#). DFT calculation results indicated that *T-shaped* complex formed in hexane has the most stable structure compared to those formed in hexadecane and CCl₄.

Similarly, the optimized geometries for *face-to-face parallel-sandwich* complexes between IL and DBT ([CH₂COOHPy][HSO₄] \supset DBT) in three solvent systems are illustrated [Figures 5.3b, d and f](#). Also, in CCl₄ ([Figure 5.3b](#)), three hydrogen bonds (C33-H39-O42, C33-H39 \cdots O4, and C1-H2 \cdots O41), are formed by the pyridinium hydrogen, giving bond distances of 3.793 Å, 2.022 Å, and 1.992 Å, respectively. Another pyridinium C-H \cdots π / DBT interaction enables the “sandwich”

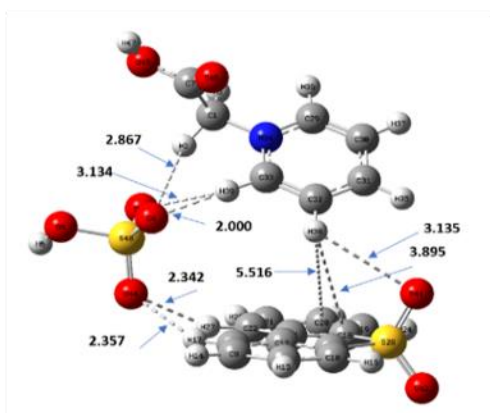
formation, especially PyC23–H38···C18(DBT) at 5.361 Å, which is nearly parallel with the DBT plane. Hydrogen bonding has also been formed between the anion [HSO₄][−] and DBT, resulting in DBT–C22–H27···O42 and DBT–C13–H17···O42 and giving bond distances of 3.487 Å and 2.475 Å, respectively. The corresponding bond distances for complexes formed in hexane and hexadecane can be found in [Figure 5.3d and f](#), respectively. Very similar to the case of [CH₂COOHPy][HSO₄][−]DBTO₂, the interactions for face-to-face parallel-sandwich complexes between [CH₂COOHPy] with DBT is the strongest in hexane, followed by that in hexadecane and CCl₄.



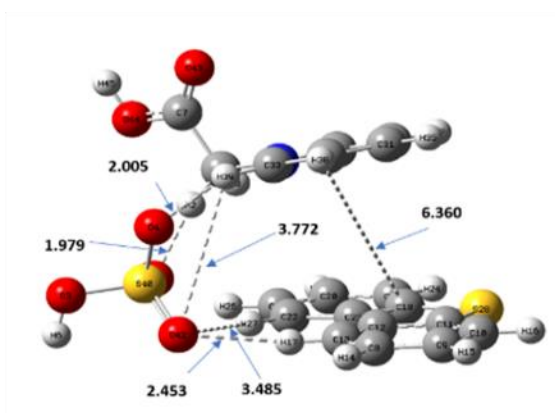
(a) $[(\text{CH}_2)_1\text{COOHpy}][\text{HSO}_4] \supset \text{DBTO}_2$ – complex
Edge tilted-T-shaped in CCl_4



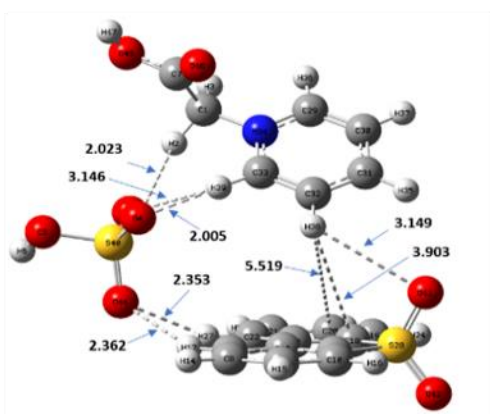
(b) $[(\text{CH}_2)_1\text{COOHpy}][\text{HSO}_4] \supset \text{DBT}$ – face
Face parallel Sandwich type in CCl_4



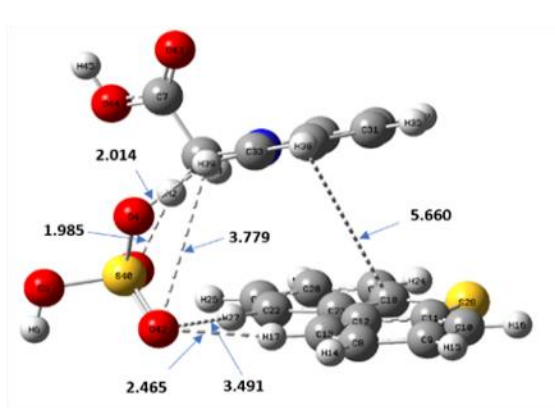
(c) $[(\text{CH}_2)_1\text{COOHpy}][\text{HSO}_4] \supset \text{DBTO}_2$ – complex
Edge tilted-T-shaped in hexane



(d) $[(\text{CH}_2)_1\text{COOHpy}][\text{HSO}_4] \supset \text{DBT}$ – face
Face parallel Sandwich type in hexane



(e) $[(\text{CH}_2)_1\text{COOHpy}][\text{HSO}_4] \supset \text{DBTO}_2$ – face
Edge tilted-T-shaped in hexadecane



(f) $[(\text{CH}_2)_1\text{COOHpy}][\text{HSO}_4] \supset \text{DBT}$ – face
Face parallel Sandwich type in hexadecane

Figure 5.3: Geometry optimized structures of (a, c, e) $[(\text{CH}_2)_1\text{COOHpy}][\text{HSO}_4] \supset \text{DBTO}_2$, and (b, d, f) $[(\text{CH}_2)_1\text{COOHpy}][\text{HSO}_4] \supset \text{DBT}$ in solvents. Color code: carbon = grey; hydrogen = white; nitrogen = blue; oxygen atom = red; sulphur atom = yellow.

5.2.2.3 Insight into the Mechanism of Tuned Extractive Desulfurization by Acid Ionic Liquid [CH₂COOHPy] [HSO₄]

The suggested mechanism of desulfurization of DBT by the acid ionic liquid [CH₂COOHPy] [HSO₄] is shown in [Figure 5.4](#) and [Scheme 5.2](#). Briefly, DBT in the oil phase is extracted by the ionic liquid. This oxidation of DBT occurs through the peroxy-carboxyl groups, which are obtained from the oxidation of carboxyl groups of the [CH₂COOHPy] [HSO₄] in the presence of H₂O₂. The peroxy-carboxyl groups are able to oxidize the DBT into DBT oxide (DBTO) and DBT dioxide (DBTO₂) in two-steps, while being reduced to carboxyl groups, leading to regeneration (recycling) of the ionic liquid. As these reactions proceed, the amount of DBT present in the oil phase keeps on decreasing until an equilibrium is reached.

The detailed reaction pathways for the desulfurization of DBT by the acidic IL are described in [Scheme 5.2](#). In first step, [PyCH₂COOH] attacks on acidic H⁺ to generate [PyCH₂COOOH]. Then DBT's sulfur atom attacks on [PyCH₂COOOH], leading to the reduction of the [PyCH₂COOOH] to [PyCH₂COOH] and the attachment of the hydroxyl (-OH) group to Sulphur atom in DBT. To remove H from hydroxyl group attached to S, H₂O acts as base and DBTO (resonance stabilized) is formed from this step. In last step, [PyCH₂COOOH] further oxidized DBTO to DBTO₂ in similar way as mentioned above. The final product DBTO₂ is polar and water soluble.

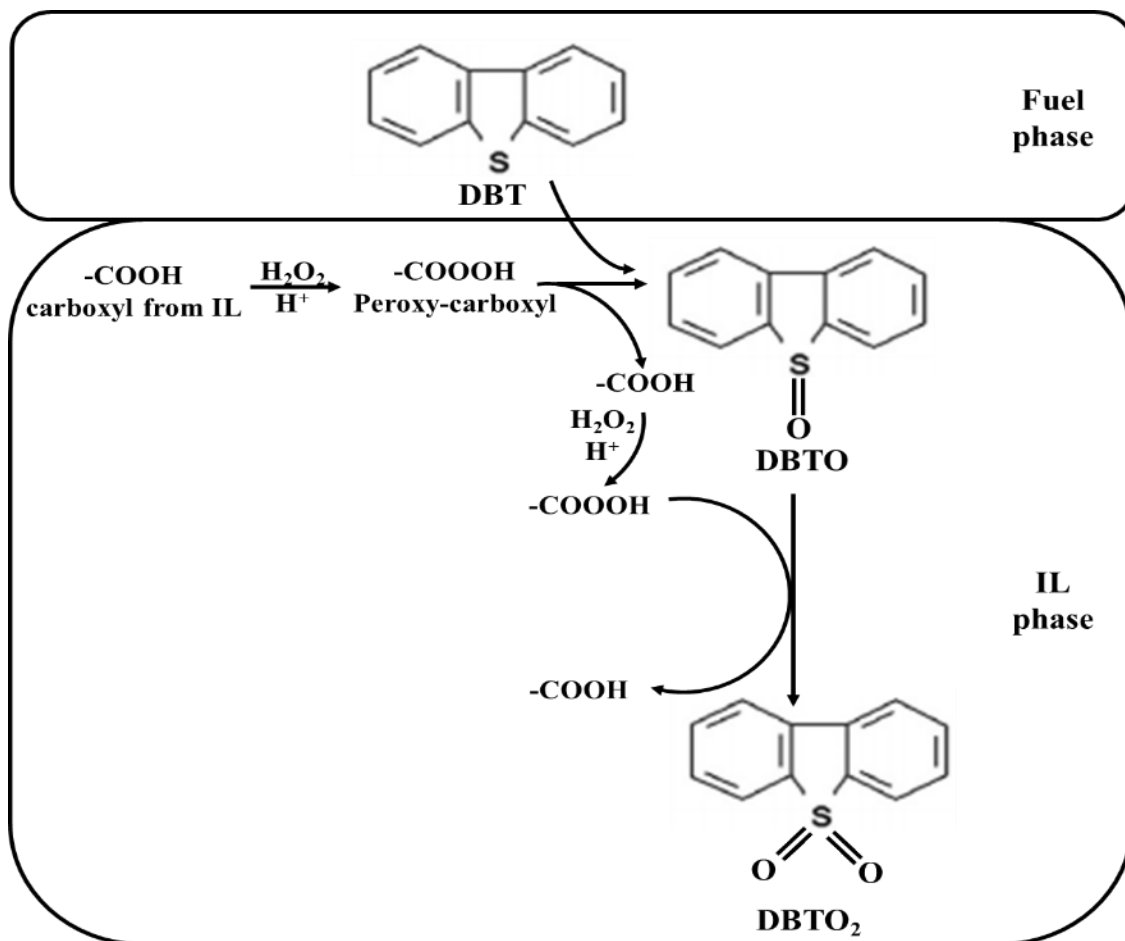
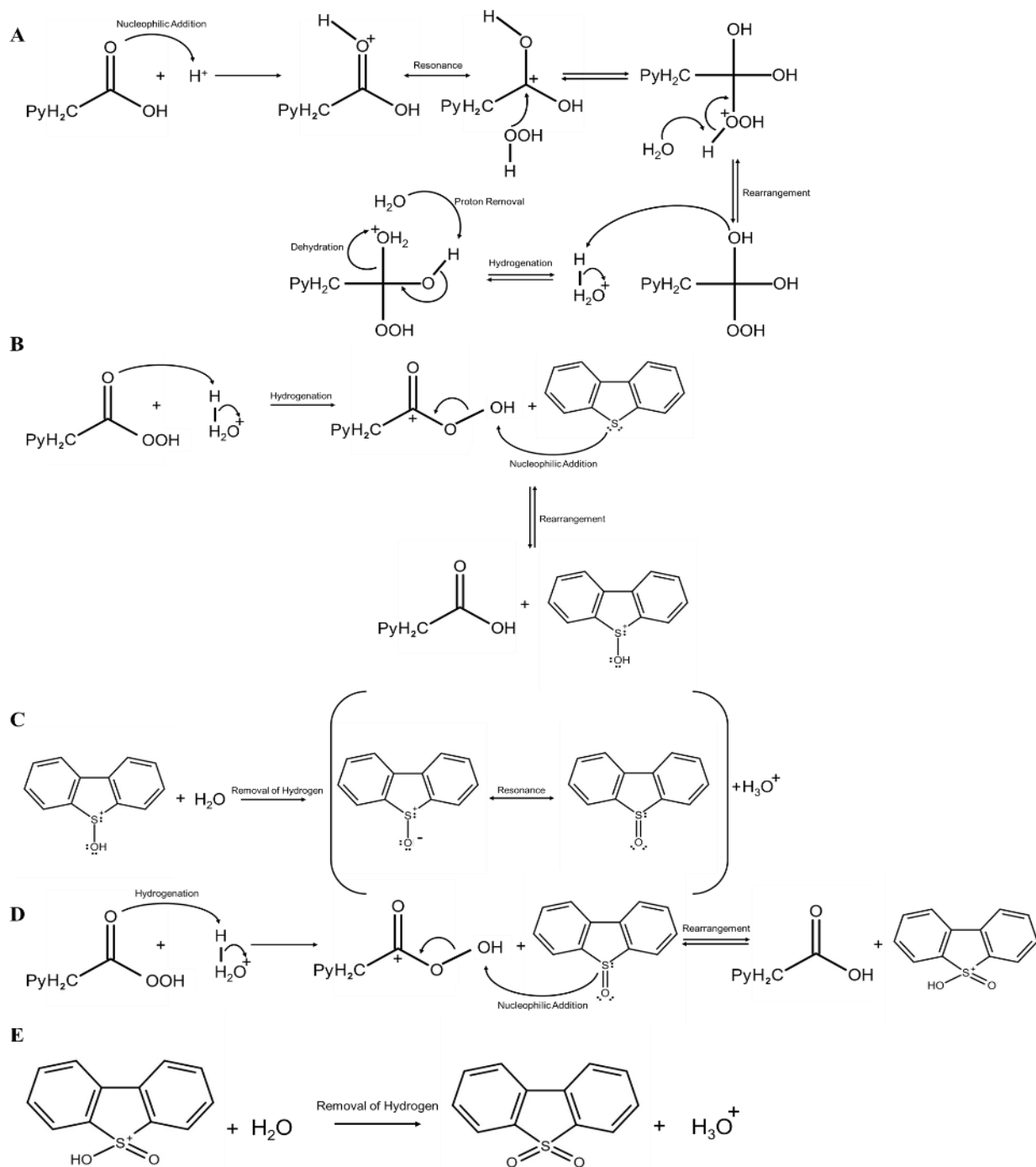


Figure 5.4: Reaction mechanism of desulfurization of DBT in fuel by using IL and H₂O₂.



Scheme 5.2: Desulfurization mechanism reaction by the acidic ionic liquid $[\text{CH}_2\text{COOHPy}][\text{HSO}_4]$ to remove DBT.

5.3 Conclusion

We employed DFT calculation to develop a mechanistic understanding of desulfurization performed by two specific pyridinium-based ionic liquids - [BPy] [BF₄] and [CH₂COOHPy] [HSO₄].

Based on DFT-based structural analysis, it was found that there are two types of possible π - π interactions between [BPy] [BF₄] and DBT/DBTO₂, resulting in the formation of complexes with different geometries. Similar analyses performed for the acidic ionic liquid [CH₂COOHPy] [HSO₄] revealed the occurrence of similar potential π - π interactions between [CH₂COOHPy] [HSO₄] and DBT/DBTO₂. The interaction energies for all configurations of ([BPy] [BF₄]) \supset DBTO₂ and ([CH₂COOHPy] [HSO₄]) \supset DBTO₂ in both the solvents were nearly two-fold higher (more highly negative) than those for the corresponding configurations of ([BPy] [BF₄]) \supset DBT and ([CH₂COOHPy] [HSO₄]) \supset DBT. The hydrogen bonding between the oxygen atom (S=O) of the DBTO₂ and the pyridinium hydrogen, as well as the higher polarity of the DBTO₂ could be responsible for these differences.

The mechanisms of tuned extractive desulfurization by the two ionic liquids were also discussed in detail in the present chapter. Overall, an oxidative desulfurization mechanism has been predicted for both the ionic liquids based upon the experimental data from the previous chapters in this thesis as well as the modeling data obtained in the present chapter. In experimental studies, [BPy][BF₄] was found to be effective in the extraction of DBT from model fuel as both EDS and OEDS reactions reached equilibrium within 1 h, while a comparison between the desulfurization efficiency data for EDS, ODS and OEDS processes using the [CH₂COOHPy] [HSO₄] revealed why OEDS resulted in the highest DBT removal. Both the ILs act as both catalysts and extractants.

When the IL is added first, it acts as an extractant and sequesters the DBT from the fuel phase into the interface of the fuel and IL phases. Upon the subsequent addition of H_2O_2 , the IL also acts as a catalyst for the oxidation of DBT to DBTO and DBTO_2 . This mechanism was affirmed by DFT in the present chapter. DFT simulations revealed that both $[\text{CH}_2\text{COOHPy}][\text{HSO}_4]$ and $[\text{BPy}][\text{BF}_4]$ can bind with DBT in multiple geometrical configurations, which suggests that both ILs can act as extractants. These simulations also showed that the interaction energies of $[\text{CH}_2\text{COOHPy}][\text{HSO}_4]$ as well as $[\text{BPy}][\text{BF}_4]$ with DBTO_2 are higher than with DBT, which further strengthens the proposed oxidative mechanism for these ILs.

To conclude, DFT calculations and mechanistic investigations can provide insights into how different ionic liquids perform desulfurization of fuels. In the future, further experimental and computational studies will be conducted with different solvent systems to obtain a deeper insight into the solvation effect for regeneration of ionic liquids that have already been used (once or more) for desulfurization of a fuel.

References

1. Yang, W. Direct calculation of electron density in density-functional theory, *Physical Review Letters* 66 (1991), 1438-1441.
2. Baker, E.B. The application of the Fermi-Thomas statistical model to the calculation of potential distribution in positive ions, *Physical Review* 36 (1930), 630-647.
3. Imamura, Y., Otsuka, T., Nakai, H. Description of core excitations by time-dependent density functional theory with local density approximation, generalized gradient approximation, meta - generalized gradient approximation, and hybrid functionals, *Journal of Computational Chemistry* 28 (2007), 2067-22074.
4. Hunter, C.A., Sanders, J.K. The nature of π - π interactions, *Journal of American Chemical Society* 112 (1990), 5525-5534.
5. Lehn, J.-M. (1995). *Supramolecular Chemistry*, 1st ed., Weinheim: VCH.
6. Lehn, J.-M. (1995). *Supramolecular Chemistry*, 1st ed., Weinheim: VCH.
7. Hohenstein, E.G., Sherrill, C.D. Effects of heteroatoms on aromatic π - π interactions: Benzene-pyridine and pyridine dimer, *Journal of Physical Chemistry A* 113 (2009), 878-886.

Chapter 6: Conclusions and Future Works

6.1 Conclusions

A novel oxidative desulfurization of DBT was characterized by the synthesis of [BPy][BF₄]. It looked at various ways to optimize DBT's EDS and OEDS based on a model fuel with [BPy][BF₄]. To prepare [BPy][BF₄], two-step synthetic method was employed. A series of ¹H-NMR, ¹³C-NMR, and FTIR spectroscopy measurements were performed on the synthesised ionic liquid.

An assessment of the effects of various operational parameters – such as extraction time, temperature, ionic liquid volume-to-model fuel, and oxidant volume-to-model fuel - on the desulfurization efficiency of [BPy][BF₄] was performed. Due to the direct effect that temperature has on the DBT removal reaction kinetic rate constant, DBT removal efficiencies improved with the increase of temperature. The highest temperature was set to 40°C from an energy savings and operating cost perspective. The desulfurization efficiency of [BPy][BF₄] decreased as the proportion of ionic liquid decreased compared to model fuel, since a large amount of DBT in the reaction mixture made the ionic liquid almost saturated. The efficiency of desulfurization was also improved with an increase in H₂O₂ amount.

[BPy][BF₄] can be regenerated and reused up to eight times without degrading significantly in its desulfurization efficiency. This study showed that desulfurization occurred at greater levels in the model fuel than in the real diesel fuel, which may be due to other contaminants found in diesel fuel that may affect the selectivity of the ionic liquid towards the DBT. Overall, this study discussed the significant potential for [BPy][BF₄] as a desulfurization agent in the industry.

The desulfurization efficiency of pyridinium-based ionic liquid, [CH₂COOHPy] [HSO₄], was tested using both a model fuel (n-hexadecane), as well as a real diesel fuel. Using this approach, the effects of multiple variables on the desulfurization efficiency of the ionic liquid were explored. Desulfurization methods included extractive, oxidative, and oxidative-extractive methods; for removal sulfur-containing compounds (e.g., DBT, 4,6-DMDBT).

Several parameters including reaction time, the concentration of an oxidant used (H₂O₂), the ration of Ionic liquid and sulfur-containing compounds, were studied. With [CH₂COOHPy] [HSO₄], it was found that OEDS led to faster and more effective removal of sulphur (DBT) from fuel models. It took 20 minutes for the OEDS reaction to reach equilibrium at ambient temperature. In contrast, DBT removal in EDS took around 50 minutes to plateau and even then, resulted in only 40 % desulfurization efficiency. However, ODS was only effective in removing DBT, resulting in a maximum desulfurization efficiency of 2.7 % in over 65 minutes. Overall, finding that an extraction time of 40 minutes caused the highest sulphur removal with OEDS is promising. The efficiency of desulfurization was also found to differ for different sulphur-containing compounds. By combining catalytic oxidation, sulphur is removed as follows: DBT \geq 4, 6-DMDBT. The removal efficiency of DBT and 4,6-DMDBT reached nearly 100 % (99.9 %) within 20 minutes.

Furthermore, this study found that desulfurization in the model fuel was significantly higher than in real diesel. This may be due to other contaminants in diesel fuel that affect the selectivity of the ionic liquid toward DBT. Some of the components (which could act affect the selectivity of the IL toward DBT) that were found in the diesel fuel used in the present study were n-decane, n-undecane, n-dodecane, n-tetradecane, n-pentadecane, n-hexadecane, n-heptadecane and n-octadecane (Table A.6). Overall, the study provided another major insight into the usefulness of ionic liquids for desulfurization in industrial environments.

Density functional theory (DFT) calculations provided a better understanding of the interactions between the aromatic sulfur compounds found in fuels and the pyridinium-based ionic liquids analyzed previously. In the study, cations and anion were found to be important to EDS. Hydrogen bonds exist between the [BPy]⁺ cation and [BF₄]⁻ anion as well as the [CH₂COOHPy]⁺ cation and [HSO₄]⁻ anion.

It is possible for [BPy] [BF₄] and DBT/ DBTO₂ to interact with each other in two different ways, leading to complexes with different structural specifications. The DFT analysis has also revealed that the interaction energies for ([BPy] [BF₄]) ⊃ DBTO₂ were nearly ten times greater than those for ([BPy] [BF₄]) ⊃ DBT. DBTO₂ is able to produce hydrogen bonds between its oxygen atom (S=O) and the pyridinium hydrogen, which could account for its increased polarity. The study also pointed to π-π interactions between [CH₂COOHPy] [HSO₄] and DBT/DBTO₂. Further, the interaction energy for ([BPy] [BF₄]) was nearly two-fold higher than that for ([CH₂COOHPy] [HSO₄]) ⊃ DBTO₂ is almost 2 times greater than for ([CH₂COOHPy] [HSO₄]) ⊃ DBT.

It was confirmed that both ionic liquids undergo an oxidative process to remove sulfur. For [BPy] [BF₄], lone pairs on the sulphur atom of DBT cause the cleavage of H₂O₂, thereby attaching an –OH group in H₂O₂ to DBT. DBTO is formed when H₂O removes H⁺ from the –OH group. H₂O₂ further oxidizes the DBTO to form water-soluble DBTO₂. In the meantime, [PyCH₂COOH] is first converted to [PyCH₂COOOH] by H₂O₂ in case of desulfurization by [CH₂COOHPy][HSO₄]. [PyCH₂COOOH] is then attacked by the sulphur atom in DBT, which results in –OH group attaching to the sulphur atom. After that, H₂O removes the H⁺, forming DBTO, which is further oxidized to water soluble DBTO₂ by [PyCH₂COOOH].

6.2 Future Perspectives

This thesis presents research findings on the key factors affecting the performance of ionic liquids combined with moderate and environment-friendly extraction conditions in desulfurization. In the future, the results of these studies may be helpful in optimizing desulfurization parameters (like temperature, oxidant concentration, fuel volume ratio, extraction time, etc.) for different ionic liquids. The DFT and mechanistic analyses can also provide insight into how different types of ionic liquids desulfurize fuel. It is necessary to further study how to scale up EODS in order to apply these ionic liquids to industrial applications.

Also, ionic liquids remain relatively expensive in comparison to conventional solvents, and their toxicity and disposal strategy are unknown. The future should examine these aspects in more detail. It is possible to develop and study new ionic liquids or their analogs (such as deep eutectic solvents) to overcome the costs challenge. Additionally, ionic liquids currently in use should be examined more thoroughly for their recyclability. In order to retain a desulfurization efficiency, an ionic liquid should be able to sustain its desulfurization ratio over a longer period of time. It is possible to reduce desulfurization costs through studies that optimize the different reaction components, including H_2O_2 . Also, it might be useful to evaluate desulfurization efficiency of ionic liquids across a wider range of experimental parameters (such as oxidant concentrations and temperatures).

Appendix A

A.1 ^1H -NMR and ^{13}C -NMR Analyses of [BPy][BF₄]

Aromatic rings produce substantial de-shielding effects in their protons, the external magnetic field induces a current in the aromatic ring that opposes this magnetic field. The aromatic protons are unscreened and absorb at low magnetic field values hence most aromatic protons absorb in the range of 7-8 ppm. In the spectrum, the appearance of a band at 0.84 ppm, is observed characteristic of the final protons of the butyl chain (10) because they are more shielded. Similarly, the signals at 1.24, 1.86 ppm, corresponding to the hydrogens in position (9) and (8) of 2 protons each. in position (7) a signal is observed at 4.63 ppm with two protons. The aromatic rings the protons of positions (3) and (5) are equivalent, i.e., their overlapping signals are equivalent, with a value of 8.13 ppm with one proton each. In position (4) a signal is presented at 8.58 ppm with a proton of the aromatic ring. The protons in positions (2) and (6) are equivalent, with a displacement of 9.13 ppm with a proton each, due to their proximity with positively charged nitrogen the lack of electrons, influences this displacement and the area of the signal. The observed peaks were well fitted to the structure of the synthesized ionic liquid and the data are summarized in [Table A.1](#).

Table A.1: Comparison of ^1H -NMR chemical shifts of [BPy][BF₄] with references.

H position	Chemical shift (ppm)	Chemical shift (Present work) (ppm)
10; (3H), CH ₃	0.90 (triplet)	0.84 (triplet)
9; (2H), CH ₂	1.30 (multiplet)	1.24 (quartet)
8; (2H), CH ₂	1.90 (multiplet)	1.86 (quartet)
7; (2H), NCH ₂	4.59 (triplet)	4.63 (triplet)
3,5; (2H), aromatic protons	8.14 (multiplet)	8.13 (triplet)
4; (1H), aromatic proton	8.59 (multiplet)	8.58 (triplet)

2,6; (2H), aromatic protons 9.04 (multiplet) 9.13 (doublet)

^{13}C -NMR is complementary to ^1H . It determines the magnetic environment of carbon atoms. A peak is observed at 13.10 ppm indicative of the carbon at the end of the butyl chain in position 10, and as they approach nitrogen and the aromatic ring, their displacement increases, signals to 18.80, 32.78 and 60.64 ppm in positions 9, 8 and 7. There are 3 peaks in the range of 110 to 160 ppm, characteristic of an aromatic ring, the signal at 128.16 ppm refers us to the positions (5) and (3) because carbon atoms are equivalent. The two signals at 144.78 and 145.58 ppm, are to the positions (6) and (2), due to the double bond present in (2) their displacement is greater, shorter is the bond and greater interaction with nitrogen. The signal at 149.06 ppm in position (4) completing the carbons of the aromatic ring. The data from the ^{13}C -NMR spectrum of the ionic liquid are summarized in [Table A.2](#). They clearly indicate the presence of the structure of [BPy][BF₄].

Table A.2: Comparison of ^{13}C -NMR chemical shifts of [BPy][BF₄] with references.

C position	Chemical shift (ppm)	Chemical shift (Present work) (ppm)
10; (1C), CH ₃	13.23	13.10
9; (1C), CH ₂	18.66	18.80
8; (1C), NCH ₂	32.57	32.78
7; (1C), NCH ₂	60.56	60.64
3,4 (2C), aromatic proton	128.03	128.16
6 (2C), aromatic protons	144.58	144.78
2 (2C), aromatic protons	145.43	145.58
4 (1C), aromatic protons	110 – 160	149.06

A.2 FTIR Analysis of [BPy][BF₄]

The molecular structure of [BPy][BF₄] was characterized by FTIR with the IR spectrum of [BPy][BF₄] being shown in [Figure A.1](#). The small band at 3618.26 cm⁻¹ is characteristic of traces

of water present in the sample. The peaks at 3070.51 and 2937.43 cm^{-1} indicate C–H stretching vibrations, representing hybridizations of sp^2 (aromatic) and sp^3 (aliphatic), respectively. Peaks at 1708.84 and 1635.55 cm^{-1} are the characteristic overtone bands for aromatic rings. The bands at 1583.47, 1488.96 and 1467.75 cm^{-1} are for the aromatic C=C stretching vibrations.

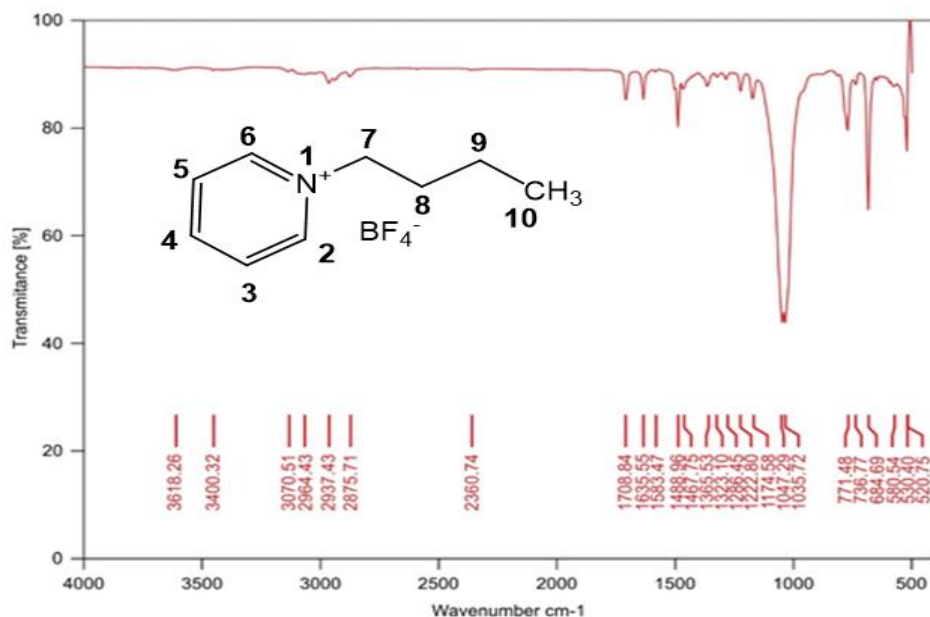


Figure A.1: FTIR spectrum of [BPy][BF₄]

In the region of the fingerprint, there are flexion bands for sp^3 C–H at 1467.75 and 1365.53 cm^{-1} . The peaks at 1222.80, 1174.58, 1047.29 and 1035.72 cm^{-1} are due to the coalescence of aromatic stretching and sp^3 C–H bending. Meanwhile, the sharp peaks at 771.48 and 684.69 cm^{-1} are due to aromatic sp^2 C–H bending. The IR data of the [BPy][BF₄] synthesized in this work are consistent with those reported previously.²

Table A.3: FTIR spectrum of [BPy][BF₄].

Peak frequency (cm-1) This work	Band assigned	Peak frequency Reference (a) (cm-1)	Peak frequency Reference (b) (cm-1)
3618.26		3618.26	3618.26
3400.32		3400.32	3400.32
3070.51		3070.51	3070.51
2964.43		2964.43	2964.43
2937.43		2937.43	2937.43
2875.71		2875.71	2875.71
2360.74		2360.74	2360.74
1708.84		1708.84	1708.84
1635.55		1635.55	1635.55
1583.47		1583.47	1583.47
1488.96		1488.96	1488.96
1467.75		1467.75	1467.75
1365.53		1365.53	1365.53
1323.10		1323.10	1323.10
1286.45		1286.45	1286.45
1222.80		1222.80	1222.80
1174.58		1174.58	1174.58
1047.29		1047.29	1047.29
1035.72		1035.72	1035.72
771.48		771.48	771.48
736.77		736.77	736.77
684.69		684.69	684.69
580.34		580.34	580.34
520.75		520.75	520.75

3070.51	Aromatic (C–H), str/b	3126, 3024	3141, 3098, 3077
2964.43, 2875.71	Aliphatic (C–H), str	2961, 2937, 2872	2965, 2942, 2880
1488.96	Aromatic, str/deform	1488	1491
1708.84	Aromatic (C–C), str	1633	1636
1365.53	Me (C–H), b, asym	1381	1387
1323.10	Me (C–H), b, sym	1310	1325
1047.29	C–H, b, I	1061	1069
771.48	Me (C–H)	776	773
684.69	CH ₂ , b	685	687
1708,	C=N	-	-
1223	C-N	-	-

A.3 Calibration Curve Obtained Using UV-Vis Spectrophotometer to Analyze Sulfur Removal

To calculate DBT (sulfur) removal, a calibration curve was first obtained using DBT standards in a UV-Vis spectrophotometer. 50 mg of DBT was dissolved in 500 mL n-hexane to form 100 ppm DBT content in the model oil. From 100 ppm DBT, it was diluted to 50 ppm, 30 ppm, 20 ppm, 15 ppm, 10 ppm, 7 ppm, 5 ppm, and 1 ppm of DBT. The samples were used to generate a standard calibration curve using a 6000 UV-vis Spectrophotometer by measuring absorbance at the wavelength 284 nm (Figure A.2).

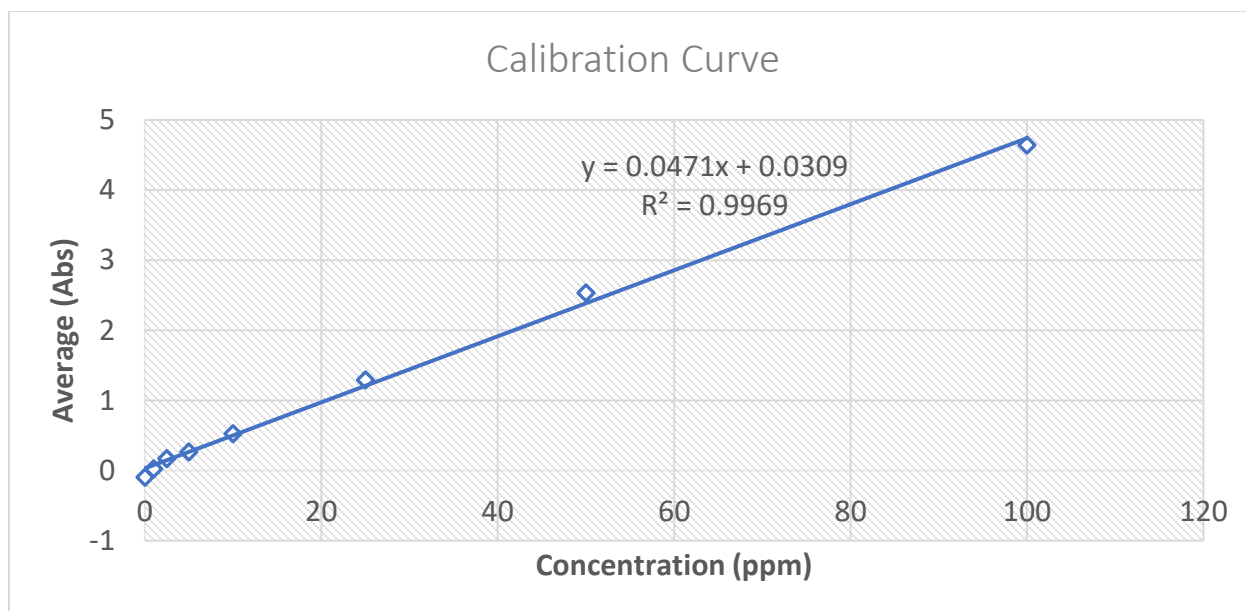


Figure A.2: Calibration curve used to measure DBT removal.

A.4 Diesel Sample Analysis by Gas Chromatography

Original diesel samples were analyzed for their content using the gas chromatograph GC7890. [Figure A.3](#) shows the gas chromatogram of the sample. [Table A.4](#) shows the compounds (and their respective peak areas and peak area percentages on the chromatogram) that were identified from the gas chromatogram. n-hexadecane was present in the highest abundance, followed by n-pentadecane and n-heptadecane.

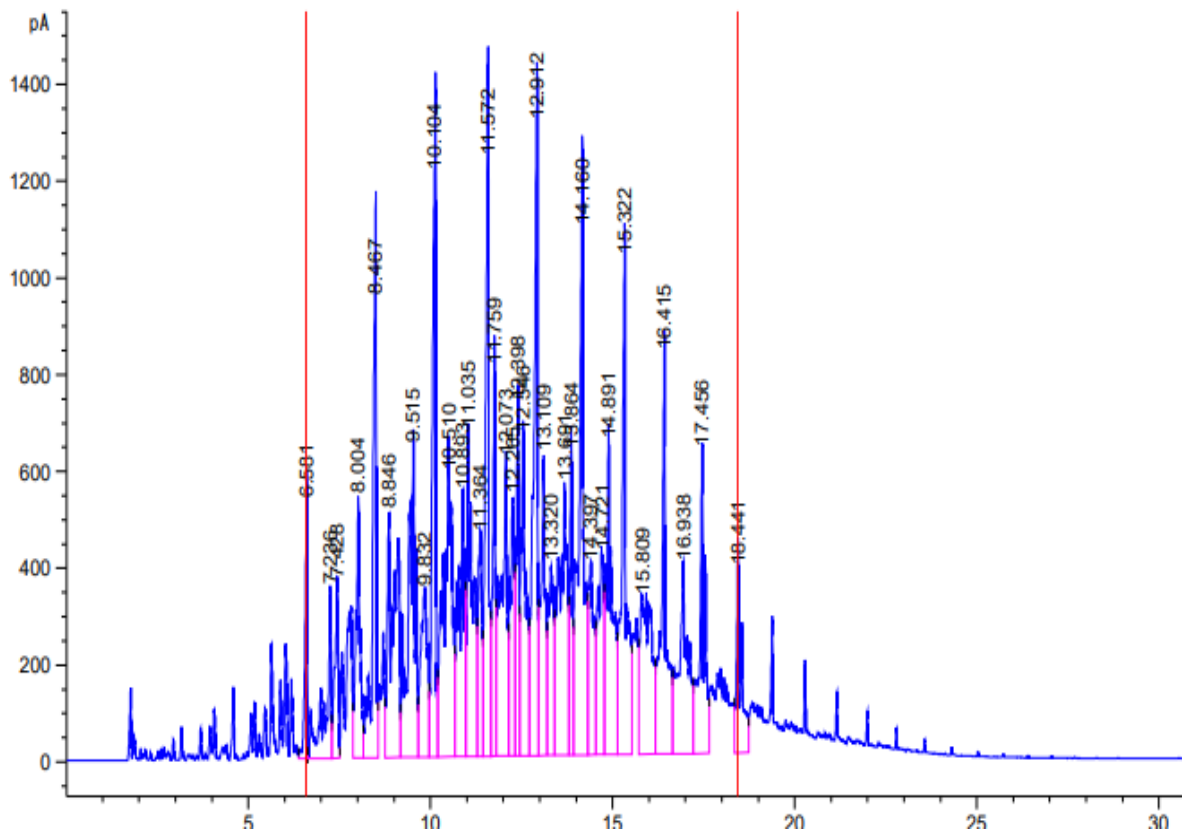


Figure A.3: Gas chromatogram of real diesel fuel.

Table A.4: Components of diesel fuel identified using gas chromatography.

Component name	Total area (pA-s)	Area %
n-pentane	0	0
CS2	0	0
n-hexane	0	0
n-heptane	0	0
n-octane	0	0
n-nonane	0	0
n-decane	4065.05	1.93
n-undecane	4398.39	2.08
n-dodecane	3372.74	1.60
n-tetradecane	3375.09	1.60

n-pentadecane	7724.75	3.66
n-hexadecane	7731.70	3.66
n-heptadecane	6820.92	3.23
n-octadecane	3425.15	1.62
n-eicosane	0	0
n-tetracosane	0	0
n-octacosane	0	0
n-hexatriacontane	0	0
n-tetracontane	0	0
n-dotriacontane	0	0

Appendix B

B.1 HPLC-UV-vis-TOF of the Model Oil Layer after Desulfurization with IL

The concentrations of different sulfur-containing compounds (BT, DBT and 4,6-DMDBT) were measured in the present study using HPLC-UV-vis-TOF. These analytical experiments also helped understand the plausible reaction mechanism of desulfurization by the IL synthesised in this study.

The HPLC-UV-vis-TOF calibration curves for the three sulfur compounds are shown in [Figures B.1 \(BT\)](#), [B.2 \(DBT\)](#) and [B.3 \(4,6-DMDBT\)](#).

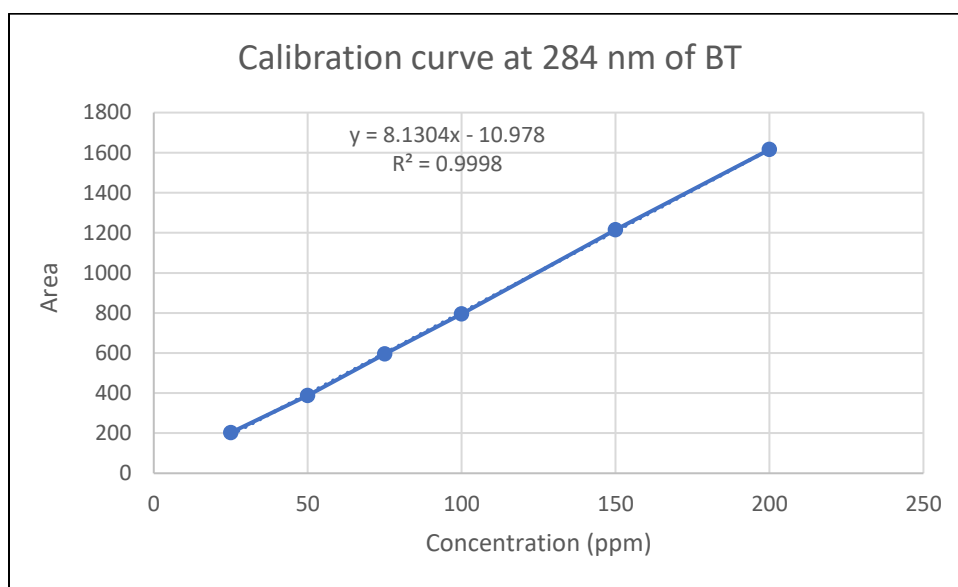


Figure B.1: HPLC-UV-vis-TOF calibration curve for BT.

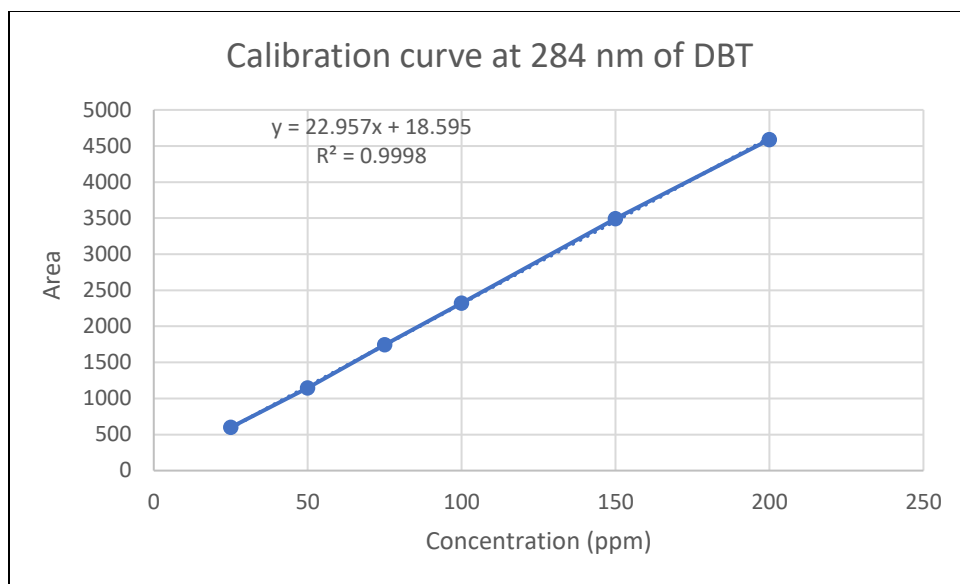


Figure B.2: HPLC-UV-vis-TOF calibration curve for DBT.

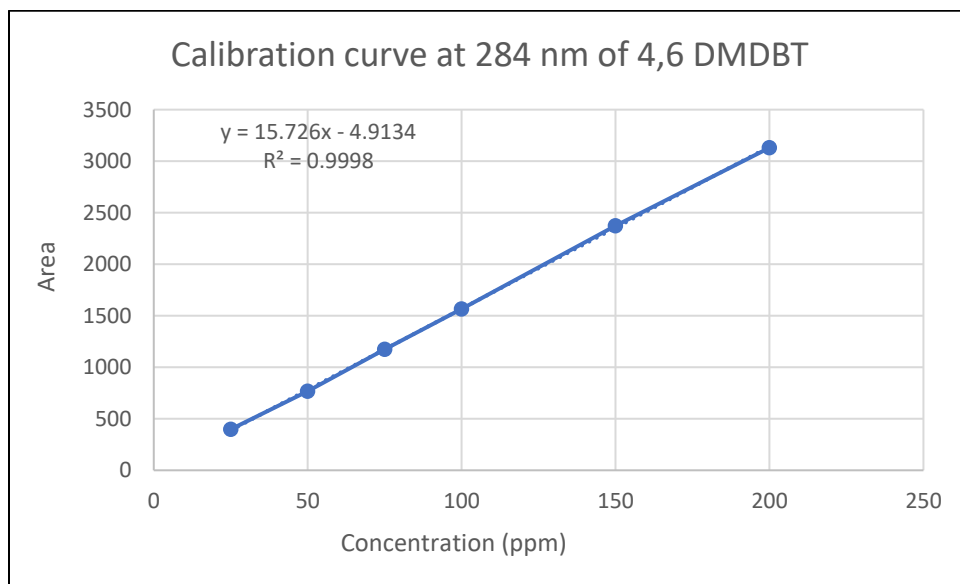


Figure B.3: HPLC-UV-vis-TOF calibration curve for 4,6-DMDBT.

The multi-standard HPLC-UV chromatogram (at wavelength 284 nm) for the three sulfur compounds BT, DBT and 4,6-DMDBT is shown in [Figure B.4](#). Based on the peaks observed for the standards of these sulfur-containing compounds, the chromatogram peak for BT arrives at 1.674 min, DBT at 2.465 min and 4,6-DMDBT at 4.485 min.

HPLC-UV chromatograms and mass spectra (Figures B.5-B.7) of samples collected from the model fuel phase (top layer) (Figure B.5) were analysed. No peak was observed at the retention time for BT, 1.674 min based on the peak that was observed in the chromatogram for BT, DBT and 4,6-DMDBT standards (Figure B.4). It is likely that when BT was converted to sulfone during the oxidation reaction, some of it was extracted into the IL phase (bottom layer) and the remaining amount was converted to styrene compounds, as indicated by the peaks in the chromatogram (at retention times 1.40 min, 2.24 min, 3.57 min, 4.40 min, and 5.09 min) (Figure B.5). This could explain why samples from the model fuel phase (top layer) yielded no specific BT peak at the expected retention time for this compound.

Meanwhile, as can be seen in the DBT chromatogram in Figure B.6, a peak was observed at the retention time of 2.44 min, indicating the presence of remaining DBT in the top layer. Similarly, as seen in the 4,6-DMDBT chromatogram in Figure B.7, a small peak was observed at the retention time of 4.38 min, suggesting the presence of a small amount of 4,6-DMDBT in the model fuel layer after the desulfurization. Other peaks were also observed in this chromatogram, which indicates the transformation of a fraction of the 4,6-DMDBT molecules into other compounds (with retention times between 1 min and 2 min) after desulfurization by the IL.

User Chromatograms

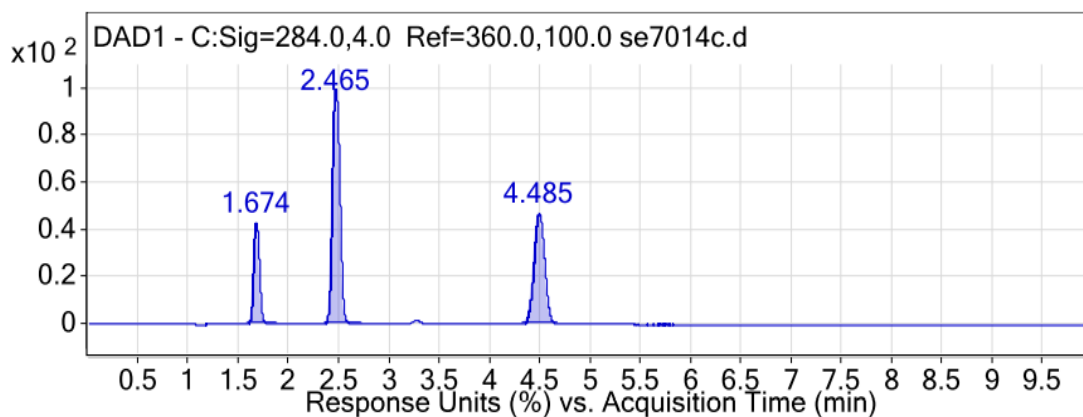


Figure B.4: Multi-standard HPLC-UV chromatogram (at wavelength 284 nm) for the three sulfur compounds BT, DBT and 4,6-DMDBT. Peaks from left to right: BT, DBT and 4,6-DMDBT.

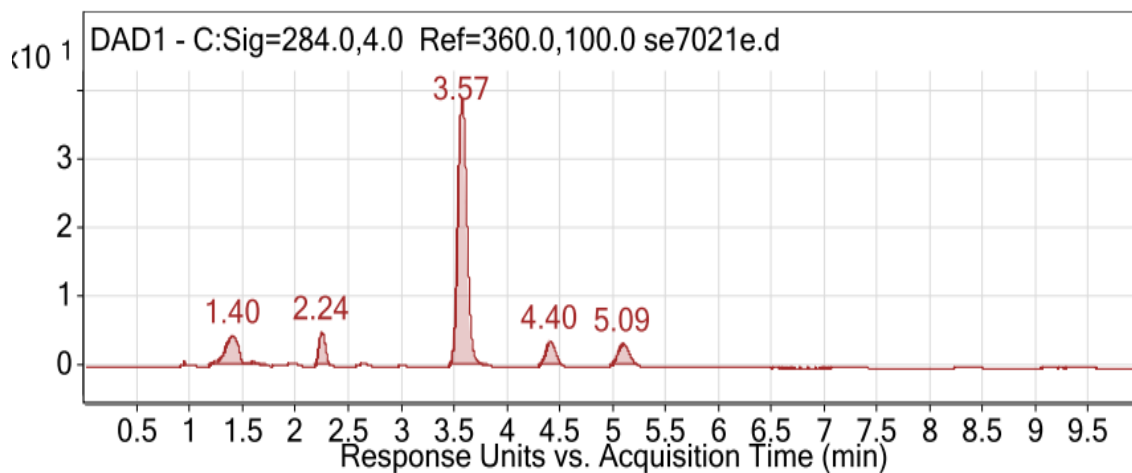


Figure B.5: HPLC-UV chromatogram (at wavelength 284 nm) used for qualitative determination of the efficacy of BT removal.

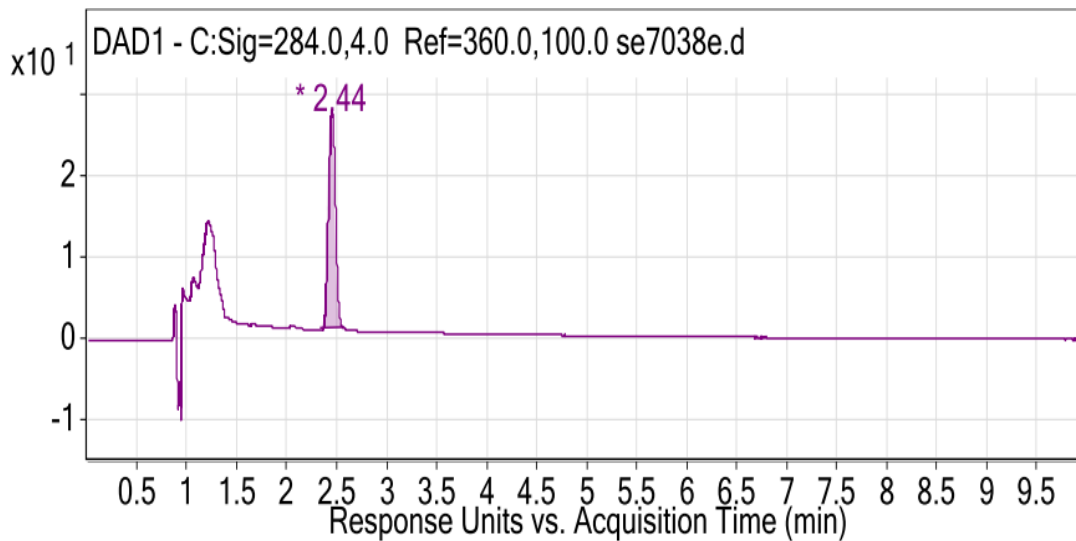


Figure B.6: HPLC-UV chromatogram (at wavelength 284 nm) used for qualitative determination of the efficacy of DBT removal.

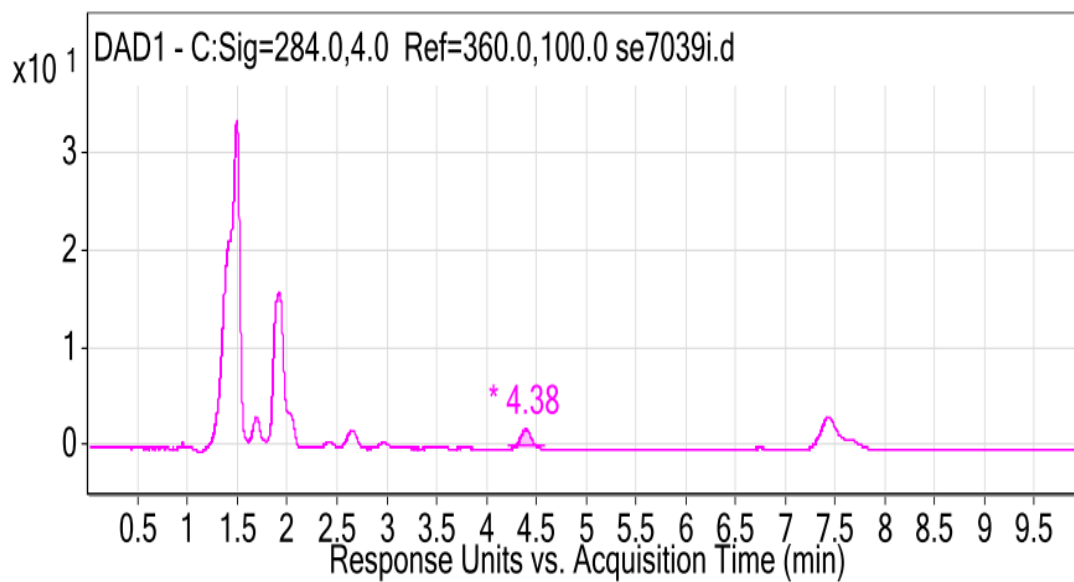


Figure B.7: HPLC-UV chromatogram (at wavelength 284 nm) used for qualitative determination of the efficacy of 4,6-DMDBT removal.